TABLE DES MATIÈRES

Page

LISTE DES TABLEAUX

Page

LISTE DES FIGURES

Page

LISTE DES ABRÉVIATIONS, SIGLES ET ACRONYMES

ACS	Grade de pureté conforme aux standards de *l'American Chemical Society*
AgNP-X	Nanoparticules d'argent (X fait référence à la taille des nanoparticules)
AgNP-X/f	Filtrat de la solution colloïdale des nanoparticules d'argent
ASTM	Organisme de normalisation concernant les matériaux
ATR	Réflectance totale atténuée
AuNP-X	Nanoparticules d'or (X fait référence à la taille des nanoparticules)
AuNP-X/f	Filtrat de la solution colloïdale des nanoparticules d'or
BPO	Peroxyde de benzoyle
CEC	Capacité d'échange cationique
DLS	Analyse par diffusion dynamique de la lumière
DTG	Thermogravimétrie différentielle
EDX	Spectroscopie à rayon X à dispersion d'énergie
ENP	Nanoparticules synthétiques
EPDM	Éthylène-propylène-diène monomère
FEI	*Field Electron and Ion Company*
FTIR	Spectroscopie infrarouge à transformée de Fourier
IR	Infrarouge
kcps	Kilo comptes par seconde
MA	Anhydride maléique
MilliQ	Grade d'eau ultra-pure de type I
MMT	Nanoparticules d'argile de nature montmorillonite
Na^{+}MMT	Montmorillonite à base de sodium
NBR	Caoutchouc poly acrylonitrile butadiène (ou élastomère nitrile)
NBR-g-MA	Caoutchouc nitrile greffé par de l'anhydride maléique
nClay(s)	Nanoparticule(s) d'argile lamellaire
nClay/0	Nanoparticule d'argile non modifiée
nClay/1 (ou 2)	Nanoparticule d'argile organiquement modifiée de type 1 (ou 2)
3005PF	Modèle commercial de gants de protection jetables en caoutchouc nitrile

OH	Groupe hydroxyle
PB	Polybutadiène
phr	Parties pour cent parties de caoutchouc
PVP	Polyvinylpyrrolidone (polymère hydrophile)
RCN	Nanocomposite argile à base de caoutchouc
RCNg	Nanocomposite argile à base de caoutchouc – greffé
RCNq	Nanocomposite argile à base de caoutchouc – trempé
rpm	Rotation par minute
SAXS	Diffusion des rayons X aux petits angles
SEM	Microscopie électronique à balayage
SiO_4^{4-}	Anion tétraèdrique de silicate ou nésosilicate
TEM	Microscopie électronique en transmission
TGA	Analyse thermogravimétrique
TOC	Teneur en carbone organique total
UHR-SEM	Microscopie électronique à balayage à ultra-haute résolution
XRD	Diffractométrie de rayons X

LISTE DES SYMBOLES ET UNITÉS DE MESURE

$\overline{D}$	Coefficient de diffusion intrinsèque
2θ	Angle de diffraction des rayons X
Å	Ångström
c	Concentration massique
$C_{(t,x)}$	Concentration de la substance pénétrante à l'instant t et à la position x
c_1	Concentration de la substance diffusante à la surface d'entrée
c_2	Concentration de la substance diffusante à la surface de sortie
C_∞	Concentration de la substance pénétrante à l'équilibre
CX	Composé aliphatique à X atomes de carbone
D	Coefficient de diffusion
d	Distance inter-réticulaire dans la loi de Bragg
D_0	Facteur pré-exponentiel de diffusion
D_a	Coefficient de diffusion de la zone amorphe d'un polymère
D_{long}	Coefficient de diffusion à longs termes
D_{short}	Coefficient de diffusion à courts termes
E_D	Énergie d'activation de diffusion
f_i	Facteur d'orientation des lamelles silicates
h	Épaisseur d'un échantillon de test d'immersion
I	Intensité de la diffraction des rayons X
I_{eq}	Intensité de la diffraction équatoriale des rayons X
J	flux de matière
k	Constante caractéristique de l'élastomère en termes de diffusion
m_0	Masse initiale d'un échantillon de test de prise de masse
M_∞	Prise de masse à l'équilibre lors d'un test d'immersion
m_∞	Masse d'un échantillon de test d'immersion à l'équilibre
M_t	Prise de masse à l'instant t lors d'un test d'immersion
m_t	Masse d'un échantillon de test d'immersion à l'instant t
n	Indice du mécanisme de la diffusion

P	Coefficient de perméabilité
R	Constante des gaz parfaits
R_{diff}	Taux de diffusion de la substance pénétrante
R_{relax}	Taux de relaxation des chaines macromoléculaires de l'élastomère
S	Coefficient de solubilité à l'équilibre
t	Temps
T	Température absolue
T_i	Température initiale de dégradation en thermogravimétrie
x	Distance (dans la direction de l'épaisseur d'une membrane)
α	Facteur de forme des nanoparticules d'argile
β	Facteur d'immobilisation
Θ	Angle entre la direction de diffusion et l'unité vectorielle normale d'une surface
λ	Longueur d'onde
τ	Facteur d'impédance géométrique
φ	Angle azimutal de la diffraction des rayons X
ϕ	Fraction volumique des nanoparticules dans un nanocomposite

INTRODUCTION

0.1 Contexte de l'étude et problématique

Les propriétés barrières d'un matériau correspondent à sa capacité à limiter le passage de substances à travers sa structure. Un matériau doté de propriétés barrières élevées sert ainsi à séparer deux milieux de concentrations différentes. La maitrise de cette propriété est fondamentale pour des applications assez variées comme en aérospatiale, en pharmaceutique, en filtration, et notamment en industrie d'emballage et d'isolation de produits conditionnés (McKeen, 2016). Pendant de nombreuses années, utiliser les métaux, le verre et le papier laminé étaient les méthodes de séparation les plus répandues pour sceller et isoler un contenu. Cependant, ces matériaux soulèvent plusieurs problèmes de durabilité, d'efficacité, de poids et de coût (Raheem, 2013).

Depuis près de deux décennies, l'intérêt s'est orienté vers les polymères pour remplacer les matériaux d'emballage conventionnels en raison de leur fonctionnalité, de leur légèreté, de leur facilité de mise en forme et de leur bonne qualité esthétique (Cui et al., 2015). En effet, le marché mondial des polymères est passé d'environ 5 millions de tonnes dans les années 50 à près de 100 millions de tonnes à nos jours. Plus de 40% des plastiques sont utilisés pour l'emballage et pour l'isolation. Près de la moitié d'entre eux est utilisée sous forme de films, de membranes et de feuilles (Rhim, Park et Ha, 2013; Silvestre, Duraccio et Cimmino, 2011). Malgré leur grande polyvalence, la perméabilité inhérente des matériaux polymériques est une propriété limitante. En effet, la présence de volumes libres dans leur structure constitue une voie de passage qui facilite la diffusion des molécules pénétrantes. Des techniques ont été développées afin d'améliorer leur propriétés barrières. Parmi les différentes approches, on trouve le traitement de la surface polymérique par un dépôt imperméable, le mélange des polymères par ajout d'une phase résistante à la pénétration ainsi que la mise en forme en multicouches (Dini, 2013).

Plus récemment, les nanocomposites polymère à base de nanoparticules lamellaires ont attiré l'attention en raison de leurs caractéristiques exceptionnelles. L'étendue de leur surface spécifique contribue à l'amélioration des propriétés du polymère de la matrice même à de faibles concentrations (Valapa et al., 2017). En particulier, l'incorporation de nanoargiles dans la structure polymérique s'est montrée comme l'un des moyens les plus prometteurs d'améliorer les propriétés barrières. Cela est dû au fait que l'ajout de particules lamellaires imperméables rend le trajet du pénétrant plus long et tortueux dans la matrice (Cui et al., 2015; Tan et Thomas, 2016). Il est communément admis que la présence des nanoargiles entraîne une amélioration systématique des propriétés barrières. Cependant, leur efficacité est principalement déterminée par l'étendue de leur dispersion et le degré de leur orientation dans la matrice. Hormis cela, les facteurs affectant l'amélioration de ces propriétés dans les matrices polaires (hydrophiles) sont différents lors de l'impaction de polymères non polaires, indiquant ainsi que la performance doit être quantifiée au cas par cas (Hsieh, Cheng et Wu, 2017).

Le caoutchouc nitrile (NBR) fait partie des matériaux polymériques utilisés comme matrice des nanocomposites renforcés par des nanoargiles afin de consolider ses propriétés barrières. C'est un des élastomères synthétiques les plus employés et sa consommation mondiale atteindra plus de 1,5 millions de tonnes en 2023 (The Global Nitrile Butadiene Rubber Market, 2018). Le NBR possède une forte résistance aux solvants hydrocarbonés aliphatiques (solvants à chaines carbonées linéaires), aux carburants ordinaires et aux huiles. Cependant, sa résistance est relativement faible aux solvants organiques à caractère polaire (Massey, 2003). Dans le but de réduire la perméabilité à ces substances, plusieurs travaux de recherche se sont consacrés pour concevoir un nanocomposite dont les lamelles nanoargiles atteignent un état exfolié dans la matrice nitrile, pour lequel les lamelles sont totalement séparées. Cependant, il a été montré qu'il est difficile d'obtenir une dispersion uniforme de ces lamelles en raison de leur tendance à s'agglomérer dans la matrice. Lorsque les chaines élastomères ne sont pas capables de s'intercaler entre les plaquettes nanoargiles, un composite à phases séparées est obtenu, dont les propriétés restent du même ordre que les microcomposites traditionnels.

À la limite de mes connaissances, il y a assez peu d'études menées sur la relation structure-propriété de ces nanocomposites caoutchouteux. En outre, des articles antérieurs sur cette problématique indiquaient la nécessité d'études plus exhaustives pour comprendre le mécanisme de renforcement de ces systèmes (Aabitha, Rane et Rajkumar, 2015; Thomas, George et Thomas, 2017).

0.2 Les objectifs

Suite aux observations précédentes, l'objectif principal de la thèse consiste à optimiser un matériau nanocomposite à base caoutchouc nitrile chargé de nanoargiles et présentant des propriétés barrières optimisées face à des solvants organiques. En d'autres termes, le but du projet est d'améliorer la dispersion des nanoargiles dans la matrice élastomère et atteindre un maximum d'exfoliation de leurs lamelles tout en maintenant une orientation perpendiculaire au sens de pénétration du diffusant.

Afin d'atteindre cet objectif, trois objectifs spécifiques sont fixés :

1. Mettre en place un protocole expérimental qui permettra de réussir **la synthèse d'un nanocomposite nitrile/nanoargiles**. Différentes techniques reportées dans la littérature seront testées. La morphologie de chaque nanocomposite ainsi que leur résistance aux solvants organiques vont être examinées;
2. **Optimiser la dispersion, l'exfoliation et l'orientation des nanoargiles dans la structure de la matrice** en élaborant des méthodes permettant d'améliorer l'affinité chimique entre les chaines macromoléculaires de la matrice et la surface des lamelles nanoargiles;
3. **Évaluer les propriétés barrières du nanocomposite optimisé** et assurer une compréhension des modes de transport de la substance pénétrante à travers la membrane nanocomposite. En outre, sera examinée l'influence de l'optimisation morphologique du matériau sur les paramètres de la cinétique du transport moléculaire.

Après chaque synthèse de matériau, les paramètres de la mise en forme seront enregistrés, la morphologie de la structure et la configuration des nanoargiles seront inspectées et les propriétés barrières seront évaluées. Compte tenu des résultats obtenus, les paramètres de synthèse seront optimisés et le cycle sera repris.

0.3 Organisation de la thèse

La thèse débute par une revue de la littérature présentée dans le chapitre 1. Ce chapitre commence par introduire des notions de base sur les théories de transfert de masse dans la matière. Il discute ensuite les mécanismes de transport moléculaire dans les systèmes polymériques, puis spécifiquement dans les membranes nanocomposites. Le chapitre s'achève par un aperçu sur l'état de l'art actuel concernant les travaux sur les propriétés barrières des nanocomposites à base d'argiles et les difficultés rencontrées.

L'objectif principal et les objectifs secondaires de la thèse sont atteints à travers trois articles de revues.

Le premier article intitulé « *Influence of processing parameters on barrier properties of nitrile/nanoclay nanocomposite membrane against organic solvent* » constitue l'objet du chapitre 2. Cette section débute par la mise en place des techniques expérimentales qui permettent la synthèse des nanocomposites. La morphologie des matériaux obtenus est ensuite examinée par diffraction des rayons X et par microscopie afin de valider les résultats de l'intercalation. Puis, une analyse par diffusion des rayons X aux petits angles (SAXS) est utilisée pour sonder l'étendue de l'orientation des plaquettes nanoargiles dans la matrice. L'étude morphologique est corrélée avec les résultats associés aux propriétés barrières des échantillons. L'article en question est publié dans « *Journal of Polymer Research* » (février 2019).

En se basant sur les résultats obtenus dans la section précédente, le chapitre 3 est dédié au développement des nanocomposites avec une morphologie avancée à l'aide du greffage par

anhydride maléique ainsi qu'à travers le traitement organique des nanoargiles. Une analyse morphologique plus approfondie est menée pour sonder la structure en combinant des observations microscopiques et des analyses de diffractométrie des rayons X. Les résultats associés à cette partie ont été soumis pour publication dans « *European Polymer Journal* » en mars 2019 sous la forme d'un deuxième article de revue ayant pour titre « *Morphological investigation of maleic anhydride-grafted nitrile rubber/nanoclay nanocomposites* ».

Le chapitre 4 est alloué à l'évaluation des propriétés barrières des nanocomposites optimisés, obtenus dans le chapitre précédent. L'effet des paramètres comme la température et la taille des molécules pénétrantes est également évalué. Les résultats menés dans cette section sont présentés dans un troisième article de revue intitulé « *Molecular sorption and diffusion of organic solvents through maleated rubber/layered silicate nanocomposites* ». Le papier a été soumis pour publication dans « *Journal of Polymer Testing* » en mars 2019.

La méthodologie adoptée pour étudier les propriétés barrières des membranes synthétisées est détaillée dans une publication jointe en annexe I. Dans certaines sections de ce rapport, il est fait référence à cette publication pour informations complémentaires sur la modélisation analytique du phénomène de transport obéissant aux lois de la diffusion (lois de Fick) et les solutions associées. Il s'agit d'un article de revue intitulé « *Sorption and diffusion of gold and silver nanoparticles in solution through nitrile rubber membrane* » et publié dans « *Journal of Applied Polymer Science* » en date du 23 juin 2017.

Suite à la présentation des conclusions de l'étude, une section à la fin du rapport sera réservée pour proposer des recommandations, aussi bien pour l'amélioration des techniques d'évaluation des propriétés barrières que pour l'approfondissement de l'étude morphologique des nanocomposites argileux obtenus. De plus, les limites de ce travail seront présentées, ainsi que les perspectives envisageables pour des travaux futurs.

CHAPITRE 1

REVUE DE LA LITTÉRATURE

Ce chapitre débute par un rappel du principe de transport de la matière à travers différents milieux. La seconde section s'intéresse au transfert de masse à travers les systèmes polymériques. La troisième section se concentre sur les élastomères nanocomposites et leurs propriétés barrières. Cette partie traite particulièrement la résistance aux solvants des nanocomposites à base de nanoparticules d'argile. La revue s'achève par une synthèse critique de l'ensemble des travaux présentés préalablement.

1.1 Théorie du transport de matière à travers une membrane

Une membrane est une mince paroi de matériau plus ou moins poreuse qu'on interpose entre deux milieux et qui permet d'éliminer ou de concentrer certains constituants par différents processus. Le principe de séparation par membrane trouve des applications industrielles importantes dont les impacts techniques et commerciaux sont considérables. Durant ces deux dernières décennies, des efforts colossaux étaient déployés par des ingénieurs, physiciens et chimistes pour améliorer leur rendement, étendre leurs champs d'application et diversifier leurs utilisations. La nature chimique ainsi que les propriétés d'une membrane diffèrent grandement selon les phases des milieux à séparer (gazeuse, liquide), la taille des particules à filtrer, la dynamique de la substance pénétrante, etc. Le mécanisme de séparation peut être catégorisé en deux grandes familles en fonction de la nature physique de la membrane, poreuse ou non poreuse. Pour chaque cas, des travaux de recherche se sont intéressés à concevoir des modèles qui traduisent le passage du pénétrant à travers la structure de la membrane.

1.1.1 Phénomène de transport substantiel à travers une membrane non poreuse

1.1.1.1 Principe de transport par diffusion

Un grand intérêt a été apporté à l'étude de la pénétration des molécules de petite taille à travers les membranes polymères. En effet, ce concept est essentiel pour des applications qui touchent au quotidien, à savoir l'emballage alimentaire, le stockage de boissons (Singh, Wani et Langowski, 2017) et la filtration (Purkait et Singh, 2018). Cet impact industriel important du phénomène de passage des liquides et des gaz a poussé les scientifiques à approfondir leurs recherches sur les lois fondamentales qui gouvernent ces processus. Les principes fondamentaux étaient fondés par des chercheurs comme Park, Crank et Barrer (Barrer, 1951; Crank, 1979; Park et Crank, 1968). Depuis, des efforts ont été déployés pour raffiner les méthodes expérimentales et les procédés empiriques capables de quantifier les grandeurs associées aux phénomènes de transfert de masse.

Une approche atomistique stipule que le transport de molécules de faible taille à travers la structure d'une membrane résulte d'un mouvement aléatoire de ces molécules, au sein de la structure, généré par une énergie thermique, c'est le mouvement brownien. D'un point de vue phénoménologique, la différence de concentration entre les deux phases, pénétrante et pénétrée, constitue la force motrice de ce transport qui a tendance à équilibrer cette grandeur et à annuler ce potentiel. Ce mouvement suit le gradient qui va des fortes concentrations vers les faibles concentrations.

1.1.1.2 Lois de Fick

La première loi de Fick met en évidence le fait que le flux allant des zones des hautes concentrations vers les zones de plus basses concentrations a une amplitude qui est proportionnelle au gradient de ces concentrations. Cette proportionnalité correspond au coefficient de diffusion relatif au système. Mathématiquement parlant, cette première loi est énoncée comme suit :

$$J = -D \cdot \frac{dc}{dx} \tag{1.1}$$

Avec *dc/dx* est le gradient de concentration selon la direction de diffusion et *D* est le coefficient de diffusion qui est indépendant de l'unité de la substance en diffusion (cm²/s). Ce coefficient dépend de la température, de la viscosité du fluide ainsi que de la taille des particules selon la relation de Stokes-Einstein (Philipse, 2018). Cette loi s'applique uniquement dans un état d'équilibre, un état où la concentration du diffusant ne varie pas en fonction du temps et le coefficient de diffusion ne dépend pas de la concentration (Roque-Malherbe, 2018). Cependant, il est à noter que durant le processus de diffusion, la concentration de la substance pénétrante ne reste pas la même en un point donné du milieu de diffusion. En effet, cette substance s'accumule dans certaines parties du système (Roque-Malherbe, 2018), d'où la deuxième loi de Fick qui est décrite par la relation suivante :

$$\frac{dc}{dt} = D \cdot \left(\frac{\partial^2 c}{\partial x^2}\right) \tag{1.2}$$

Cette relation correspond au cas idéal où le coefficient de diffusion en lui-même ne dépend ni de la concentration du pénétrant, ni du temps, ni de la distance *x* (on considère un système monodimensionnel dont la diffusion s'effectue selon une seule direction).

Dans un milieu non homogène, la pénétration d'un liquide à travers une structure résulte de l'interaction entre le phénomène de diffusion et le processus de prise de masse dans la structure pénétrée. Réciproquement, cette prise de masse est elle-même engendrée par le phénomène de pénétration. En d'autres termes, plus il y a de la pénétration, plus se manifeste la prise de masse. Il apparait en conséquence un relâchement de la matrice du milieu de pénétration qui favorise davantage la pénétration (Rudin et Choi, 2012). Ainsi, le coefficient de diffusion *D* dépend largement de la concentration de la substance pénétrante et varie d'un point à l'autre dans le milieu. L'équation (1.2) devient alors :

$$\frac{\partial c}{\partial t} = \frac{\partial}{\partial x}\left(D \cdot \frac{\partial c}{\partial x}\right) \tag{1.3}$$

1.1.1.3 Cinétique de transport de la matière

Coefficient de diffusion :

Comme préalablement défini, le coefficient de diffusion correspond au facteur de proportionnalité dans la première loi de Fick. Plusieurs modèles mathématiques sont développés pour décrire le processus de diffusion à travers un système. Le modèle le plus basique suppose une évolution linéaire de la concentration du pénétrant qui est invariante en fonction du temps. Ainsi, l'équation associée se donne par :

$$D \cdot \frac{d^2c}{dx^2} = 0 \tag{1.4}$$

En tenant compte des conditions aux limites qui s'appliquent sur les concentrations aux bords d'un échantillon d'une membrane (pour $x = 0$, $c = c_1$ et pour $x = h$, $c = c_2$), une double intégration de cette équation (1.4) nous fournit le profil de l'évolution spatiale de la concentration du diffusant au cœur du milieu de diffusion entre ses deux faces externes :

$$c = c_1 + \frac{(c_2 + c_1)}{h \cdot x} \tag{1.5}$$

Il s'agit d'une évolution linéaire invariante en fonction du temps. Cette évolution peut être schématisée par la Figure 1-1 suivante :

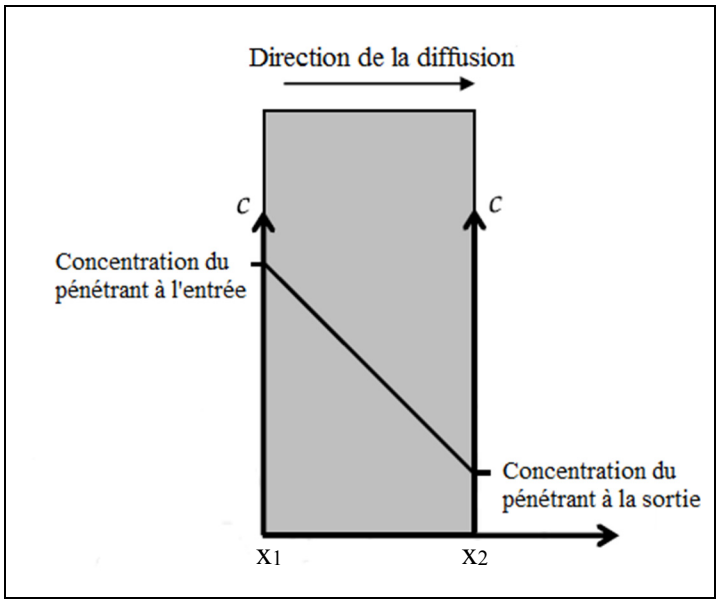

Figure 1-1. Variation de la concentration d'un diffusant à l'intérieur d'une membrane à l'état d'équilibre

Pour une compréhension plus approfondie du mécanisme de la diffusion et pour une évaluation plus précise du coefficient associé, la variation de la concentration du pénétrant en fonction du temps le long du processus ne peut pas être omise. Compte tenu de l'accumulation en fonction du temps du diffusant, la seconde loi de Fick est considérée pour la modélisation de la diffusion. Cependant, et pour plusieurs systèmes diffusants/membranes, une simplification sur le coefficient de diffusion peut être admise. Avec cette hypothèse, ce coefficient est estimé comme une constante intrinsèque du système de diffusion, une constante qui ne dépend ni de la concentration du diffusant, ni du temps, ni de l'abscisse du point d'analyse. Le profil de concentration peut être obtenu en résolvant l'équation aux dérivées partielles de la seconde loi tout en tenant compte des conditions limites et initiales nécessaires. Une solution de la seconde loi de Fick permet le calcul du coefficient de diffusion. Il est à noter, néanmoins, que la concentration du pénétrant à l'intérieur de la structure ainsi que son évolution en fonction du temps sont des paramètres qui sont délicats à évaluer expérimentalement. Des paramètres comme la masse de la substance ayant pénétrée ainsi que son évolution au cours du temps sont beaucoup plus accessibles. Une solution de l'équation de la seconde loi de Fick en termes de prise de masse sous la forme d'une série

trigonométrique a été proposée par Crank et Parker dans leurs travaux sur les mathématiques de diffusion. Cette solution est donnée par (Siepmann et Peppas, 2011) :

$$\frac{M_t}{M_\infty} = 4 \cdot \left(\frac{D \cdot t}{h^2}\right)^{1/2} \cdot \left[\frac{1}{\pi^{1/2}} + 2 \cdot \sum_{n=0}^{\infty} (-1)^n ierfc \frac{n \cdot h}{2 \cdot (D \cdot t)^{1/2}}\right] \qquad (1.6)$$

Où *ierfc* et une fonction d'erreur complémentaire intégrée de Gauss. Ainsi, en disposant des données expérimentales de prises de masse en fonction du temps, le coefficient de diffusion peut être déduit. Plus de détails sur le calcul du coefficient de diffusion à partir de la solution de la seconde loi de Fick seront présentés dans les prochains chapitres.

Perméabilité et solubilité :

Le phénomène de la diffusion fait partie d'un processus de transport plus général qui correspond au phénomène perméation. Les molécules de la substance pénétrante sont transportées d'une surface de la membrane vers la surface opposée via une combinaison de mécanismes. En premier lieu, les molécules de la substance pénétrante obéissent à un phénomène d'adsorption par lequel elles traversent l'interface membrane/liquide. Ensuite, les éléments sont conduits à l'intérieur de la structure sous l'effet d'un gradient de potentiel chimique. Enfin, le mécanisme de désorption permet à la substance de franchir la surface de sortie et émerger de la structure.

Pour que le mécanisme de diffusion ait lieu, les éléments de la substance pénétrante doivent d'abord s'infiltrer dans le matériau et franchir la surface d'exposition de la membrane. Ce mécanisme est un processus thermodynamique qui se traduit par la solubilité du système de pénétration. Elle consiste à l'affinité d'un solvant pour un matériau polymère. En effet, la solubilité du système est reliée à l'énergie d'interaction entre le polymère et le solvant. Elle est d'autant plus grande que l'énergie est élevée (Perron, Desnoyers et Lara, 2002b).

1.1.1.4 Techniques d'évaluation des paramètres de transport

Il existe plusieurs méthodes de mesure et de nombreuses techniques normalisées pour évaluer et quantifier le transport de masse dans un réseau polymérique. Le choix de la procédure à adopter dépend de certains facteurs à savoir l'état physique de la substance pénétrante ainsi que la morphologie et les dimensions de la membrane pénétrée. Ces techniques peuvent être scindées en deux catégories. La première se base sur la détermination des paramètres de la cinétique de transport à travers l'évaluation du taux de perméation du pénétrant d'une surface à l'autre de la membrane. La deuxième se base sur la détection, au fil du temps, de la concentration du pénétrant en tout point de la membrane durant le processus de transport (Duncan, Urquhart et Roberts, 2005; Follain et al., 2010).

Les méthodes de perméation s'articulent sur le principe suivant : la première phase consiste à exposer la membrane en question à une concentration donnée de la substance pénétrante. La surface alimentée est généralement confinée dans une cellule fermée pour assurer une concentration et une pression de vapeur constantes. La deuxième phase consiste à sonder la surface opposée de la membrane et évaluer la perméabilité de la substance ayant traversé la structure.

Les techniques utilisées diffèrent par la méthode adoptée pour sonder l'accumulation du pénétrant à la surface de sortie. La détection de la substance pénétrante peut être directe à travers une analyse chimique. Karimi a présenté une étude de diffusion d'une substance liquide menée sur des membranes en polyméthacrylate de méthyle et pour lesquelles le diffusant est détecté par spectroscopie infrarouge en mode de réflectance totale atténuée (Karimi, 2011). Cette méthode était également utilisée par Kwan pour évaluer le taux de perméabilité de deux séries de n-alcanes (C6-C17) et esters (C5-C17) à travers des membranes adhésives thermodurcissables (Kwan Jr, 1998).

La détection peut également être effectuée par technique gravimétrique. La quantité de la substance est mesurée indirectement. En effet, dès que le diffusant est mis en contact avec la

membrane, il commence à diffuser à travers. Par évaporation instantanée de tout le diffusant qui apparait sur la seconde face de la membrane, on obtient une variation de masse du pénétrant par rapport à l'état initial. Cette perte correspond à la quantité ayant traversé la membrane. Cette évaluation permet de remonter aux coefficients de diffusion et de perméabilité du système. La manipulation s'effectue moyennant une cellule gravimétrique conforme à la norme ASTM F1407 (*Standard Test Method for Resistance of Chemical Protective Clothing Materials to Liquid Permeation-Permeation Cup Method*, 2017). Des auteurs comme Ibrahim et al. ont adopté cette technique pour évaluer les paramètres de transfert de masse de certains solvants organiques à travers des membranes carboxyméthylcellulose mélangées à l'alcool polyvinylique (Ibrahim et al., 2013).

D'autre part, la deuxième famille de techniques d'évaluation des paramètres de diffusion dans un système se base sur la mesure des changements des propriétés du matériau d'une membrane suite à l'exposition à la substance pénétrante. En effet, le contact entre la substance chimique et la matrice polymérique cause généralement des altérations au niveau des propriétés thermomécaniques de cette dernière. Bien que ces changements de propriétés soient généralement considérés comme une conséquence indésirable de l'exposition aux produits chimiques, sonder ces changements de propriétés peut fournir des informations sur les concentrations des substances chimiques diffusantes (Duncan, Urquhart et Roberts, 2005). L'une des techniques les plus répandues et également la plus simple pour étudier expérimentalement la diffusion consiste à évaluer la cinétique d'absorption ou la cinétique de prise de masse. La manipulation consiste à préparer un échantillon du matériau à étudier dont l'épaisseur est connue. L'échantillon est ensuite immergé dans la solution diffusante de manière à ce que la surface externe du matériau soit en contact permanent avec le solvant. La concentration est supposée uniformément répartie sur toute la surface de contact. Le liquide commence à diffuser dans la structure de la membrane. On considère que le réseau de la membrane conserve sa masse tout au long du processus et une évolution de la prise de masse du système est reportée en fonction du temps. Cette quantité correspond à la masse du pénétrant ayant diffusé.

1.2 Transport de matière à travers un système polymérique

1.2.1 Diffusion à travers un réseau polymérique

La diffusivité d'une substance dans une matrice polymérique ainsi que la solubilité du système dépendent étroitement du volume libre disponible dans le réseau. Ce volume est une propriété intrinsèque du matériau et dépend de sa nature, de son état physique ainsi que de ses éléments constitutifs (Drioli, Giorno et Fontananova, 2017). Le volume libre apparait sous l'effet de l'enchevêtrement et du désordre des chaînes macromoléculaires de la structure polymérique. La taille de l'espace vide varie continuellement en fonction de la vibration et de la translation des chaînes adjacentes sous l'effet de l'agitation thermique. L'ensemble de ces cavités donne naissance à un réseau de vide au sein de la structure permettant au diffusant de se déplacer. La Figure 1-2 illustre le mouvement d'un diffusant à travers le volume libre entre les chaînes.

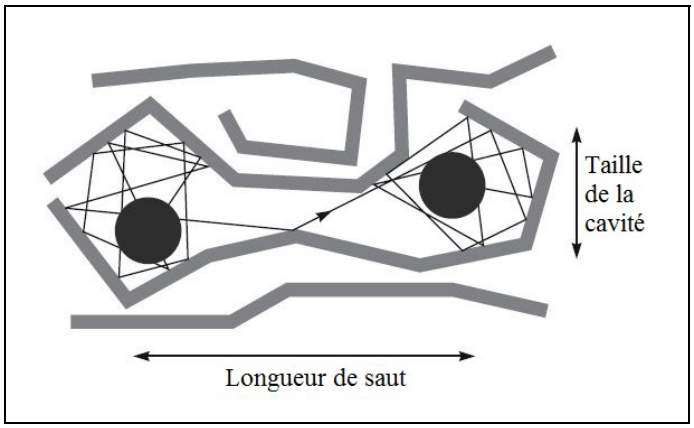

Figure 1-2. Déplacement d'une molécule de dioxyde de carbone dans la matrice d'un polyamide (6FDA-4PDA) – Illustration tirée de (Powell et Qiao, 2006)

La mobilité et le degré de liberté des chaînes affectent de près la fraction du volume libre et ainsi la diffusivité du perméant.

La nature de la structure polymérique a une influence sur les coefficients de diffusion des substances pénétrantes. La Figure 1-3 montre un graphique qui représente des courbes de variation des coefficients de diffusion, en fonction de la masse moléculaire, des substances diffusantes à travers trois membranes de natures différentes ; deux caoutchoucs mous (caoutchouc naturel et caoutchouc de silicone), et un polymère vitreux dur et rigide (polystyrène). Il a été montré que pour les entités de très faible taille comme l'hélium et l'hydrogène, les coefficients de diffusion dans tous les réseaux polymériques sont comparables et ne différent que d'un facteur de 2 ou 3. Ces entités n'interagissent qu'avec un ou deux atomes à proximité immédiats dans la matrice. L'environnement local de ces pénétrants dans les trois polymères ressemble à celui d'un liquide. Cependant, pour les substances de plus grande masse moléculaire (de 200 à 300) et de diamètres moléculaires plus importants (de 6 à 10 Å), les environnements locaux sont très différents dépendamment du milieu de diffusion. En effet, dans les membranes polymères, plusieurs segments des chaînes polymères sont impliqués dans chaque mouvement de l'espèce diffusante. Les différences entre le mouvement des segments de polymère dans les membranes souples caoutchouteuses et dans la membrane rigide en polystyrène sont considérables. Les chaînes polymères des caoutchoucs sont beaucoup plus malléables et tournent plus facilement que celles du polystyrène. L'une des manifestations de cette différence dans la flexibilité des chaînes est la différence dans les propriétés élastiques et aussi les coefficients de diffusion (Baker, 2012). Pour comprendre la diffusion dans les membranes polymères, il est donc essentiel de connaitre l'environnement local autour de la molécule perméable. Ainsi, les polymères peuvent être divisés, du point de vue des propriétés barrières, en deux grandes catégories ; les caoutchoucs et les polymères vitreux.

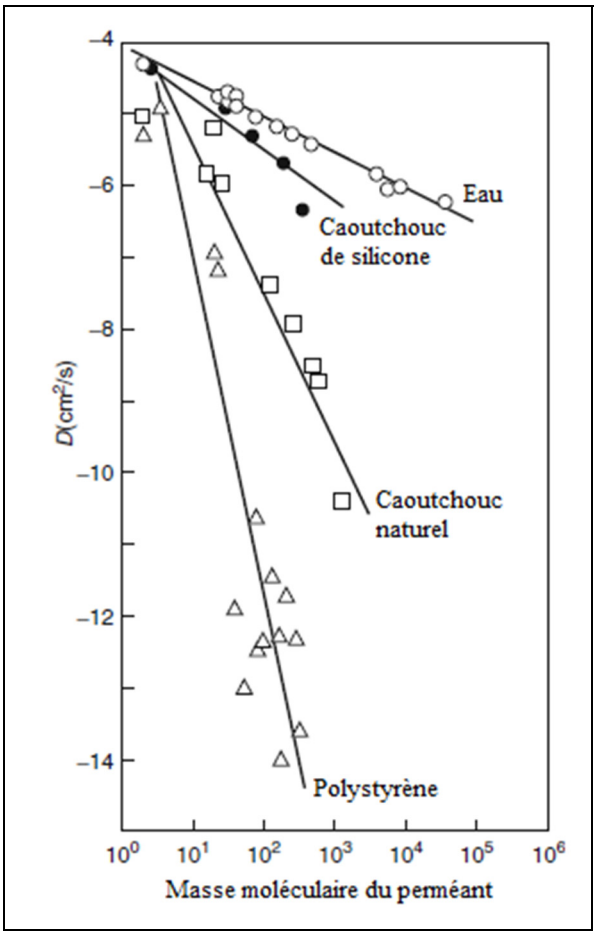

Figure 1-3. Coefficient de diffusion perméable en fonction du poids moléculaire perméable dans l'eau, le caoutchouc naturel, le caoutchouc de silicone et le polystyrène – Figure tirée de (Baker, 2012)

Il est à noter que des efforts considérables ont été déployés au cours des deux dernières décennies pour établir un lien entre la nature de la structure polymérique et leurs propriétés de perméation. Une corrélation quantitative fiable de nature structure/propriété barrière n'a pu être établie. Ce qui a été réalisé à ce jour est un ensemble de lois semi-empiriques qui ont permis de corréler les propriétés de perméation de familles apparentées de polymères en fonction des variations dans leurs structures chimiques.

1.2.2 Cas particulier : Les élastomères

Dans un polymère caoutchouteux, élastomère, les segments des chaînes macromoléculaires peuvent se mouvoir librement et établir des rotations autour de leurs axes sous l'effet de l'agitation thermique. La mobilité segmentaire et la grande quantité de volume libre entre leurs macromolécules donnent à ces structures leur souplesse et leur élasticité, et particulièrement, les caractérisent par des coefficients de diffusion élevés (Heinrich, 2011).

Un exemple présenté dans les travaux de Artis et al. montre l'évolution du coefficient de diffusion du dichloroéthane à travers la matrice de l'éthylcellulose en fonction de la fraction du volume libre de la structure. En augmentant la concentration du dichloroéthane dans la structure (de <1% à >90%), la température de transition vitreuse varie et la matrice se plastifie passant d'une structure vitreuse à une structure caoutchouteuse, puis en un gel gonflé par le solvant et enfin en solution polymérique. Le coefficient de diffusion passe d'environ 2×10^{-9} cm^2/s à 2×10^{-6} cm^2/s (Baker, 2012). La Figure 1-4 représente graphiquement cette augmentation de la diffusivité du solvant.

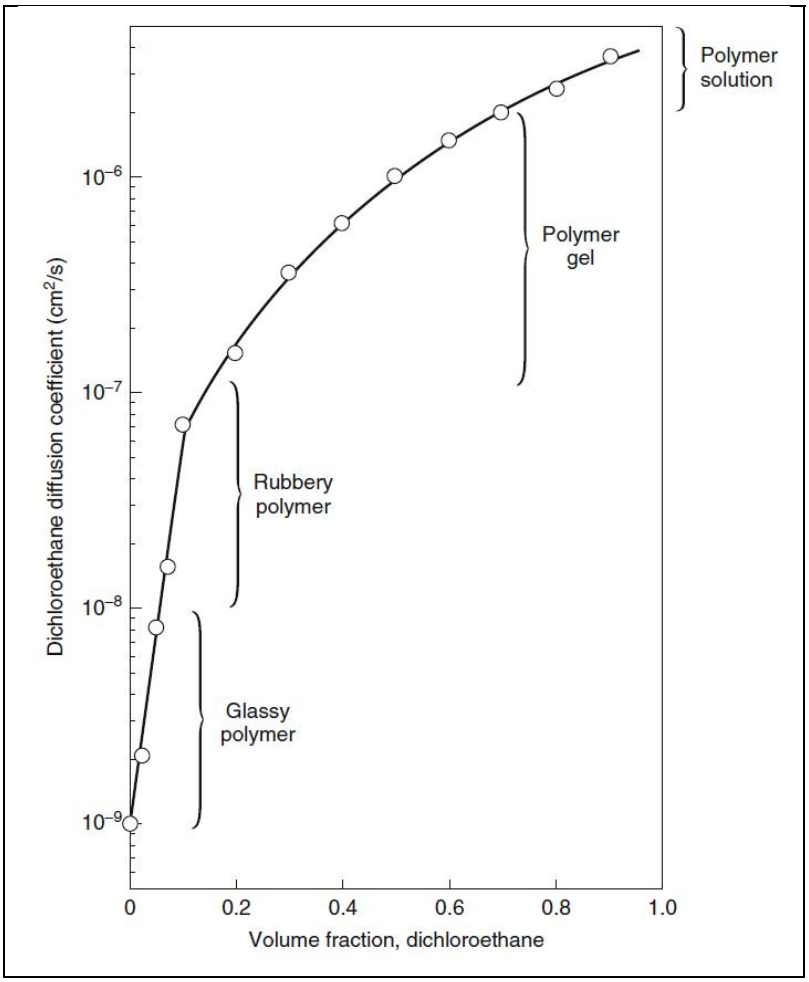

Figure 1-4. Variation du coefficient de diffusion du dichloroéthane dans la matrice du l'éthylcellulose en fonction de la fraction du volume libre dans la structure – Figure tirée de (Baker, 2012)

1.2.3 Paramètres d'influence sur le phénomène de transport

Le phénomène de diffusion fait intervenir une structure polymérique en interaction avec un solvant liquide. Lors de la mise en contact permanent entre les deux entités, des interactions physiques et chimiques sont inévitables. Ces interactions affectent plus au moins le processus de la diffusion en agissant sur les propriétés du milieu de diffusion. Pour sa part, le diffusant est caractérisé par des paramètres qui influencent d'une façon directe la diffusivité à savoir la taille des molécules du solvant. La viscosité, l'état physique ainsi que la volatilité jouent également un rôle dans la détermination du coefficient de diffusion. Quant au réseau

polymérique, la morphologie de la structure, le taux de réticulation des chaînes ainsi que son taux de cristallinité influencent le processus. Finalement, les conditions environnementales à savoir la pression et la température ont également montré des effets sur la diffusivité du système.

1.2.3.1 Propriétés du pénétrant

Étant une partie du système de diffusion, la substance diffusante influe par ses propriétés et ses caractéristiques sur le taux de transport à travers la structure. L'augmentation de la taille des molécules pénétrantes fait systématiquement diminuer le coefficient de diffusion du système (Siracusa et al., 2018). Également, la forme des pénétrants affecte le taux de diffusivité. Dans leurs travaux sur la diffusion à travers le polyéthylène à basse densité, Rusina et ses coauteurs ont évoqué le fait que pour le même volume occupé, les molécules ayant des formes aplaties ou allongées ont un coefficient de diffusion plus élevé que les molécules de forme sphérique (Rusina, Smedes et Klanova, 2010). Il est, cependant, intéressant à noter que la variation du facteur forme du pénétrant affecte la diffusion dans les réseaux polymériques vitreux plus que les réseaux caoutchouteux (George et Thomas, 2001).

Certaines études se sont penchées sur l'effet de la variation de la nature du pénétrant sur le phénomène de transport en exposant un système polymérique donné à des solvants organiques. Les travaux de Kim et al., reportés dans la revue de George et Thomas, ont montré une baisse de l'absorption à l'équilibre proportionnellement à l'augmentation de la longueur de la chaîne moléculaire du diffusant. Le système étudié était des solvants organiques allant de l'heptane au dodécane et du polystyrène réticulé (George et Thomas, 2001). Des études plus récentes effectuées par Al Minnath el al. se sont intéressées aux mécanismes de transports d'une variété de benzènes substitués (benzène, toluène et p-xylène) à travers un mélange de polymères à base de polyuréthane. Leurs résultats montrent que l'augmentation de la taille moléculaire du pénétrant engendre une diminution des valeurs de la diffusivité et dévient le mécanisme du transport (Al Minnath, Unnikrishnan et Purushothaman, 2011). D'autres travaux similaires ont été consacrés à la diffusion de

différents solvants organiques à travers des membranes polymériques (Mathew et al., 2002; Tiemblo et al., 2002).

D'autre part, la littérature contient également des études qui traitent l'effet de la nature du pénétrant à travers des membranes élastomères. À titre indicatif, le transport moléculaire d'une série d'hydrocarbures aromatiques à travers des mélanges de polypropylène/caoutchouc nitrile isotactique a été étudié. Les coefficients de diffusion et de perméation diminuaient avec l'augmentation du volume molaire des solvants. (George, Varughese et Thomas, 2000). Les mêmes observations ont été notées avec un système de solvants aromatiques contre un mélange élastomère naturel et nitrile (Mathai, Singh et Thomas, 2002).

1.2.3.2 Température

La variation de la température est responsable de l'agitation thermique des molécules dans le système. Cette agitation concerne les solutés dans le liquide de même que les chaînes macromoléculaires du réseau polymérique. Cette approche justifie la dépendance, de type Arrhenius, du coefficient de diffusion du système à la température.

$$D = D_0 \cdot \exp(-E_D/(R \cdot T)) \tag{1.7}$$

En comparaison avec les deux premiers processus de transport cités, le processus de diffusion est le plus sensible au paramètre de la température. Il a été également montré que l'énergie d'activation est un paramètre thermique qui dépend de la taille de la substance pénétrante plus que sa dépendance de la masse (Drioli, Barbieri et Brunetti, 2017).

On compte plusieurs travaux dans la littérature qui ont montré l'effet de la variation de la température sur la diffusion de solvants à travers des systèmes polymériques. À titre d'exemple, Soney et al. ont étudié le transport moléculaire de certains hydrocarbures aromatiques à travers des membranes élastomères vulcanisées de styrène-butadiène. L'étude était menée dans un intervalle de température allant de 25 à 65°C. Il a constaté que

l’augmentation de la température active le processus de diffusion. Les auteurs ont pu également estimer l'entropie et l'enthalpie de sorption du système en se basant sur la relation de Van’t Hoff. Il est à mentionner, néanmoins, que l'absorption du solvant à l'équilibre avait légèrement diminué en raison du taux plus élevé de désorption aux hautes températures (George, Thomas et Ninan, 1996). Aminabhavi et al. ont évalué la résistivité des fluoroélastomères aux solvants ketones et nitriles en se basant sur la technique gravimétrique. Les tests de prise de masse ont été effectués à des températures allant de 30 à 60°C. Leurs résultats ont montré que la cinétique de la migration moléculaire des solvants est conforme au modèle de la diffusion à travers les structures polymériques pour tous les paliers de température et que les coefficients de diffusion obéissaient à la loi d’Arrhenius (Aminabhavi, Harlapur et Ortego, 1997). Aji et al. ont travaillé sur un mélange d’élastomère nitrile et d’éthylène-acétate de vinyle. Entre autres, l’effet de la température (23-75°C) sur la diffusion et la sorption de benzènes substitués par un méthyle a été observé. La même tendance que les travaux précédents a été remarquée. Selon les auteurs, la température active le processus de pénétration sous l’effet de la mobilité des chaînes dans le réseau polymère. Plus loin, les paramètres thermodynamiques issus de l’étude de la variation de la température ont permis la prédiction le taux de réticulation dans le système (Joseph, Mathai et Thomas, 2003).

1.2.3.3 Additifs

Dans l'industrie du caoutchouc, une grande variété d’additifs particulaires est utilisée à des fins diverses comme le renforcement, la réduction des coûts des matériaux et l'amélioration de la mise en forme (Pal et al., 2010). Au cours du phénomène de diffusion, ces espèces imperméables se logent et s’accumulent dans la structure de la membrane. Par conséquent, ces entités forment un obstacle qui s’oppose à la pénétration du diffusant (Tan et Thomas, 2016).

La relation entre la diffusion et la présence de ces espèces dépend de leur nature, de leur degré d’adhésion ainsi que de leur compatibilité avec la matrice polymérique. Le taux

d'obstruction dépend également de la taille de ces entités, de leur forme et de leur orientation dans le réseau (Choudalakis et Gotsis, 2009b).

Dans la revue de Mattozi, on trouve une relation qui exprime une proportionnalité entre le coefficient de diffusion global d'une membrane D et le coefficient de diffusion de la zone amorphe de la structure D_a (Mattozi, 2007):

$$D = D_a/(\tau \cdot \beta) \tag{1.8}$$

Avec β est un facteur d'immobilisation et τ est le facteur d'impédance géométrique. Karimi a montré que ce facteur augmente rapidement avec l'augmentation de la concentration ainsi que de la taille des entités imperméables (Karimi, 2011).

Des travaux se sont intéressés à étudier l'effet des plastifiants sur la diffusivité. Un plastifiant est une molécule ajoutée aux formulations des matériaux plastiques généralement pour les rendre plus flexibles, plus résistants et plus faciles à manipuler. Ainsi, l'ajout d'un plastifiant à la structure d'un élastomère permet de faire augmenter la mobilité entre les chaînes macromoléculaires. Comme mentionné préalablement, cette mobilité est étroitement liée à la pénétration du diffusant; l'ajout de plastifiant favorise le transport du diffusant dans la structure. En contrepartie, un agent plastifiant contribue à affaiblir la solubilité du système. Dans les revues de Soney, l'ajout du tricresyl phosphate comme plastifiant au polymère permet d'améliorer le coefficient de diffusion du pénétrant à travers sa structure (Soney, 2001).

1.3 Propriétés barrières des polymères nanocomposites

De plus en plus, les efforts se multiplient pour développer de nouvelles technologies afin d'améliorer les propriétés barrières des membranes polymériques. Il est reconnu que la stratégie la plus prometteuse jusqu'à présent consiste à utiliser des polymères nanocomposites. Il s'agit d'une classe de composites polymériques dans laquelle la matrice est chargée par des particules dont au moins l'une des dimensions est inférieure à 100 nm.

Certains de ces nanocomposites ont montré une capacité inédite à améliorer les propriétés barrières par rapport aux polymères non chargés et aux microcomposites, et cela à des taux de chargement relativement faibles (Kotal et Bhowmick, 2015; Valapa et al., 2017). Parmi les particules nanométriques les plus utilisées on compte les nanoargiles qui sont à la fois très abondantes, peu coûteuses, stables chimiquement et aussi respectueuses de l'environnement. En outre, et contrairement à d'autres nanoparticules comme celles d'or, d'argent et de dioxyde de titane, les nanoargiles ne sont pas reportées toxiques. Cela est principalement dû à la nature inerte de leur structure chimique ainsi que leur facteur forme élevé (Zhang et al., 2017).

1.3.1 Les nanoparticules d'argile lamellaire

Les minéraux argileux sont des substances naturelles rocheuses qui englobent plusieurs catégories. Les phyllosilicates constituent une famille de ces minéraux et correspondent à des argiles lamellaires. Les phyllosilicates sont composés d'un empilement interconnecté de feuillets de silicates. Chaque feuillet est formé d'une superposition de couches tétraédriques et octaédriques. Une couche tétraédrique plane est basée sur une continuité d'anneaux de tétraèdres de silicate (SiO_4^{4-}) dont des groupes hydroxyles (OH) occupent leurs centres. Les couches octaédriques, quant à eux, dictent la nature du phyllosilicate dépendamment de la nature ainsi que la charge du cation qui les compose (Al^{3+}, Fe^{2+}, Mg^{2+}, etc.) (Laske, 2015; Zabihi et al., 2018). Comme le montre la Figure 1-5, les couches sont connectées en partageant les groupes hydroxyles ainsi que l'atome d'oxygène apical résultant des liaisons hexagonales des tétraèdres de silicium.

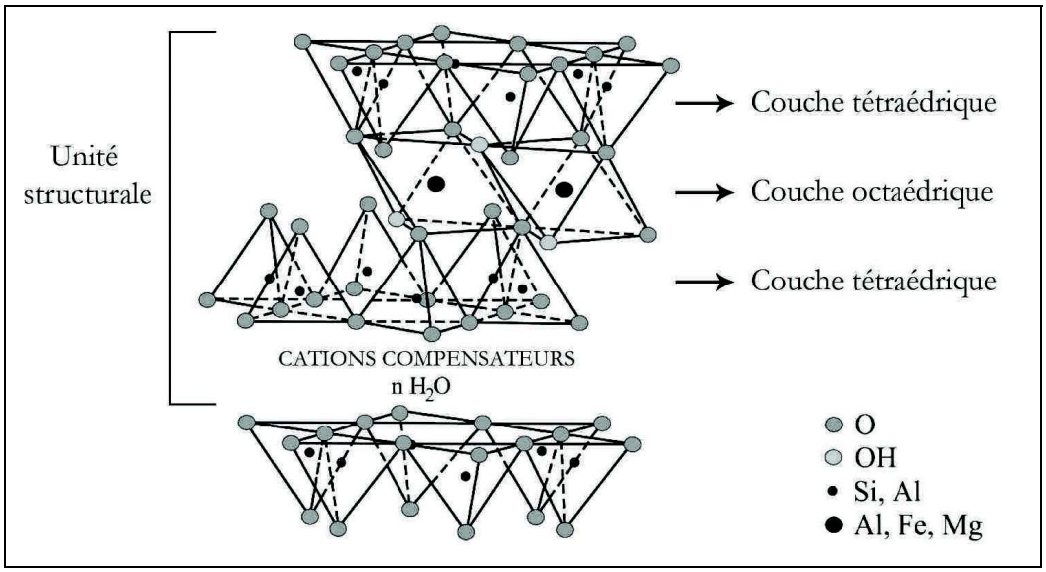

Figure 1-5. Modèle cristallographique de la structure phyllosilicate – Figure tirée de (Domenech, 2012)

En particulier, les smectites sont des 2:1 phyllosilicates ; chaque lamelle de ces argiles est formée d'une couche octaédrique d'aluminium en sandwich entre deux couches tétraédriques de silicium. Il est à noter que l'origine de la grande diversité des argiles lamellaires provient du fait que les cations d'aluminium (Al^{3+}) situés dans leurs couches octaédriques peuvent être partiellement substituées par d'autres cations de même taille. Si une telle substitution isomorphe s'effectue par un cation de moindre valence, il en résulte un excès de charge négative. Afin d'assurer l'électroneutralité de l'ensemble des couches, des cations de métaux terreux alcalins déjà présents dans le minéral comme ceux du calcium, du potassium ou du sodium contrebalancent cette altération de charge. Ces cations compensateurs ne pénètrent pas à travers les couches tétraédriques et se logent plutôt dans le vide interlamellaire (Cui, 2009). C'est grâce à la présence de ces cations que les argiles lamellaires naturelles sont dotées de leur nature hydrophilique. Dans le cas particulier où les cations Al^{3+} sont substitués par des cations Mg^{2+}, le smectite résultant se transforme en montmorillonite (MMT), l'une des familles les plus commercialisées des argiles lamellaires (Dlamini, Li et Mamba, 2019). Les argiles montmorillonites sont le plus souvent commercialisées sous forme de poudre fine dont la taille de ses grains est d'environ 10 µm. Chaque grain constitue une agglomération d'amas de cristaux d'argile. Au sein de chaque cristal se trouvent des agrégats de tactoïdes

aléatoirement orientés. Ces tactoïdes correspondent à des empilements des lamelles, ou feuillets, unitaires décrits préalablement. Un tactoïde de montmorillonite compte environ une dizaine de lamelles (Chu et al., 2013). La structure du MMT à différentes échelles est schématisée dans la Figure 1-6. Une lamelle mesure environ un nanomètre d'épaisseur. Sa dimension latérale est de quelques dizaines à quelques centaines de nanomètres. Cela leur confère un facteur forme très élevé. Un tactoïde préserve son intégrité grâce aux forces électrostatiques et aux faibles forces de Van Der Waals qui s'établissent entre les feuillets élémentaires dans le vide interlamellaire. Dans l'hypothèse où une séparation complète des lamelles peut avoir lieu, un gramme de MMT lamellaire peut fournir une surface spécifique réactive d'environ 750 m^2 (Naveau et al., 2011).

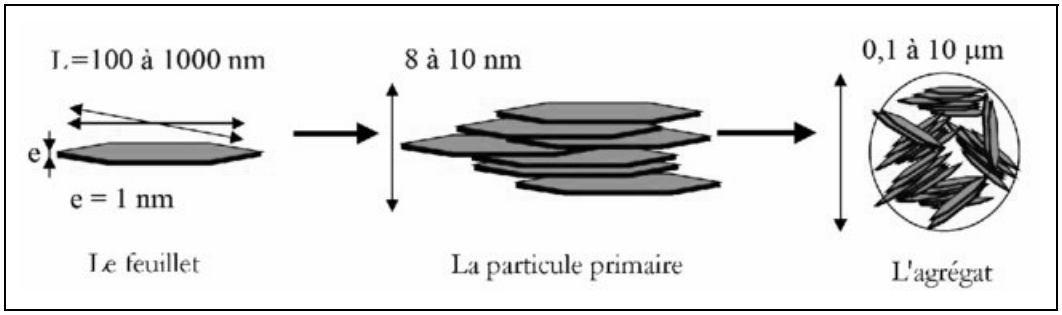

Figure 1-6. Représentation de l'organisation multiéchelles de la montmorillonite – Figure tirée de (Espinosa et Stalin, 2017)

1.3.2 Souci de dispersion dans les nanocomposites

Un nanocomposite, c'est quoi ? Un nanocomposite est une classe de matériaux hybrides dont au moins l'une des phases se trouve à l'échelle nanométrique. En particulier, les nanocomposites polymères se composent par une matrice polymérique chargée par des renforts nanométriques.

1.3.2.1 Les nanocomposites à base de nanoparticules d'argile

Le MMT par sa grande surface spécifique, son facteur de forme élevé, sa haute résistance et son faible coût semble être prometteur comme phase de renfort pour les nanocomposites.

Avec un chargement en MMT de seulement 5% en masse, les propriétés mécaniques et thermiques étaient grandement améliorées. Depuis, les études se sont poursuivies pour révéler des caractéristiques uniques et inédites d'une large gamme de polymères renforcés par du MMT. En plus des propriétés thermomécaniques, des améliorations ont été apportées aux propriétés barrières, aux propriétés de transparence, au retardement de feu, etc.

À l'échelle microstructurelle, de telles bonifications ne peuvent être atteints que si le maximum de la surface spécifique du MMT rentre en contact avec les chaînes polymères et un maximum d'interface soit établi entre les feuillets silicates et la matrice. Ainsi, la clé de réussite de la synthèse d'un nanocomposite à base d'argile lamellaire consiste à désassembler les lamelles qui composent les tactoïdes et atteindre un niveau élevé d'exfoliation. Cependant, mélanger physiquement les MMT avec un polymère ne produit pas nécessairement un nanocomposite. En effet, les groupes hydroxyles AlOH qui constituent les bordures des lamelles d'argile ainsi que les réseaux de tétraèdres silicates sur leurs surfaces font en sorte que 8 à 10% de la superficie de la lamelle soit couverte de molécules d'eau. Cette nature hautement hydrophilique est incompatible avec les structures des réseaux polymériques majoritairement hydrophobes et empêche la dispersion des nanoparticules d'argile. La littérature rapporte assez peu de polymères combinés avec succès à des MMT à l'état naturel, exception faite de l'alcool polyvinylique et de l'oxyde de polyéthylène.

1.3.2.2 Fonctionnalisation des nanoparticules d'argile

Afin d'améliorer l'affinité chimique entre les MMT et les polymères organiques de nature hydrophobe, il est nécessaire d'appliquer des modifications chimiques sur les surfaces des lamelles silicates. Intuitivement, les modifications consistent à attribuer à ses surfaces une nature organique et apolaire pour favoriser l'interaction interfaciale entre le polymère et les nanoparticules. Ces modifications s'effectuent sur la surface dans les sites de déficit de charges occupés par les cations terreux hydratés à travers une substitution cationique. Les éléments chimiques introduits sont des tensioactifs fonctionnels ; ce sont des molécules composées qui possèdent une partie hydrophile polaire pour assurer le processus de

substitution et une partie organique hydrophobe pour interagir avec les macromolécules polymériques. L'étendue de fonctionnalisation dépend du nombre des sites d'échange cationique sur la surface de la lamelle. Cette spécification est caractéristique pour une argile et se considère comme sa capacité d'échange cationique (CEC). Pour les MMT, la CEC s'évalue entre 60 et 120 meq/100g. Parmi les cations tensioactifs, on compte les alkyles-ammonium, les alkyles-phosphonium, etc. Il est à noter que les alkyles-ammonium quaternaires sont de loin les plus utilisés. La structure de ces molécules est basée sur celle du cation ammonium avec une substitution de l'une ou de plusieurs de ces atomes d'hydrogène par des chaînes aliphatiques dont le nombre d'atomes de carbone varie de six à une vingtaine. LeBaron et Pinnavaia étaient les premiers chercheurs à appliquer des modifications de surface sur des silicates lamellaires. Ils ont utilisé des cations hexadecyltrimethylammonium pour assurer la compatibilité avec de la polydimethylsiloxane. Ils ont montré qu'avec seulement 5% de nanoparticules modifiées, la résistance à la traction de l'élastomère silicone a augmenté de 152 à 361 MPa (LeBaron et Pinnavaia, 2001). Il est à mentionner que lesdites chaînes peuvent être terminées par des groupes réactifs comme les groupes hydroxyles. En raison de l'encombrement causé par les tensioactifs volumineux, il a été montré que leur présence fait augmenter la distance interlamellaire et aide ainsi l'intercalation des chaînes polymériques entre les lamelles. L'étendue de cet espacement dépend de la nature des cations tensioactifs, du nombre des chaînes aliphatiques par cation, de la longueur de ces chaînes ainsi que de leur agencement dans le vide interlamellaire. La Figure 1-7 présente certaines de ses configurations. Ray a établi une liste exhaustive des cations tensioactifs les plus commercialisés avec des détails sur leurs propriétés physiques et leur structure (Ray, 2013).

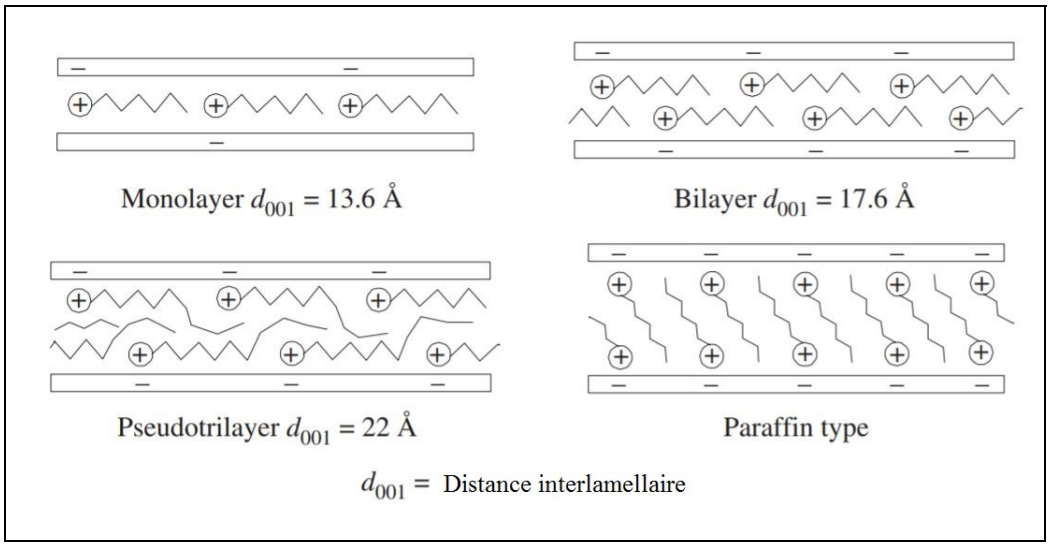

Figure 1-7. Configuration schématique des ions alkyle-ammonium dans l'espace interlamellaire de la smectite – Figure tirée de (Christidis, 2011)

1.3.2.3 Stratégies de compatibilisation nanoargile/polymère

La stratégie de fonctionnaliser les surfaces des lamelles silicates par des molécules tensioactives permet d'augmenter la distance interlamellaire et d'espacer les plaquettes d'environ un nanomètre. Cependant, l'intercalation des macromolécules de la matrice nécessite un espacement d'au moins 3 à 4 nm, dépendamment de la nature du polymère. Ainsi, d'autres techniques ont été mises au point pour augmenter davantage l'affinité chimique entre les lamelles argiles et le réseau polymérique. Il faut d'abord souligner le fait que ces techniques peuvent être une alternative à la modification organique et s'appliquent sur les nanoargiles à l'état vierge comme elles peuvent être appliquées suite à l'introduction des agents tensioactifs pour renforcer l'intercalation. Étant donné le caractère hydrophile des MMT à l'état naturel, certains chercheurs ont opté pour l'intercalation des lamelles silicates par des solvants et par des solutions à faible masse molaire avant l'introduction du polymère (Daab et al., 2018; Sirinakorn et al., 2018). Une telle substance peut être de l'eau, des alcools, des glycols, etc. En effet, l'espace interlamellaire initial du MMT est estimé à 0,96 nm. Cette distance augmente à 1,7 nm suite à l'introduction de l'éthylène glycol. L'intercalation sera facilitée pour un polymère compatible avec le solvant introduit. Srikhirin et ces coauteurs tentaient de l'intercalation de deux types de MMT par deux

polydiacétylènes. Le processus était précédé par une dilution des nanoargiles dans une solution d'éthanol aqueux. L'intercalation a été confirmée par la diffraction des rayons X et pour l'un des systèmes polydiacétylène/MMT la distance interlamellaire était de 3,68 nm (Srikhirin, Moet et Lando, 1998). Dans les travaux de Gilman, les MMT étaient prédispersées dans de l'éther couronné. Par la suite, les lamelles étaient intercalées avec réussite par du polystyrène et du nylon-6 (Gilman et al., 2001). La littérature évoque une approche d'intercalation similaire qui consiste à introduire des liquides organiques dans les MMT afin de mieux disperser des matrices polymères. Ces intercalants sont généralement solubles dans l'eau et doivent contenir, soit des groupes fonctionnels (hydroxyle, carbonyle, etc.), soit un anneau aromatique volumineux pour aider à espacer les lamelles (Fajrin et al., 2017; Gates et al., 2016). Ces entités établissent des raccords avec la lamelle silicate par liaison électrostatique à travers un cation métallique résiduel ou par chélation de ce cation (Abubakar Zauro et Vishalakshi, 2018). En visant toujours les sites à charge positive issus des substitutions isomorphes, des chercheurs ont utilisé des intercalants à caractère amphilyophile. Dans cette catégorie, les molécules les plus utilisées sont les alkyles-pyrrolidones. Dans les travaux de Beall, du n-dodecyl-pyrrolidone est dispersé avec les nanoargiles à une fraction de 2:1. Un espacement de 3,5 nm est atteint avec cette configuration. En effet, deux chaînes alkyle se réunissent sur un même cation métallique pour donner naissance à un encombrement rigide qui engendre un éloignement des lamelles silicates (Beall et Powell, 2011). Une telle configuration est représentée par la Figure 1-8.

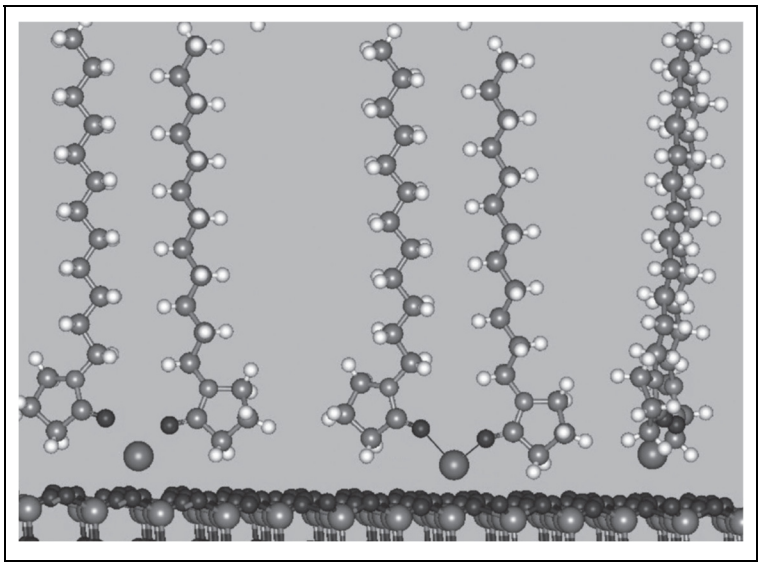

Figure 1-8. Modèle moléculaire de l'ion dipolaire dodécyl-pyrrolidone lié à du sodium – Figure tirée de (Beall et Powell, 2011)

La littérature discute également une stratégie prometteuse qui se base sur une intercalation à deux niveaux. Elle consiste à appliquer un traitement des molécules d'alkyle-ammonium sur les MMT en premier lieu, puis le faire suivre par l'introduction d'une molécule ou d'un oligomère doté d'un groupement polaire pour renforcer l'intercalation. Une application de cette méthode se manifeste dans les travaux d'Usuki et al (Kato et al., 2011). Les nanocomposites préparés sont des polyoléfines chargés par des MMT. L'intercalation du premier niveau est effectuée par des ions de chlorure d'octadécyl-ammonium. En second lieu, les lamelles silicates organiquement traitées étaient introduites par des oligomères polyoléfines greffées par de l'anhydride maléique. Les résultats ont montré une augmentation considérable de l'étendue de l'intercalation, mais aussi une forte dépendance de la présence du groupement anhydride (Kato et al., 2011). D'autres stratégies intéressantes ont été adoptées pour aboutir à des états d'intercalation élevés à savoir l'intercalation par silylation, par des composés époxy et par des anions organiques (Bee et al., 2018; Fu et al., 2016). Pour des applications qui nécessitent une forte stabilité thermique, des intercalants inorganiques sont utilisés.

1.3.3 Techniques de fabrication de nanocomposites à base de nanoparticules d'argile

La compatibilité chimique facilite l'intercalation des polymères dans les nanoargiles, mais ces traitements sont loin d'être suffisants pour atteindre un état d'exfoliation là où les lamelles silicates sont totalement dispersées dans la matrice. Le choix judicieux de la technique de mise en forme du nanocomposite joue un rôle primordial dans l'obtention d'une structure homogène et influence ainsi les propriétés du matériau résultant. Les procédés de fabrication peuvent être catégorisés en trois familles ; la polymérisation *in situ*, le mélange en solution et la mise en forme à l'état fondu (Benbayer, 2014).

1.3.3.1 Polymérisation *in situ*

La technique de polymérisation *in situ* consiste à faire gonfler les tactoïdes nanoargiles par introduction de monomères dans les galleries interlamellaires. Ensuite, le processus de polymérisation est amorcé à partir de ces monomères en partant de l'intérieur de l'espace entre les lamelles silicates et s'achève par la formation complète du polymère de la matrice. La polymérisation contribue davantage à l'écartement des lamelles sous l'effet de l'augmentation du volume occupé par les macromolécules. La polymérisation en situ est, par effet, une procédure très prometteuse pour concevoir des nanocomposites argiles dont la structure s'approche de l'état d'exfoliation. D'ailleurs, cette technique a été la première à être utilisée dans les travaux précurseurs d'Okada et son équipe à Toyota pour réussir la polymérisation du monomère ε-caprolactame dans des lamelles MMT pour produire du nanocomposite argile à base de polyamide 6 (Lennerová, Kovanda et Brožek, 2015; Okada et al., 1989). Il est recommandé de combiner cette technique avec un traitement chimique des surfaces des lamelles avec des tensioactifs qui sont compatibles avec les monomères pour faciliter leur introduction.

1.3.3.2 Mélange en solution

La technique de mélange en solution s'articule principalement sur le choix d'un solvant adéquat qui permet à la fois de gonfler les nanoparticules d'argile et de faire dissoudre le polymère de la matrice. En dispersant une faible concentration de nanoargiles dans le solvant, les faibles forces de Van der Waals cèdent les liaisons entre les lamelles silicates et donne naissance à une structure éclatée des nanoparticules. À cette dispersion s'ajoute la solution du polymère dissous dans le même solvant. Les chaînes macromoléculaires s'intercalent aisément et s'adsorbent sur les surfaces silicates délaminées. Suite à l'élimination du solvant, les lamelles tendent à se regrouper en gardant les chaînes polymères agrippées entre elles faisant apparaitre une structure intercalée (Valapa et al., 2017).

La synthèse de nanocomposites par mélange en solution est très convenable pour les polymères hydrosolubles tels que le poly(vinylpyrrolidone), le poly(alcool vinylique), le poly(oxyde d'éthylène), etc. Ces polymères sont ainsi solubles dans l'eau, un milieu dans lequel les nanoargiles sont gonflables sans même avoir recours au traitement organique par les tensioactifs. Pour d'autres systèmes polymère/MMT, plusieurs solvants peuvent être utilisés. La littérature reporte l'utilisation de ce procédé avec des solvants non aqueux pour préparer des nanocomposites basés sur une variété d'élastomères à savoir le caoutchouc naturel et naturel epoxydé, le poly(isoprène), le poly(styrène-butadiène), le poly(butadiène), le caoutchouc éthylène-propylène-diène monomère, le poly(acrylonitrile-butadiène) avec des solvants organiques comme l'acétone, le toluène et le chloroforme (Galimberti, 2011). Toutefois, la procédure requiert des volumes considérables de solvant ce qui est défavorable pour l'environnement et rend l'application assez limitée à l'échelle industrielle.

1.3.3.3 Mise en forme à l'état fondu

Pour commercialiser les nanocomposites, la fabrication des nanocomposites par mise en forme à l'état fondu est la technique la plus adéquate. Elle peut s'effectuer par les mêmes méthodes traditionnellement utilisées pour la synthèse des polymères classiques et ne requière aucun solvant. La production en continu, comme l'extrusion, revêt un engouement

particulier au niveau industriel. Ce procédé est adopté pour la préparation de la grande majorité des nanocomposites à base d'argile (Mittal, 2009).

Dans cette approche, le polymère de la matrice est porté à l'état fondu sous une température élevée. La charge en nanoargiles est ensuite mélangée avec le polymère fondu sous une contrainte de cisaillement exercée par le dispositif de mise en forme. À l'état fondu, les chaînes macromoléculaires surmontent l'état d'enchevêtrement et acquièrent plus de liberté de translation. Elles s'introduisent puis diffusent dans les galeries interlamellaires des nanoargiles. Pour les élastomères, le matériau est ramené à l'état latex pour lequel la structure devient souple. Comme avec les élastomères conventionnels, le mélange doit se préparer avant toute vulcanisation. Le processus de mise en forme est animé davantage sous l'effet des contraintes de cisaillement qui contribuent à la délamination des feuillets silicates et à forcer l'intercalation des macromolécules. Toutefois, un minimum de compatibilité chimique doit exister entre le couple polymère/nanoargile afin d'assurer un niveau élevé de structure intercalé/exfolié. Ainsi, inclure des nanoargiles fonctionnalisées est très courant avec la technique de mise en forme à l'état fondu (Beall et Powell, 2011; Cui et al., 2015).

Plusieurs études sont axées sur les nanocomposites basés sur des MMT, avec et sans modification organique, en utilisant le procédé d'intercalation à l'état fondu. Particulièrement avec les élastomères, des auteurs comme Liang et Ghari ont discuté récemment les avancées sur l'intercalation à l'état fondu du caoutchouc naturel (Ghari et Jalali-Arani, 2016; Liang et al., 2015). Pandey et Adak ont traité le même point avec le polyuréthane pour des applications sur les propriétés barrières (Adak, Joshi et Butola, 2018; Pandey et al., 2017). Un nombre important de travaux ont été fait sur la mise en œuvre de nanocomposites à base d'élastomères nitriles, les plus récentes de ces études ont traité les effets des différentes modifications chimiques ainsi que les paramètres de synthèse sur la structure du matériau résultant (Bhadran et al., 2018; Zhang et al., 2016).

Bien que la mise en forme à l'état fondu soit l'une des méthodes les plus attrayantes pour la génération commerciale de nanocomposites polymères, des limitations s'imposent. Étant

donné que la mise en forme s'effectue à haute température, ces conditions peuvent être néfastes autant pour les molécules organiques de modification des argiles que pour la matrice polymérique elle-même. Le composé peut se dégrader sous cet effet et perdre ses propriétés. En outre, et à une certaine limite de contraintes de cisaillement appliquées, les lamelles silicates peuvent se briser ce qui réduit considérablement leur facteur forme caractéristique. Ainsi, les paramètres de mise en forme doivent être judicieusement choisis afin de garder l'intégrité du nanocomposite et profiter au mieux de l'effet des nanoargiles.

Préface du chapitre 2 :

Le chapitre suivant constitue l'objet de l'article 1. L'objectif de cet article est d'évaluer l'influence des techniques de mise en forme et l'effet des paramètres de synthèse associés sur la morphologie d'un nanocomposite à base de caoutchouc nitrile chargé de nanoargiles. Sont adoptées trois des techniques les plus reconnues dans la littérature; l'extrusion, le mixage et la voie chimique. Le chapitre s'achève par examiner l'influence de ces paramètres sur les propriétés barrière du nanocomposite. Ses propriétés de résistance chimique et de transfert de masse sont corrélées à sa morphologie.

CHAPITRE 2

ARTICLE 1 : INFLUENCE OF PROCESSING PARAMETERS ON BARRIER PROPERTIES OF NITRILE RUBBER/NANOCLAY NANOCOMPOSITE MEMBRANE AGAINST ORGANIC SOLVENT

Mohamed Zemzem, Ludwig Vinches, Stéphane Hallé

Département de génie mécanique, École de Technologie Supérieure,
1100 Notre-Dame Ouest, Montréal, Québec, Canada H3C 1K3

Article publié dans :
Journal of Polymer Research, volume 26(3), février 2019
https://doi.org/10.1007/s10965-019-1725-5

2.1 Abstract

The present study focuses on the influence of layered silicate nanoparticles on barrier properties of a rubber/nanoclay nanocomposite (RCN). Most of the previous works deal with the importance of the surface chemistry of the nanoclay on the performance of the material. In this paper were rather investigated the effect of the processing conditions. Elastomer nanocomposites based on nitrile butadiene rubber and layered silicate nanoparticles were prepared using three different techniques: chemical dissolution, mixing in an internal mixer and melt-mixing with a twin-screw extruder. Chemical resistance to methanol was assessed using gravimetric method and mass transfer kinetic parameters were then deduced. Mass uptake results clearly showed that extruded RCN exhibited the highest chemical resistance. Barrier properties were subsequently correlated to the morphological structure of the rubber/nanoclay system. Small-angle X-ray diffraction patterns indicated that this improvement was due to a preferred alignment of the nanoparticle in the structure. Further, inspection revealed an anisotropic orientation profile of the nanoclay layers over the thickness of a sheet-like extruded material. In addition, a neat decrease of chemical sorption

was spotted with mixing and chemically processed RCN materials over the unfilled rubber. The state of dispersion of clay nanoparticles was also probed in these nanocomposites using X-ray diffraction. The findings suggested an intercalation during processing. Further, transmission electron microscopy observations were suggesting a bimodal state of dispersion over spotting individual nClay platelets along with the layered stacks. Improvement of mass transport kinetic parameters was recorded over increasing the shear stress as well as the residence time when RCN were prepared in the internal mixer.

Keywords: Nitrile rubber, layered silicate nanoparticles, rubber/clay nanocomposite, mass transfer kinetics, mass uptake.

2.2 Introduction

Rubber/nanoclay nanocomposite has attracted substantial attention in the past decade due to their outstanding properties even at considerably low nanoparticle proportions (Caldona et al., 2017). These materials combine the easiness of polymer processing with the strength of the nanometric platelets-like fillers. The high aspect ratio of their layers was reported, in several works, to greatly reduce fluid permeability by creating a tortuous pathway to the penetrant substance (Mittal, 2010; Sedničková et al., 2017). For an optimal performance, the ideal state would be having a complete separation of the nano-platelets leading to a maximum of active interface in the rubber/nanoclay system (Jauhari et al., 2017; Suter, Groen et Coveney, 2015). However, total delamination is technically difficult to achieve due to the non-compatibility between the rubbery matrix and the hydrophilic nature of the bare clay nanoparticles surface (Suter, Groen et Coveney, 2015). The synthesis of a successful RCN depends upon the thermodynamic interaction between the rubbery matrix and the hosted nanoparticles (Hári et al., 2017).

It has been reported that several factors affect the dispersion and the distribution of the nano-platelets in the matrix of the nanocomposite as well as their contribution to the intercalation process (Hsieh, Cheng et Wu, 2017). For instance, Fornes, Hunter and al. depicted the

significant effect of the nano-layers surface modification using alkyl ammonium cations (Fornes, Hunter et Paul, 2004a; 2004b; Fornes et al., 2002). Among others, Wang and Chen elucidated the effect of the nature and the concentration of nano-filler/matrix compatibilizers (Wang et al., 2004). From another perspective, an increasing number of studies proved that the preparation conditions could substantially influence the morphology of the nanocomposites. Specifically, mastering processing parameters might play a key role in achieving a better dispersion (Modesti et al., 2005; Puglia et al., 2016; Yang et Ozisik, 2006) and controlling nanoparticles alignment within the structure (Domenech, Peuvrel-Disdier et Vergnes, 2013; Koo et al., 2005; Treece et Oberhauser, 2007). In particular, Lertwimolnun and al. recorded the influence of the type of extruder, whether equipped with a single screw or a co- and counter-rotating twin-screws, on the morphology of layered silicate/natural rubber system (Lertwimolnun et Vergnes, 2006). Besides, the works of Varghese and al. were devoted demonstrating the effect of the processing conditions while mixing such as the mean residence time and the amount of shear stress (Varghese, Karger-Kocsis et Gatos, 2003). More specifically, Wu, You-Ping and al. as well as Kim and al. established relations between processing conditions and morphological structure of nitrile rubber based nanocomposites (Kim, Oh et Lee, 2004; Wu et al., 2003). However, the effect of these processing conditions was far from being fully explained and these parametric studies were not related to the barrier performance of the material.

In the current paper, some factors that may affect layered silicates delamination, dispersion and orientation within the rubbery matrix were treated based on morphological analyses. A correlation was then established with the chemical resistance properties of the nanocomposites.

2.3 Reagents and materials

Nitrile rubber (NBR) was chosen as the polymeric matrix for the nanocomposites under investigation. Powdered acrylonitrile-butadiene rubber (Baymod N34.52) with an Acrylonitrile content of 33.0±1.0% was kindly provided by Matexion, ON, Canada. The

rubber is characterized by a Mooney viscosity of 45±5 at 100°C and a specific gravity of 0.98.

Nanomer® I.44P, an organically modified layered silicate nanoparticle (nClay) in powder form was used as a nano-filler for the preparation of the nanocomposite. It consists on nanoclay of Na^+ type montmorillonite subjected to a surface treatment with 35-45 wt. % of dimethyl dialkyl (C14-C18) amine (Sigma-Aldrich, Canada).

Acetone for components dissolution and dispersion as well as methanol for swelling experiments were of ACS grade purity and were both supplied from Fisher scientific, Canada.

2.4 Experimental

2.4.1 Preparation techniques of rubber/clay nanocomposites

Three main techniques were adopted in order to assess processing parameters effect on barrier properties of the nitrile rubber nanocomposite.

2.4.1.1 Chemical dissolution

The preparation of the nanocomposite by the chemical method was carried out in two parts; each component was first dissolved separately in the same adequate solvent. The two resulted solutions were then mixed together.

Based on solubility parameters data from the literature, acetone was chosen to dissolve nitrile rubber (Forrest, 2001). Dissolution was carried out at room temperature and with a ratio of rubber to solvent of 2:5, weight/volume. The solution was continuously stirred for 20 hours at 700 rpm. Those stirring parameters were found to be the optimum match to achieve a total dissolution of the nitrile powder in the solvent.

On the other hand and at the same temperature conditions, 5 parts per hundred of rubber (phr) of the clay nanoparticles were dispersed in acetone at 1:30 weight/volume ratio at the same stirring speed of 700 rpm for 20 hours. Subsequently, both obtained solutions were mixed together and stirred for additional 20 hours to ensure a total mixture of the components. The stirring speed was slightly reduced to 600 rpm because of the increase in the viscosity of the system. Afterward, the mixture was cast over in a thoroughly cleaned sheet of Teflon to avoid sticking issues. The sample was then kept in ambient condition under a ventilated hood until the evaporation of most of the solvent. The resulted nanocomposite sheet was vacuum-dried in the oven for 24 hours at about 65°C to ensure a complete drive out of the residual acetone.

2.4.1.2 Extrusion

The required nanocomposites were prepared in a Haake Polylab OS – RheoDrive 4 twin screw extruder (Rheomex OS PTW16). The screws (40, length/diameter) were operating in counter rotation mode. The rotation speed was set at 100 rpm for which the maximum torque allowed by the extruder was attained. The feeding rate was set at 50 rpm to keep moderate pressure during extrusion. The temperature settings at the barrel and at the flat-die were set at 160°C. This value must not be exceeded to avoid the degradation of the material. To enhance distribution, nClay and elastomer powders were dry mixed by shaking in a sealed glass container prior to being fed into the hopper. The outgoing nanocomposites were air cooled at ambient temperature then cut into strips of about 10 cm in length.

2.4.1.3 Mixing

Nanocomposites with a mass fraction of 5% of nClay/1 (RCN/1-5%) were prepared by compounding in a Brabender mixer equipped with twin roller blades (Rheomix OS). For all samples, the components were mixed at a fixed temperature of 135°C. Bellow this temperature, the mixture was noticed to be still powdered and did not completely transform into latex form. The compounding speed was set up to 100 rpm. Higher speeds would increase the temperature of the processed material in the chamber. In order to evaluate

mixing conditions effect on the performance of the synthesized materials, nanocomposites were mixed at three different residence times going from 5 to 25 minutes; 5 min was set arbitrary as minimum time of mixing. However, nanocomposite was found to degrade at a mixing time over 30 min. In addition, processing was operated at different values of torque ranging from 25 to 155 N.m. Torque values were controlled by the material loading volume in the mixing chamber. 155 N.m. correspond to a loading of 70% of the mixing chamber which is the maximum filling allowed in the blender. Formulation of the nanocomposites mixing parameters was portrayed in Tableau 2-1.

Tableau 2-1. Formulation of the mixing parameters of the RCN/1-5% in the internal mixer

Processing method	Nanocomposite specimen	Residence time (minute)	Torque (N.m)	Loading volume (g)
Internal Mixer	01	5	25	35
	02	5	50	70
	03	5	95	140
	04	5	155	210
	05	15	155	210
	06	25	155	210

Afterward, all compounds were press-molded in the form of sheets of 125 × 125 × 2 mm at 150°C under 10 MPa pressure using a hydraulic press in accordance with D3187-06 ASTM standard. Curing time was defined by the rheological data obtained from MCR 501 Anton Paar rheometer. The compressed sheets were used in what follows for mass transfer experiments and for morphological characterization.

2.4.2 Morphological study

The galleries basal spacing (d-spacing) of the layered silicate nanoparticles, in their native form and after being incorporated in the synthesized rubber nanocomposites, was

investigated using X-ray diffraction technique. The diffractometer was equipped with a nickel-filtered CuKα radiation. Samples were tested at a generator voltage of 45 kV and a wavelength of λ=1.541 Å (XRD - Philips PANalytical X'pert PRO). Experiments were performed at room temperature. Each run was performed in step mode at a scan rate of $1°.min^{-1}$ and within the range of scattering angles (2θ) from 2.5 to 10°. The d-spacing was then calculated according to Bragg's equation given by $\lambda = 2d \cdot \sin(\theta)$ (Ren et al., 2005).

The morphological study was consolidated with transmission electron microscopy (TEM) observations. Analyses were carried out meaning an FEI Tecnai G2 F20 TEM operating at 200 kV.

The alignment of the clay nanoparticles in the elastomeric matrix was also investigated by the mean of Small-angle X-ray diffraction experiments (SAXS - Bruker Nanostar diffractometer). Measurements were conducted on a pinhole geometry camera using a 2D wire detector at 28 cm of distance between the sample and the detector. The wire detector allowed energy resolution reaching 1.54 Å.

2.4.3 Mass uptake experiment

Swelling behavior of the nanocomposite membranes was assessed gravimetrically. Vacuum dried rectangular shaped membrane samples of 60 × 10 mm were cut from the press-molded nanocomposite sheets. A sharp-edged steel die was used for the cut. Dry weights of the samples were placed in screw-tight test bottles containing about 10 mL of methanol and maintained at room temperature. At regular intervals of time, samples were removed from the solvent, gently dried with a paper towel before being weighed on an analytical balance (±0.01 mg). This experimental procedure was repeated until reaching swelling equilibrium and for which no more solvent was up-taken by further immersion. For each specimen, three replicates were performed in order to obtain statistically valid data.

The output from a mass uptake experiment was the percent weight gain (%), which is calculated as:

$$\%Mass\ uptake(t) = \left(\frac{m_t - m_0}{m_0}\right) \times 100 \quad (2.1)$$

Where m_0 is the initial weight of the sample and m_t is its weight at a given time *t*.

2.4.4 Kinetic parameters of mass transfer

In the literature, different methods were adopted to describe the transport phenomena and to estimate the ability of the material to act as an effective barrier. Most of these approaches were formulated from the Fickian model which is based on an assessment of the diffusivity of a penetrant substance in a polymer.

The concentration independent diffusion coefficient, *D* ($cm^2.s^{-1}$), provides a measure of the molecular diffusion rate within the polymer structure. Mass transport at the molecular level occurs in the direction of the penetrant concentration gradient through a membrane-like specimen of thickness h. The normalized weight gain of the penetrant solvent can be described by the following simplified equation. More details about the resolution of Fick's relation can be accessed in our previous works (Vinches et al., 2012; Zemzem, Vinches et Hallé, 2017a; 2017b).

$$\frac{m_t - m_0}{m_\infty - m_0} = \frac{4}{h}\left(\frac{Dt}{\pi}\right)^{0.5} \quad (2.2)$$

The solubility, *S*, of the studied materials is related to the chemical nature of both penetrant and polymer; it is the capacity of the polymer to uptake the solvent. The permeability coefficient, *P*, is defined as the volume of the permeant which passes through a unit area of the membrane per unit time on a normalized thickness, all within a unit pressure difference across the system.

This parameter depends on both solubility and diffusion coefficients of the process; it is therefore defined as (George et Thomas, 2001):

$$P = D \times S \tag{2.3}$$

2.5 Results and discussions

2.5.1 Morphology study and X-ray diffraction patterns

X-ray diffraction techniques had been used to elucidate the morphology of the rubbery nanocomposites. Multilayered structures had been identified due to the periodic arrangement of the nClay platelets as well as the lamellar structure of the ordered intercalate in the nanocomposites. Over intercalation, layers periodicity is preserved and interlayer spacing can be calculated. Intercalation of polymeric macromolecules between the nClay layers increases the d-spacing and causes a shift of the characteristic peaks of the XRD patterns toward smaller angles (Xi et al., 2004).

XRD patterns of two RCN membranes prepared by an extruder, internal mixer and chemical method were represented in Figure 2-1. Diffraction patterns of nClay powder and unfilled nitrile rubber were also included in the same figure for comparison purposes. A characteristic peak on the nClay curve was spotted at 2θ = 3.55°. The peak is associated to the (001) plane reflection of the silicate layer aggregates and corresponds to a basal spacing of 24.89 Å. This value was found to agree reasonably well with the specifications of the supplier (Khoeini et al., 2010). It is worth noting that a second accompanying peak could be observed at 2θ = 7.15° (12.36 Å). According to the literature, this peak was associated to the diffraction of the plan (002) which arises due to some re-aggregation of the nano-platelets (Rajasekar et al., 2009; Sinha Ray et al., 2002). It should be mentioned that NBR powder is characterized by an amorphous structure. The associated XRD pattern would show no peaks (Kader et al., 2006). Despite this morphology, press-molded specimen exhibited four well-distinguished peaks in its XRD curve. The emergence of these reflections may be due to some

rearrangement of the polymer chains and, accordingly, the onset of areas of crystallinity in the structure of the press-molded sheet.

It was observed that the first peak of each RCN was associated to the nClay dispersed in the NBR material. All three peaks were observed to be shifted toward lower angles compared to that of the nClay powder. This clearly indicated the intercalation of NBR macromolecules between the nanoparticles platelets. Peaks positions of the (001) plane scattering and the associated basal spacing for the nClay and the nanocomposites prepared by the internal mixer and by solution were presented in Tableau 2-2. The d-spacing increased with about 5.5 Å. As a side note, a small difference could be noticed in the peaks related to both described processing techniques. The difference barely reached 0.1° and it revealed that the chemical processing method slightly improved intercalation over mixing technique. For the extruded sample, the peak related to the (001) plane was located at 2.85° corresponding to a d-spacing of 31 Å. Here again, intercalation could be deduced from the growth of the interlayer spacing. However, it should be mentioned that this increase is slightly higher than that of the two other described techniques.

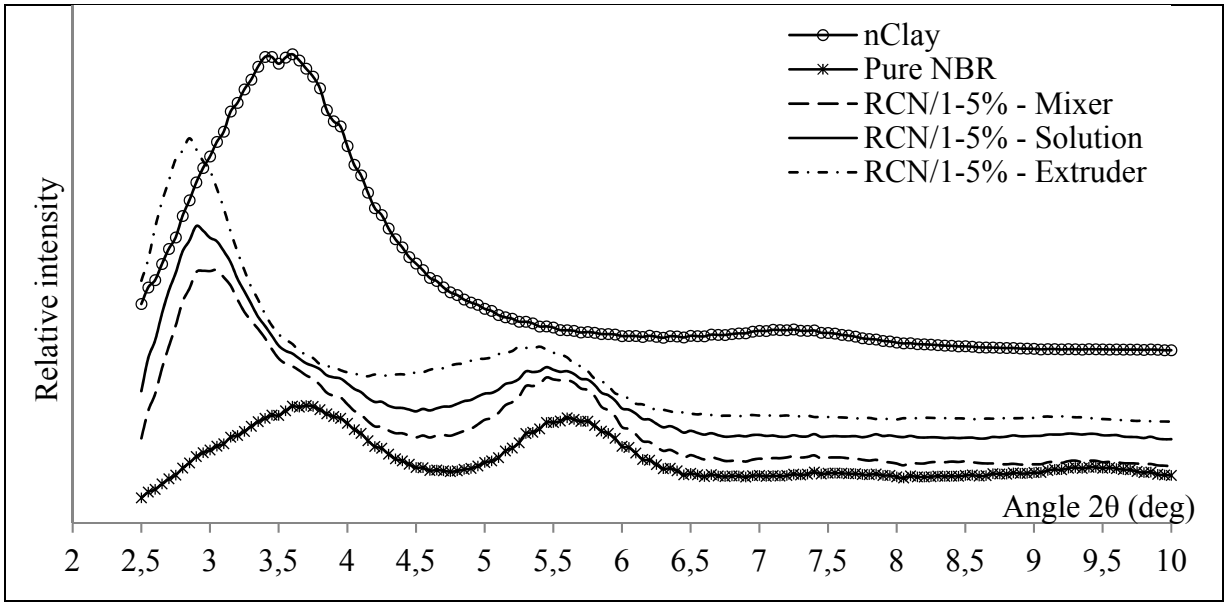

Figure 2-1. X-ray diffraction patterns of nClay in powder, pure NBR and two RCN/1-5% of nClay processed by mixer and chemical method

Tableau 2-2. Peaks positions of the (001) plane reflexions and the associated basal spacing for the nClay and the nanocomposites prepared by the extruder, by the internal mixer and by solution

	2θ (deg)	$d_{(001)}$ (Å)
nClay	3.55	24.89
RCN/1-5% Mixer	3.00	29.45
RCN/1-5% Solution	2.90	30.46
RCN/1-5% Extruder	2.85	31.00

Since the extruded sample exhibited the highest extent of intercalation according to XRD results, its morphology was analyzed through transmission electron microscope observation. Figure 2-2 presents a TEM micrograph of an extruded RCN sample. The dark lines represent the silicate layers embedded within the polymeric network appearing as a bright domain. It can be seen that the state of dispersion of the nClays within the rubbery matrix exhibits a bimodal structure. In fact, the presence of layered silicate stacks (encircled in the figure) along with few single-detached platelets (pointed with arrows) is suggesting the co-existence of both intercalation and exfoliation states.

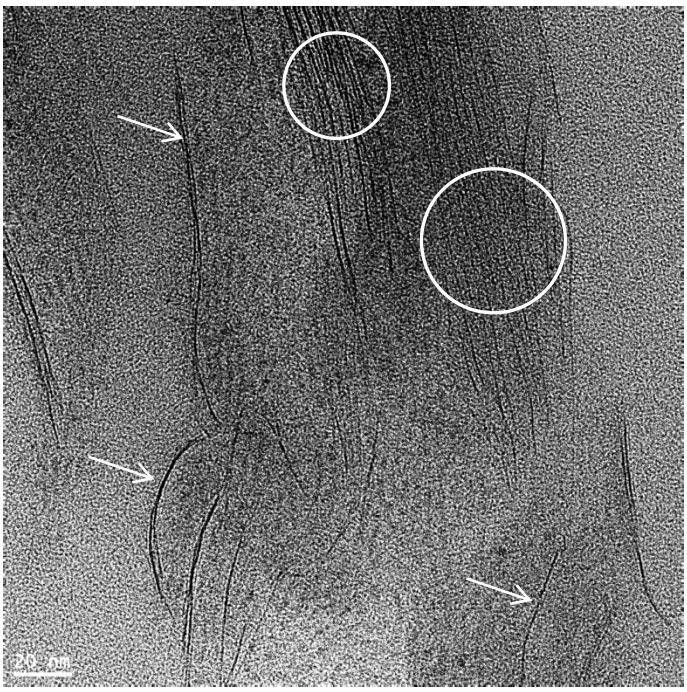

Figure 2-2. Transmission electron micrograph of layered silicates reinforced nitrile rubber processed by extrusion

Along with the intercalation and the state of dispersion, alignment and orientation of the nClay platelets play a major role in tuning barrier properties in nanocomposite systems. Clay nanoparticle sheets are three dimensional and are usually randomly oriented in the bulk of the nanocomposite matrix. With some processing techniques, shear stress could be applied during the elaboration process and, according to studies (Domenech, Peuvrel-Disdier et Vergnes, 2013; Koo et al., 2005; Treece et Oberhauser, 2007), the nano-layers could then align in a direction parallel to the membrane's surface along the flow axis. A possible orientation of the nClay layers within the nanocomposite structure was investigated using small-angle X-ray scattering technique through probing the interlayer space of the nanoclays.

SAXS patterns associated with samples from both techniques, internal mixer and extruder, were compared in Figure 2-3. The 2D scattering spectrogram of the first technique (Figure 2-3 (a)) exhibited well defined concentric circles around the primary incident beam. The delimited rings in the figure, which are formed of dark dots, correspond to the diffraction

interval of 2θ ranging from 2.4° to 3.5°. This diffraction range is characteristic of the previously described intercalated nanocomposite peaks. These blob-like nearly isotropic patterns of scattering are indicative of a roughly random orientation of the nClay platelets within the RCN structure (Wang et al., 2007).

The lamellar phase morphology for the extruded samples was shown in Figure 2-3 (b) and (c). The associated 2D patterns revealed a lack of diffracted intensity at both sides of the central spot. This anisotropic azimuthal angular dependence of the scattering intensities is a signature of a preferred orientation parallel to the planar direction (Kamal et al., 2012; Kiersnowski, Gutmann et Pigłowski, 2007). This finding is strongly dependent on the processing technique. In fact, the extruder is designed in such a way that only a close fit is maintained between the internal surface of the barrel and the external surface of the screws. As these screws rotate, the processed mixture is subjected to a high shear force and is conveyed to the end of the barrel in a spiral fashion. As a result, the compound reaches the die segment with randomly distributed and arbitrary oriented nanoclays within the elastomeric matrix. At this point, the flowing mixture passes through the screws segment at a high temperature and hits the die zone with a significant velocity. Furthermore, the narrowly converging design of the flat die inlet results in an additional shear stress applied to the bulk mass. These forces contribute to a partial alignment of the nanoclay platelets parallel to the inner surface of the die's cavity.

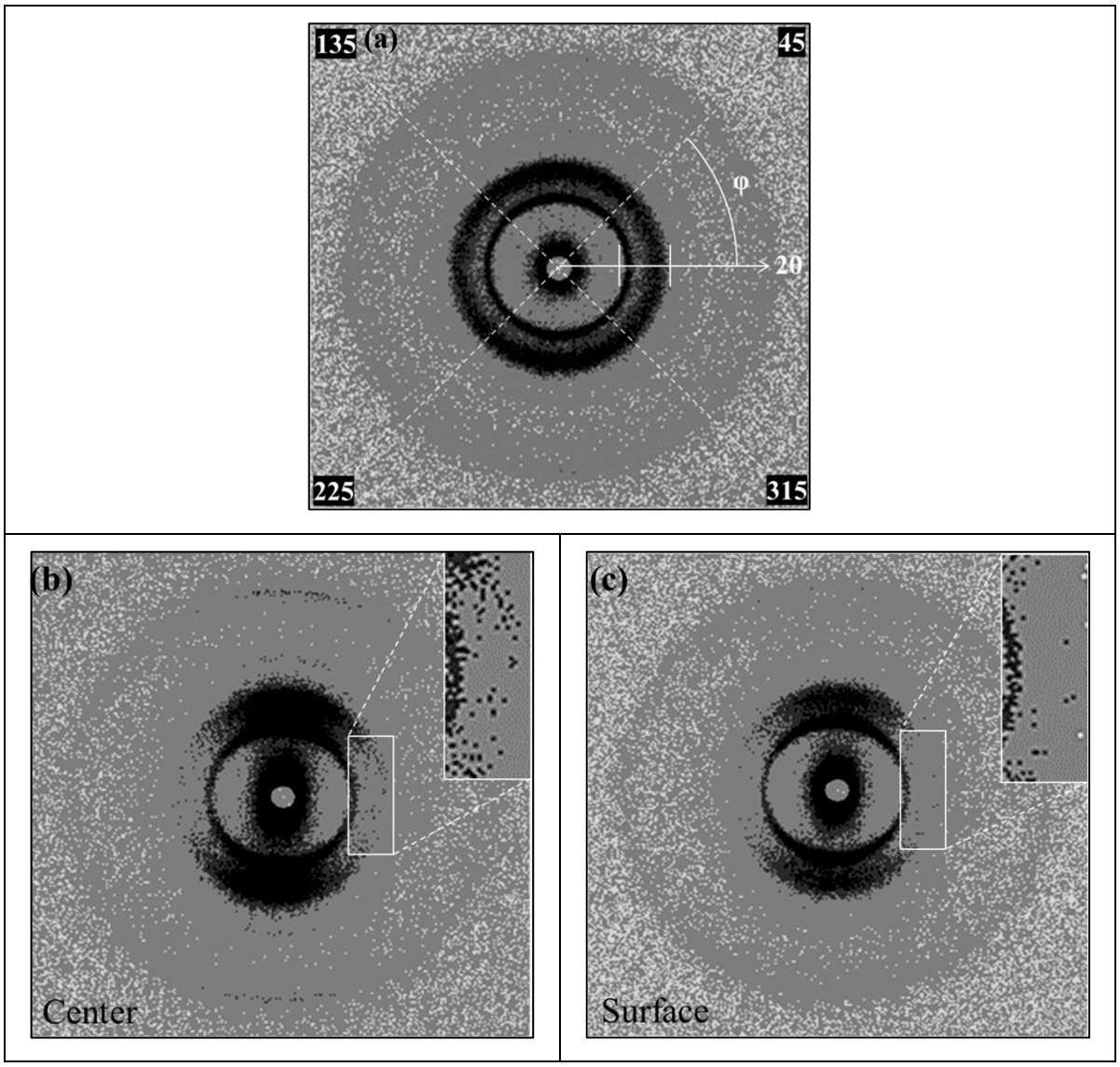

Figure 2-3. Two-dimensional SAXS Patterns (a) of a mixed RCN specimen, (b) of an extruded RCN at the center of the specimen, (c) of an extruded RCN at its surface

For further inspection, orientation profile of the nano-platelets could be anisotropic along the thickness of the extruded specimen due to the concentration of the applied shear stress at the surface of the extrudate. Were then examined the diffractions of an extruded RCN at the center (Figure 2-3 (b)) and at the surface (Figure 2-3 (c)) of the sample. By examining the described SAXS patterns (see the enlarged areas at the up-right corners of the figures), it was noticed the loss of some of the diffracted intensity at both sides of the spectrogram at the

surface of the specimen when compared to the one at the center. This orientation profile along the thickness of an extruded sample was schematically illustrated in Figure 2-4.

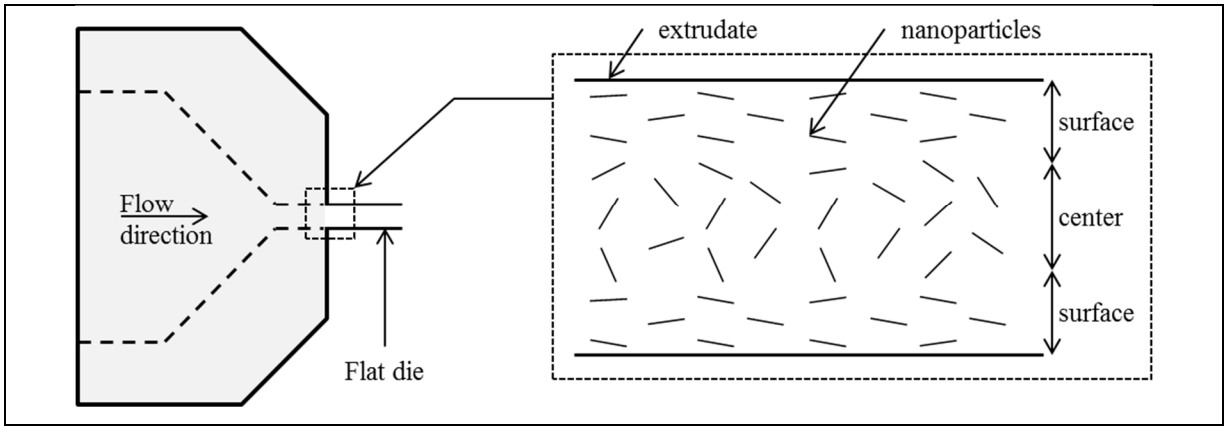

Figure 2-4. Schematic diagram of the flat die associated with the extruder and illustration of the alignment profile of the clay nanoparticles along the thickness of the extrudate

For the sake of quantitative assessment of the nClay alignment, two-dimensional SAXS diffractions were firstly plotted over the azimuthal angle (φ) as seen in Figure 2-5. The resulted intensity was then integrated over φ to determine the Bragg scattering intensity (I) as a function of the diffraction angle 2θ. As mentioned before, the study was conducted along a diffraction angle interval ranging from 2.4° to 3.5°, which matches with the main diffraction peaks of the nanoclays in the nanocomposite.

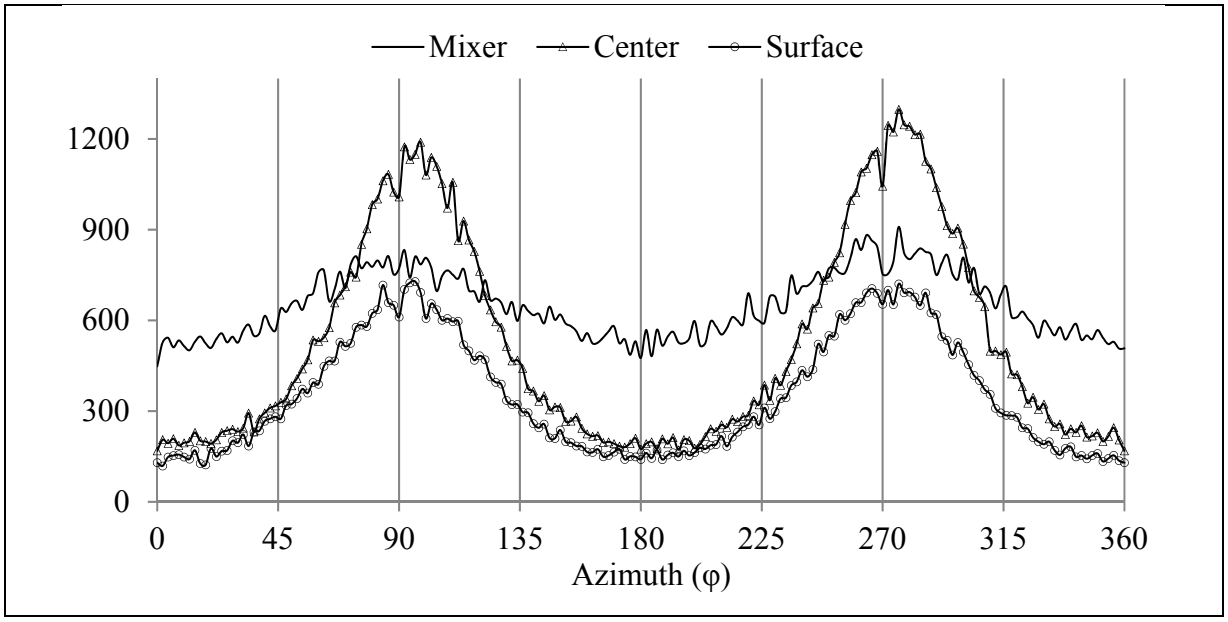

Figure 2-5. Plots of the diffraction intensities of the three 2D-SAXS patterns over the azimuthal angle

In the next step, order factors of the nanoparticles were estimated. The 2D SAXS patterns were subdivided into four equal quadrants, as pictured in Figure 2-3 (a). A particular area was then distinguished; the total integrated intensities over the φ angles from -45° (or 315°) to 45° then from 135° to 225° were denoted as the equatorial intensities zone (I_{eq}). In order to probe the alignment along the thickness of an extruded sample, the SAXS diffraction pattern of the RCN prepared in the internal mixer stood for a reference. Hence, the order factor was defined by:

$$f = (I_{eq}^{mixer} - I_{eq}^{extruder})/I_{eq}^{mixer} \quad (2.4)$$

Where I_{eq}^{mixer} and $I_{eq}^{extruder}$ correspond to the I_{eq} of a mixed and an extruded specimen, respectively. According to this relation, an isotropic diffraction has an orientation factor equal to zero. In addition, the more alignment we have in the extruded samples, the lower the intensity $I_{eq}^{extruder}$ and the closer we get this factor to unity. Based on intensity data from Figure 2-5, alignment factors of an extruded membrane at the center and at its surface are equal to 0.552 and 0.665, respectively.

Finally, and as a side note, it is worth mentioning that even at the surface of the extruded sample, nClay platelets were partially, and not totally, aligned. In fact, a specimen with perfectly aligned nanoparticles would exhibit a scattering feature with sharp diffraction spots along the direction perpendicular to the surface of the nClay layers (Schnablegger et Yashveer).

2.5.2 Sorption kinetics and mass transfer phenomena

2.5.2.1 Mass uptake in RCN/methanol systems

In order to examine the effect of nanocomposite processing technique on mass transfer of the solvent through the material, relative mass uptake data were plotted as a function of time. In Figure 2-6, percentage increases in the mass of RCN at 5% of nClay prepared by the three processing methods were plotted as a function of exposure time in methanol. Curve of mass uptake of pure NBR was also presented in the same plot to assess the nClay effect on chemical resistance. The average standard deviation of these measurements was less than 2.8%. It is worth noting that all curves exhibit similar behavior. Initially, the swelling rate starts at a high level. This is due to the large concentration gradient of the penetrant on the surface of the material at first exposure; the polymer sample was sustained to intense solvent stress. Then, the swelling rate decreases proportionally to the decreases of the concentration gradient until equilibrium for which no more solvent was absorbed over immersion. Moreover, mass uptake is similar until approximately 10 hours of immersion. However, pure NBR exhibits the highest amount of equilibrium mass per cent uptake (S) over all RCN samples. In fact, pure NBR attained saturation at (44.2 ± 2.2) % while this state markedly reduced and reached (31.6 ± 2.4) %, (29.9 ± 2.0) % and (27.1 ± 2.3) % with mixed, chemically casted and extruded samples respectively. This result clearly indicates that the presence of silicate nano-layers dispersed in the rubbery matrix reduces the chemical permeability in the sheet of the nanocomposite. In addition, a decrease of the solubility is expected in the nanocomposite due to the reduced polymer matrix volume. As a matter of fact, a dispersion of the nanoparticles decreases the rate of transport by increasing the average path length required to transport the penetrant solvent. Hence, the platelets act as

impermeable barriers to the diffusing molecules, forcing them to follow longer and more tortuous paths in order to diffuse through the nanocomposite (Bharadwaj, 2001).

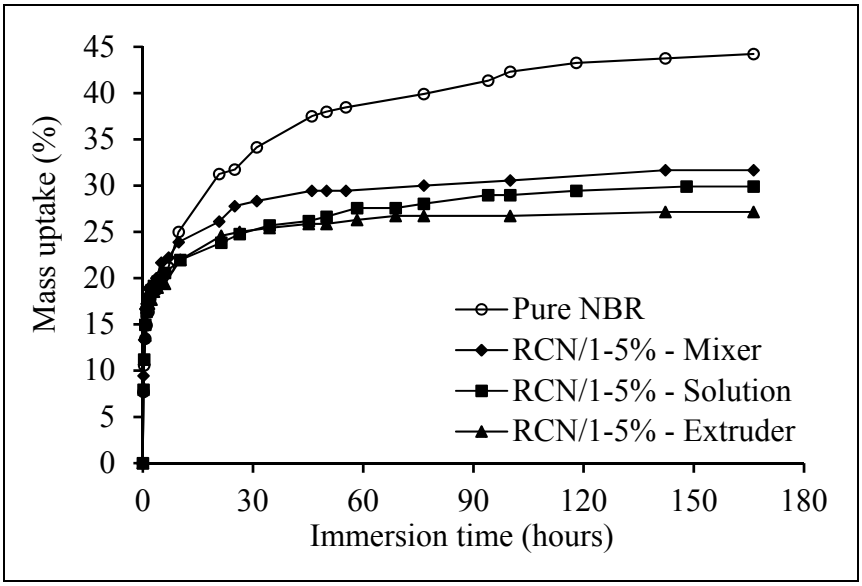

Figure 2-6. Effect of processing technique: Sorption plot of pure NBR and RCN/1-5% in methanol

It is also noteworthy that the enhancement of barrier properties of NBR nanocomposites formed by the extrusion-blending process presented in this study is more noticeable than that found in NBR nanocomposites obtained by the mixing or chemical-blending process. A point of fact is that the tortuosity is the highest when the nano-platelets are aligned perpendicular to the diffusion direction.

As analytically modeled by Nielsen (Choudalakis et Gotsis, 2009a), the nanocomposite/matrix permeability ratio expression of a non-uniform nanoparticles orientation takes the following form:

$$\frac{P_{nanocomposite}}{P_{matrix}} = \frac{1-\phi}{1+\frac{\alpha}{2}.\frac{2}{3}(\beta+\frac{1}{2})\phi} \qquad (2.5)$$

Where, ϕ is the volume fraction of the nanoparticles, α is their aspect ratio (length/width) and β is an order parameter to quantify the degree of their orientation around the diffusion direction (Choudalakis et Gotsis, 2009a):

$$\beta = (3\cos\Theta - 1)/2 \quad (2.6)$$

Where, Θ is the angle between the diffusion direction and the unit vector normal to the surface of a platelet. Obviously, the greatest reduction of the permeability is achieved when β =1 for which the nano-platelets are oriented perpendicularly to the membrane's thickness. This result is in accordance with the morphology analysis of the extruder-blended nanocomposite presented in the previous section. Therefore, the permeability is controlled by the microstructure of the nanocomposite and the behavior of the fillers within the rubbery matrix.

Within the range of experimental error, equilibrium mass percent uptake of chemical-blending specimen seems to be slightly inferior to that of the mixed one. This difference can be explained by the fact that layered silicates were somewhat more intercalated in the chemically processed nanocomposite. Indeed, at the first phase of preparation, nClay were dispersed in acetone along with NBR powder. From literature, the nano-platelets swell during prolonged exposure to acetone. This interaction creates larger galleries for polymer chains intercalation and therefore more filler/matrix contact surface which affected permeability (Pavlidou et Papaspyrides, 2008). The same conclusion could be confirmed from X-ray diffraction patterns. In fact, only a slight difference was spotted in the peaks related to both processing techniques (0.1°) at low 2θ angles.

2.5.2.2 Kinetic parameters of mass transfer

Processing parameters are related to the rate of stress applied to the synthesized compound. Variation of this constraint would affect the dispersion state of the nanoparticles in the polymeric matrix and could modify the morphology of the resulted nanocomposite (Sadhu et Bhowmick, 2004; Yang et Ozisik, 2006). In what follows, were investigated the effects of

shear stress (torque) rate and residence time in an internal mixer on RCN material filled with 5% of nClay. It is interesting to mention that although extrusion had shown better results in improving the barrier properties of the material, the mixing parameters were chosen to be examined given the importance of this technique in the field of rubber nanocomposites processing.

Figure 2-7 and Tableau 2-3 depicted the response of the kinetic parameters of mass transport *D*, *S* and *P* to the variation of the described parameters. In Figure 2-7 (a) it was noticed that the diffusion coefficient of the methanol/RCN system decreased with increasing the torque. The diminishing continues until reaching a state of equilibrium at around $(9.76 \pm 0.35) \times 10^{-9}$ $cm^2.s^{-1}$ for 95 N.m. At this rate, the maximum achievable nClay dispersion was thought to be reached and a critical morphology was established. Besides, 155 N.m matches with 210 g compound load, which fills 75% of the mixer's chamber and the maximum allowed load. As disclosed in Tableau 2-3, torque had no significant effect on equilibrium mass percent uptake and permeability coefficient varies proportionally with *D*.

Figure 2-7 (b) showed that the diffusion coefficient decreases continuously with the increasing of the residence time of mixing. *D* ranged from $(9.94 \pm 0.42) \times 10^{-9}$ to $(6.62 \pm 0.60) \times 10^{-9}$ $cm^2.s^{-1}$ in an interval of time of 20 min. The residence time limit was set at 25 min because the temperature inside the mixer was spotted to rise over time and at 30 min the nanocomposite started degradation. As reported from the literature, longer residence time at a steady level shear stress is likely to promote nano-platelets delamination and improve nanoparticle dispersion (Varghese, Karger-Kocsis et Gatos, 2003). Similarly to the torque effect, the extent at which the nClay was distributed in the polymer matrix enhanced the barrier properties of RCN material.

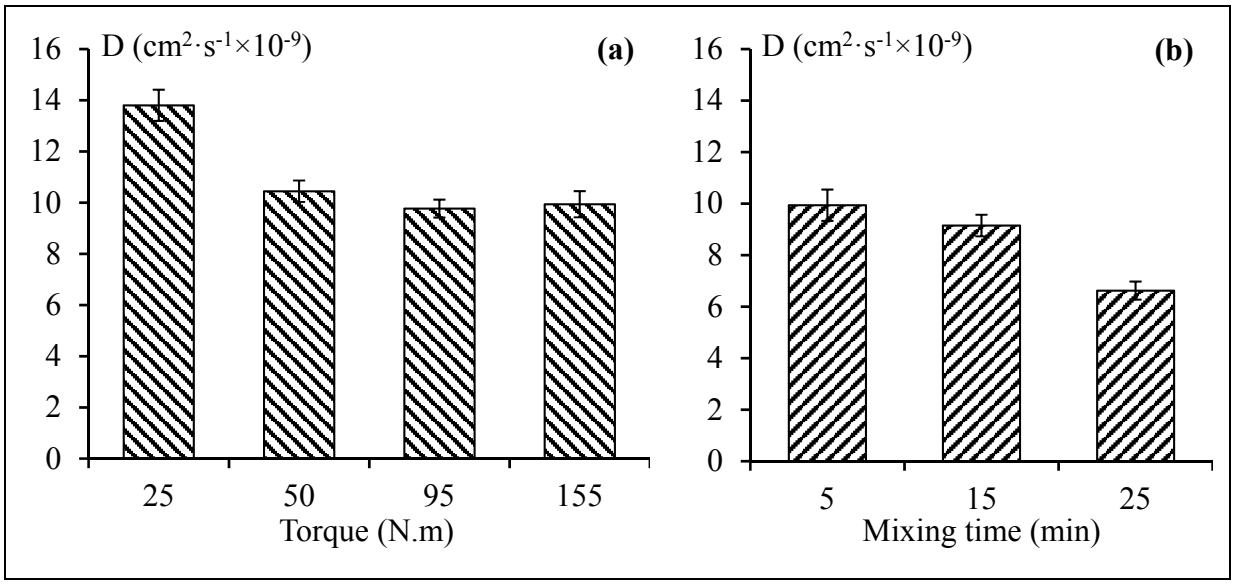

Figure 2-7. Effect of (a) torque in mixer and (b) mixing time on diffusion coefficient of methanol in RCN/1-5%

Tableau 2-3. Effect of mixing time and torque on the kinetic parameters of mass transport of methanol-RCN/1-5% system

	S (%)	P ($cm^2 \cdot s^{-1} \times 10^{-9}$)
25 N.m	29.7	410
50 N.m	30.1	315
95 N.m	31.9	312
155 N.m	29.7	295
5 min	29.7	295
15 min	31.6	289
25 min	30.9	204

2.6 Conclusions

NBR/nClay nanocomposite materials at 5% of nanoparticles were prepared using three of the most commonly used techniques for polymer compounds processing: Mixing in an internal mixer, chemical casting and extrusion with twin screw extruder. Mass uptake experiments indicate a chemical resistance improvement over the addition of the nano-fillers. More pronounced enhancement was spotted with the extruded material which was believed to be caused by nanoparticle arrangement in a preferred pattern. Nano-platelet orientation in the flow direction was then confirmed by SAXS analysis. In addition, it was observed that nClay follow an anisotropic orientation profile along the thickness of an extruder RCN. Apart from that, nanocomposites were produced at three mixing times and subjected to four different shear stresses. Kinetic parameters of the chemical transfer through the nanocomposite were demonstrated to be affected by mixing conditions. Diffusion and permeation coefficients were spotted to decrease with increasing torque and residence time. The dispersion was improved but total delamination was far from being achieved. Advanced techniques such as the addition of suitable compatibilizers would enhance exfoliation.

Préface du chapitre 3 :

L'objectif du chapitre suivant est d'optimiser la morphologie des nanocomposite NBR/nanoargile. Il fait l'objet de l'article 02. Le but consiste à appliquer des modifications chimiques sur la structure de la matrice ainsi que sur la surfaces des lamelles nanoargiles afin d'améliorer leur compatibilité. Des analyses spectroscopiques et des observations microscopiques sont combinées afin d'évaluer l'étendue de la dispersion des nanoargiles dans la structure, le niveau de leur exfolation. La diffraction aux rayons X est aussi utilisée pour examiner l'orientation des lamelles dans la membrane.

CHAPITRE 3

ARTICLE 2 : MORPHOLOGICAL INVESTIGATION OF MALEIC ANHYDRIDE-GRAFTED NITRILE RUBBER/NANOCLAY NANOCOMPOSITES

Mohamed Zemzem, Ludwig Vinches, Stéphane Hallé

Département de génie mécanique, École de Technologie Supérieure,
1100 Notre-Dame Ouest, Montréal, Québec, Canada H3C 1K3

Article soumis à :
European Polymer Journal, en date de mars 2019

3.1 Abstract

Dispersion and orientation of clay nanoparticles embedded in nitrile-based nanocomposites were examined in the current study. Nanocomposites were prepared with both chemical casting and melt compounding techniques. Three different clay nanoparticles were used in order to assess the effect of their surface treatments on the morphology of the material. Maleic anhydride was grafted on nitrile structure for the purpose of enhancing compatibility and the corresponding nanocomposites were investigated. The study started with a thermogravimetric analysis to obtain information about the degradation behavior of the received nanoparticles and their thermal stability in the nanocomposites during processing. Results showed that the organic modifier was capable of holding their integrity under processing conditions. A Fourier-transform infrared spectroscopy was then performed to validate the grafting of maleic anhydride on the rubbery structure. Associated spectra revealed that the said monomer was effectively anchored and possible location of the grafting has been also identified. The state of dispersion of the layered silicates in the matrix was discussed at different levels. First, the extent of intercalation within the nanocomposites was probed with X-ray diffraction technique. Grafting of maleic anhydride seemed to have a pronounced effect leading the structure to a near-exfoliation state. Effect of the processing

technique was barely noticeable. Second, the state of distribution of layered silicate clusters in the nanocomposite was sensed with an energy-dispersive X-ray spectrometer coupled to a scanning electron microscope. Again, maleic anhydride provided a reduction in the size of the agglomerations and enhanced the homogeneity of the system. Finally, the intercalation and delamination of the layered silicates over grafting were validated by transmission electron microscopy. Inter-lamellar spacing was found to perfectly correlate with X-ray data. After grafting, several dispersions of separated monolayers have been witnessed. On the other hand, the alignment of the clay nanoparticles was examined by small angle X-ray scattering. A 3D-orientation approach was built based on the scattering stereographs. Orientation was found to be at its best with nanocomposites processed with melt compounding and subjected to fast cooling.

Keywords: Nitrile rubber; layered silicate nanoparticles; maleic anhydride; rubber/clay nanocomposite; exfoliation and orientation.

3.2 Introduction

Polymer/nano-fillers nanocomposites have drawn considerable attention for both industrial and scientific applications due to their unique capabilities to exhibit enhanced characteristics and value-added qualities over the unfilled virgin polymers (Kotal et Bhowmick, 2015; Ray et Okamoto, 2003). Their synergistic properties were of concern to substantial material characteristics such as enhancing barrier properties (Tan et Thomas, 2016), increasing mechanical moduli (Azeez et al., 2013) and improving flame retardancy (Morgan, 2006). Out of all the tested nano-fillers for their reinforcing ability, clay nanoparticles have gained momentum due to their availability, low cost, intrinsic anisotropy and the impressive capability to tune polymer properties at considerably low loading concentrations. Nano-clays (nClays) belong to the class of the layered mineral materials and were termed as stacks of silicate sheets (nano-platelets) of around 1 nm thick and up to several microns of lateral dimension. The piling of nano-platelets were held together by Van Der Waals forces caused

by the negative surface charges, leading to the appearing of interlayer gaps (galleries) of about 1 nm (Ray, 2013).

Up to nowadays, chemical casting and melt compounding are considered among the most efficient techniques to process nanocomposites (Thomas et Stephen, 2010; Wang et al., 2000). However, physically mixing a polymer with layered silicates nanoparticles may not lead systematically to a nanocomposite. The presence of nClays as agglomerated tactoids form or clusters of layers within the matrix would provide poor reinforcing ability making it comparable to the conventional microcomposites. The key factor to achieve a successful nanocomposite is to obtain homogeneous dispersion and good distribution of separated individual layers in the polymeric matrix. Given their high aspect ratio, monolayers could provide a large active surface area even at low amounts of loading. It was found, however, that reaching a complete separation of the nano-platelets is a quite challenging task because of the interlayer ionic bonds. Moreover, the difference in polarity in the nClays/polymer system implies weak interfacial interaction rendering complete dispersion more difficult (Vaia et al., 1996).

In order to enhance the affinity between the nanoclays and the polymeric matrix, naturally hydrophilic silicate surface could be converted to organophilic by implementing organic cations on the surface of the layers (Kim, Oh et Lee, 2004). Adding reactive functional groups to the organic modifier was found in many works to further enhance the compatibility in the nanocomposite system (Kim et White, 2005). It was seen in some studies that chemical modification by including functional moieties could be applied from the polymeric side, either. Polar molecules, such as maleic anhydride, grafted onto the polymeric backbone were found to lower the interfacial energy and improve the wetting properties of the system (Hasegawa et al., 1998; Hasegawa et Usuki, 2004). Chemical affinity causes the infiltration of polymeric macromolecules into the nClays host galleries leading to an increase in the interlayer spacing. On this basis and depending on the strength of interfacial interactions, intercalated nanoclays could be obtained. Appropriate processing parameters along with a proper chemical tailoring could lead the nanocomposite to a high level of dispersion and a

state of near exfoliation (Lertwimolnun et Vergnes, 2005). Further, some authors highlighted a particularly attractive design involving the preferred alignment of the layered silicates in the material. Nano-platelets orientation was found to provide rigidity, stiffness, and bi-dimensional stability to the polymer (Kim et al., 2001). The orientation factor cannot be discussed without referring to its tremendous effect reported on barrier properties (Osman, Mittal et Lusti, 2004).

For what was introduced, a great interest was allocated to nanocomposites based on thermoplastic polymers. Morphological studies, as well as investigation of their industrial properties, have been examined thoroughly. However, except for some studies that have been conducted in the field of rubber/nanoclay systems (Hwang, Wei et Wu, 2004; Sadhu et Bhowmick, 2004), few attempts have been undertaken to understand the morphology of elastomeric nanocomposites. Until date, little has been said about the dispersion on nClays in rubbery matrices. In addition, the existing papers this topic suggested that exhaustive work is needed to provide a good understanding of the elastomeric nanocomposites structure.

The present article was meant to establish a state of understanding about the dispersion and the alignment of layered silicate within their associated nanocomposites. The effect of organic modification of the nanoparticles and the maleic anhydride grafting of the rubber were depicted through cross-checking of various characterization techniques.

3.3 Reagents and materials

Acrylonitrile-butadiene rubber (NBR) was selected as an elastomeric matrix for the investigated nanocomposite materials in this study. Powdered NBR containing 34% acrylonitrile under the trade name of Baymod N34.52 was kindly provided by Matexion, ON, Canada. The nitrile was denoted by a Mooney viscosity of 45±5 at 100°C and a specific gravity of 0.98. Acetone for samples dissolution in chemical casting procedure was of ACS grade and was purchased from Fisher Scientific. Maleic anhydride (MA) and benzoyl

peroxide (BPO) were both acquired from Aldrich Chemical. BPO, with purity level over 98%, was used as an initiator for the grafting of MA onto the nitrile rubber.

Three commercial grades of clay nanoparticles were chosen for this study and were purchased from Sigma-Aldrich. The nClays were labeled nClay/0 for the unmodified nanoparticles. nClay/1 and nClay/2 referred to two different chemical modifications applied to the surface of the nano-platelets. nClay/0 is a natural inorganic sodium montmorillonite (Na^+MMT) with a chemical formula $(Na, Ca)_{0.33}(Al, Mg)_2(Si_4O_{10})(OH)_2.nH_2O$. nClay/1 is montmorillonite clay chemically modified with about 35 to 45 wt% dimethyl dialkyl (C14-C18) amine. nClay/2 is also a natural montmorillonite modified with 30 wt% methyl hydroxyethyl tallow (T) ammonium. The tallow structure is ~65% C18, ~30% C16, and ~5% C14. The organoclays were investigated to assess the effects of surface modification structures on the dispersion of the nClay platelets in the elastomeric matrix. Figure 3-1 showed the chemical structures of the amine surfactants that were exchanged for the sodium ion of native montmorillonite clay and used to form the organoclays nClay/1 and nClay/2.

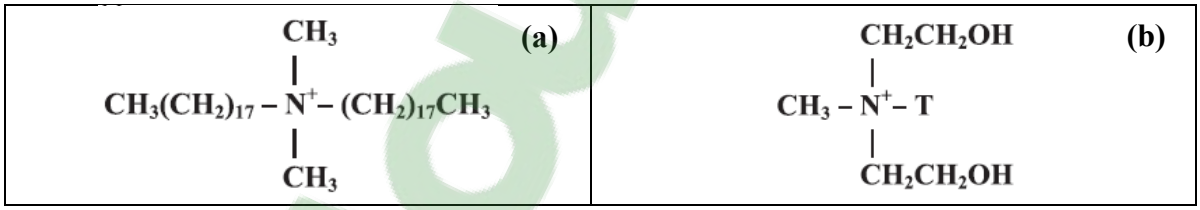

Figure 3-1. Molecular structure and nomenclature of the alkyl ammoniums used to form the organically modify sodium montmorillonite (a) nClay/1 and (b) nClay/2

3.4 Experimental

3.4.1 Nanocomposites preparation

Nanocomposites based on nitrile rubber and containing the three described clay nanoparticles were prepared. The concentration of the filler was held constant at 5% for all the samples. Different processing techniques were adopted in order to obtain an optimal configuration of

the nClays dispersion. It is worth noting that prior to every preparation; all powders were oven-dried at 65 °C for 24 h.

3.4.1.1 Solution mixing

Rubber/clay nanocomposites were synthesized by a solution-intercalation casting method. NBR powder was dissolved in acetone at 60°C. The ratio of the rubber to solvent was 2:5, weight/volume. The solution was continuously stirred at 700 rpm for 20 hours until the complete dissolution in the solvent. On the other hand, 5 parts per hundred of rubber of the nClay powder was added under constant stirring and dispersed in acetone at 1:30 weight/volume ratio and in the same stirring and temperature conditions for 20 hours. Prior to rubber/nanoparticles solutions mixing, the nClay solution was ultra-sonicated using a UIP1000hd ultra-sonic processor (Hielscher ultrasound tech) for 30 minutes at 60°C. Ultra-sonication frequency was set at 20 kHz to ensure better delamination of the nClay platelets and a standard 0.5 in diameter flat horn tip was used. Subsequently, both solutions were mixed together and stirred with a high shear hydrodynamic dispersion process for an additional 30 min at 6000 rpm. The resultant solution was then cast over in a thoroughly cleaned sheet of Teflon to avoid sticking issues. The sample was kept in ambient condition under a ventilated hood until the evaporation of most of the solvent. The obtained film was then vacuum-dried in the oven for 24h at 60-70°C for a complete drive out of residual acetone.

3.4.1.2 Melt processing

In order to guarantee a better distribution, the prescribed amounts of nClays were premixed by shaking with the rubber in a sealed glass container. Melt processing is then conducted in two steps. The powdered compound was melt-mixed in a Brabender mixer equipped with twin roller blades (Rheomix OS). For all samples, mixing was conducted at 135°C for a residence time of 5 min. Compounding speed was set at 100 rpm. The resulting mixture has been retrieved from the mixing chamber, cooled at room temperature then pelletized in a grinder for the next processing step. The obtained pellets were extruded using a Haake

Polylab OS – RheoDrive 4 co-rotating twin screw extruder (Rheomex OS PTW16). The rotation speed was set at 100 rpm. The barrel and the flat-die temperature profile ranged from 150° to 160°C.

3.4.1.3 Preparation of maleated nanocomposites

The preparation of maleated nanocomposite rubber was carried out in two stages; grafted nitrile rubber was firstly prepared by grafting NBR with maleic anhydride in the presence of benzoyl peroxide in a Brabender mixer. 1 part per hundred rubber (phr) was pre-mixed with nitrile powder for 5 min at 80°C and 100 rpm. 2 phr of MA was then added for an additional 5 min under the same mixing conditions. The resulting mixture was then extruded in accordance with the procedure described in the previous section.

The nomenclature adopted to label the nanocomposites under study was as follows. Each nanocomposite was appointed as RCN/xy-5% where x stood for the nature of the nClay (0, 1 and 2 for nClay/0, nClay/1 and nClay/2 respectively) and y referred to the processing technique (1 for solution casting and 2 for melt processing). The same terminology was used for the maleated sample with an extra g letter referring for grafting (RCNg/xy-5%). One of the prepared nanocomposites was quenched with liquid nitrogen right after extrusion. For the quenched sample, a letter q was used (RCNq/xy-5%).

Afterward, all compounds were press-molded in the form of sheets of 125 × 125 × 2 mm at 150°C under 10 MPa pressure using the hydraulic press in accordance with D3187-06 ASTM standard (*Standard Test Methods for Rubber-Evaluation of NBR (Acrylonitrile-Butadiene Rubber) - D3187-06*, 2016). Curing time was defined by the rheological data obtained from MCR 501 Anton Paar rheometer. The compressed sheets were used in what follows for morphological characterization. More details about processing parameters can be consulted in our previous works (Zemzem, Vinches et Hallé, 2019a).

3.4.2 Nanocomposites structural characterization methods

3.4.2.1 Thermal behavior analysis

The thermal degradation characteristics of the three studied clay nanoparticles and their corresponding nanocomposites were conducted using a Pyris Diamond thermogravimetric analyzer. A ceramic pan containing about 10 mg of the investigated material was used. The weight loss of the samples against temperature was measured at a heating rate of 20°C per minute. The experiment started with an isothermal plateau at 50°C for 3 min then heating was ranged from 50 to 700°C.

3.4.2.2 Fourier transform IR spectroscopy analysis

The infrared (IR) spectra were recorded on a Perkin-Elmer FTIR-ATR Spectrometer from 4000 to 400 cm^{-1} with an averaging of 5 scans and at a resolution of 1 cm^{-1}. For the analysis of the as-received powdered clay nanoparticles, 100 to 200 mg samples were disc-shaped using a hand-held press for 5 seconds at room temperature. On the other side, grafted and non-grafted nanocomposite samples were processed in a 1 mm thick film by hot pressing.

3.4.2.3 X-ray diffraction experiments

The morphology properties of the nanoparticles, as well as the synthesized rubber nanocomposites, were investigated at room temperature by an X-ray diffractometer (XRD - Philips PANalytical X'pert PRO). The layered silicate galleries basal spacing (d-spacing) was monitored using a nickel-filtered CuKα radiation at a generator voltage of 45 kV and a wavelength of λ=1.541 Å. The diffraction curves were obtained within the range of scattering angles (2θ) of 2.5-10° and at a scan rate of 1°.min^{-1}. The d-spacing was calculated according to Bragg's equation.

3.4.2.4 Scanning electron microscopy and energy dispersive X-ray spectroscopy studies

Agglomerations and clusters of clay nanoparticles could be fairly detectable with ultra-high resolution scanning electron microscopy (UHR-SEM). Observations were conducted using a Hitachi SU-8230 SEM using an accelerating voltage of 5 kV. Cross-sections of 1 mm-thick nanocomposites films were observed. Samples were microtomed by a Leica (RM2235) cryo-microtome at -100°C using a tungsten knife then coated with 2 nm-thick platinum layer.

Given the capability of the electron microscope to detect nanoclay clusters down to a few tens of nanometers, energy dispersive X-ray (EDX) module coupled to the UHR-SEM was adopted to detect characteristic chemical elements of the nanoclays. Therefore, EDX technique was employed to establish a statistical study about the look of the cluster's size distribution as a function of the nanocomposite composition as well as the nClays nature. Measurements were acquired in bi-dimensional mapping mode at a count rate of 100 kcps and for a scan time of 120 seconds. Size distribution assessment was based on meaning data collected from five different spots for each specimen. The analysis was made at a working distance of around 15 mm and with a magnification of 5K for each one of the spots. The count of the agglomerations and the evaluation of their area for size distribution calculations were established in post-treatment using ImageJ software.

3.4.2.5 Transmission electron microscopy observations

Further inspection of the state of dispersion of the nClays platelets in the elastomeric matrix comes from transmission electron microscopy analysis. Observations were carried out meaning an FEI Tecnai G2 F20 TEM equipped with a Gatan Ultrascan 4000 4k × 4k CCD Camera System Model 895 EDAX Octane T Ultra W /Apollo XLT2 SDD and TEAM EDS Analysis System operating at 200 kV. Samples as thin as 50-100 nm were cut from the cross-section of nanocomposite films at –120°C using a Leica Microsystems UC7/FC7 cryo-ultramicrotome equipped with a diamond knife. Fractured sections were transferred from the knife edge onto coated 200-mesh copper grids.

3.4.2.6 Small angle X-ray scattering measurements

In order to investigate nClay orientation in the nanocomposite material, Small angle X-ray diffraction experiments (SAXS) were conducted. A Bruker Nanostar diffractometer was adopted with a pinhole geometry camera using a 2D wire detector at 28 cm of distance between the sample and the detector. Further, a representation of the 3D orientation of the nClays platelets was constructed based on 2D SAXS patterns token from the three Cartesian directions of a 1 mm cubic sample with respect to the incident X-ray beam.

3.5 Results and discussions

3.5.1 Thermogravimetric analysis of the thermal stability

The dispersion characteristics of clay nanoparticles in the elastomeric matrix depend critically on the interfacial interaction between the filler and the host polymeric chains (Galimberti, 2011; Thomas et Stephen, 2010). For modified nClays, termed organoclays, these interactions are established through organic alkyl ammonium surfactants. On the other hand, the melt processing of elastomeric nanocomposites involves using relatively high temperatures. Since the long-chain aliphatic hydrocarbon-based cations used for organoclays surface treatment are known for their poor thermal stability (Cui et al., 2008), investigating the thermal degradation of the fillers, as well as their associated nanocomposites, is of concern. In fact, thermal degradation of the organic surfactants potentially affects the fillers/matrix interfacial bonding and thus the state of exfoliation of the nano-platelets. In addition, the decomposed residues resulting from the thermal degradation could possibly engage non-desired side reactions influencing the physical properties of the nanocomposites (Shah et Paul, 2006; Xie et al., 2001; Zanetti, Bracco et Costa, 2004). Thermogravimetric analyses were conducted to throw some light on the thermal stability of the nClays within the polymeric matrix after being subjected to melt processing conditions.

Degradation experiments were firstly applied to the three investigated powdered nClays as received from the supplier. Figure 3-2 showed, for the untreated and the two modified clay

nanoparticles, curves of weight loss over temperature (TG) at a steady heating rate as well as their associated differential curves (DTG).

Starting with nClay/0, degradation behavior over heating could be divided into two separated parts. Those parts were well defined by a peak in the 100-250°C interval and another one at around 500-700°C interval in the DTG curve. It is worth to note that sodium montmorillonites are hydrophilic minerals and usually contain considerable amounts of water trapped inside their silicate galleries. Water molecules adsorption in the inter-lamellar space is mainly driven by the hydration mechanism of the exchangeable cations (Na^+) located on the inner surfaces of the nClay layers. Small and very mobile water molecules are positioned around the alkali metal ion forming a spherical shell in which H_2O/Na^+ ratio is between 3 and 4 (Hensen et Smit, 2002). Smaller amounts are attracted to the inter-lamellar voids through the establishment of hydrogen bonds between the water hydrogen atoms and the oxygen atoms located on the external tetrahedral sheets of the montmorillonite layers (Hatch et al., 2012; Hensen et Smit, 2002). When subjected to increasing temperatures, the interlayer water was gradually abstracted from the nClays galleries until reaching around 250°C as portrayed in Figure 3-2. Indeed, it was shown with X-ray that interlayer spacing decreased by about 5-6 Å when reaching this level of temperature (Xie et al., 2001). The second peak located at the range of 500-700°C was most likely caused by the elimination of the structural water (Cervantes-Uc et al., 2007; Ray, 2013; Xie et al., 2001). In fact, considering the crystalline structure of a given montmorillonite layers, four hydroxyl groups per unit cell are covalently bonded to the edges of the octahedral and the tetrahedral ions. The signal appearing in the [500, 700°C] interval is attributed to the dehydration of the structural OH groups (Cervantes-Uc et al., 2007).

Regarding organoclays nClay/1 and nClay/2, a small signal could be detected around 100°C suggesting the disappearance of the free water located in the external surfaces lamellar structures and between the tactoids voids (Cervantes-Uc et al., 2007; Xie et al., 2001). The weakness of the signal was interpreted by the absence of interlayer water in the organically modified clay nanoparticles. As previously described for untreated nClay, peaks appearing in

the temperatures ranging from 500 to 700°C for both organoclays were most likely caused by the dehydration reactions of the structural hydroxyl groups (Cervantes-Uc et al., 2007; Ray, 2013). More importantly, the most noticeable difference in the thermal behavior between the organoclays and the untreated montmorillonite was recorded between 200 and 500°C. Strong derivative weight loss peaks appearing in this range were typically caused by the thermal decomposition reactions of the alkyl ammonium salts used for the organic treatment. It is suggested that the decomposition of the organic constituents incepts at around 200°C starting with the smaller molecules (Pramoda et al., 2003; Saad, Elhamid et Elmenyawy, 2011). As expected, the resulting spectrum for nClay/2 sample differs notoriously from the one obtained for nClay/1 organoclay due to the presence of these OH groups. It is worth noting that the observed difference in the intensity of the peaks in the DTG curves was relative to the increase of the surfactant concentration in the nanoparticle (35–45 wt% for nClay/1 versus 20-30 wt% for nClay/2) (Osman et al., 2016). Further analysis of the organic surfactants degradation could be established through analysis of Gram–Schmidt plots which provide structural information about evolved gaseous decomposition products using TGA coupled with Fourier transform infrared spectrometer.

The main reason for investigating the organic surfactant degradation is that it has some drawbacks of the thermal stability of the overall nanocomposite. First of all, decomposition of the organic treatment during melt processing can result in a de-intercalation of the polymeric chains from the nClays galleries. In addition, residues from the surfactant decomposition, positioned within the galleries, may provoke an early ignition process in the nanocomposite and cause a premature degradation of the system (Ray, 2013; Zanetti, Bracco et Costa, 2004).

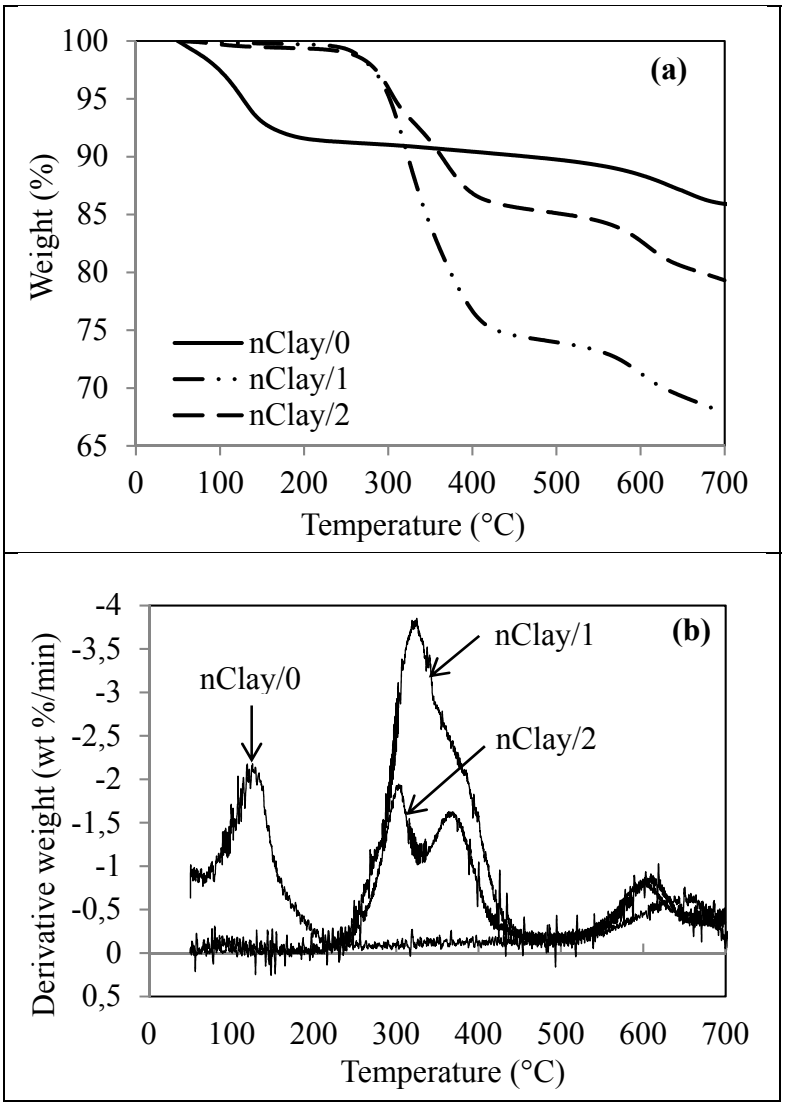

Figure 3-2. Thermal degradation of nClay/0, nClay/1 and nClay2 represented by (a) weight loss of material as a function of the temperature plots and (b) the corresponding derivative curves

Figure 3-3 (a) shows the percentage of weight loss curves obtained at a heating rate of 20°C per min for pure NBR as well as the corresponding nanocomposites RCN/0, RCN/1 and RCN/2. The initial degradation temperature (T_i), corresponding to 95% of weight loss, of the RCN/1 occurred at a lower temperature (386°C) as compared to the pure NBR (400°C). This could probably due to the degradation of the organic surfactant. The dimethyl dialkyl (C14–C18) amine may play a major catalyst role that can be responsible for the acceleration of the

degradation process (Leszczyńska et al., 2007; Osman et al., 2016; Wilson et al., 2012). The same but less pronounced effect was spotted with RCN/0 and the T_i was reported at 393°C. Surprisingly, RCN/2 kept the same T_i as for the pure NBR although it contains organically modified clay nanoparticles.

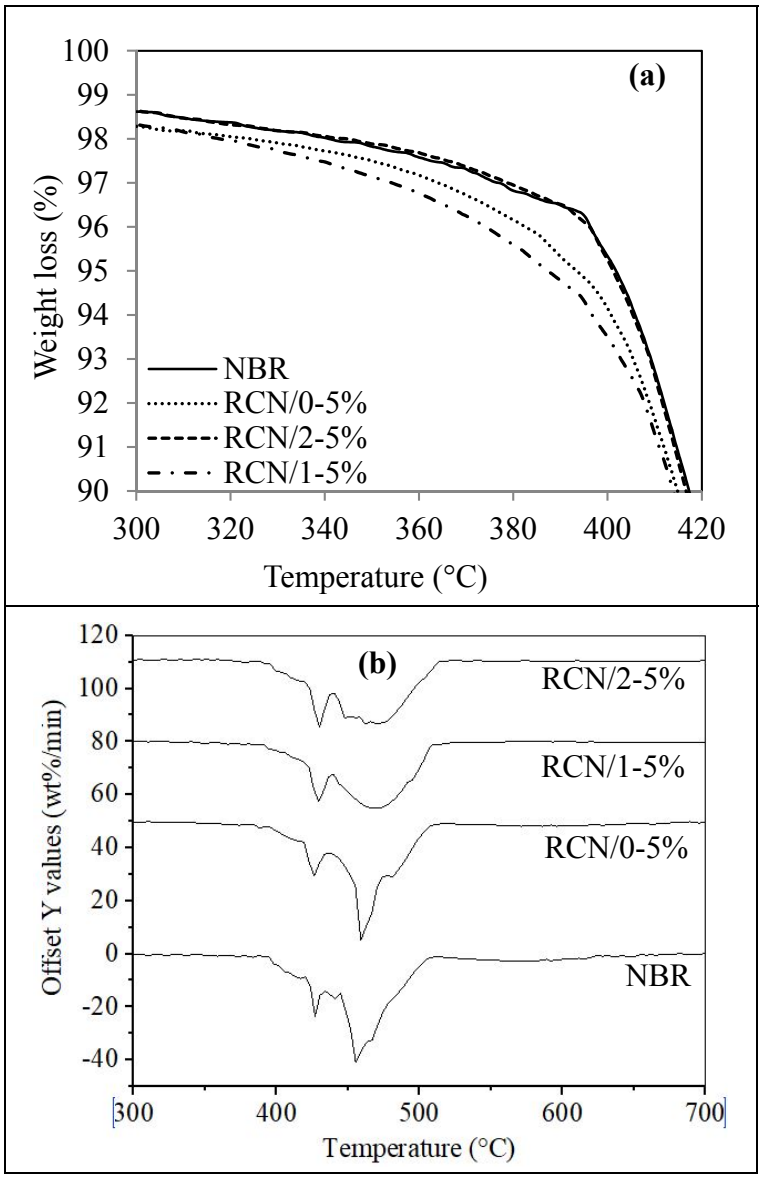

Figure 3-3. (a) TGA thermograms of pure NBR and NBR nanocomposites filled with 5% of nClay/0, nClay/1 and nClay/2 and (b) their associated DTG curves

This result highlights a remarkable effect of the chemical nature of the organic compound present in the clay on the thermal stability of the nanocomposite. In fact, the literature mentioned a “labyrinth” effect that limits oxygen diffusion in the polymer from the outside and restrains gases from evolving in the matrix with extending the initial time of degradation (Singala, Mungray et Mungray, 2012).

Regarding derivative data in Figure 3-3 (b), the DTG curves illustrate that the pyrolysis of NBR takes place in two steps; the curve exhibits a shoulder at around 430°C followed by a principal peak at about 470°C. The three associated nanocomposites exhibited similar profiles. It is interesting to mention though that the peak rate of degradation of both organoclays nanocomposites decreased by about 20 wt%/min compared to the pure rubber. Therefore, it could be said that the nClay imparts a temperature barrier due to its unique layered structure.

3.5.2 MA grafting assessment with FTIR

Co-polymerization by chemical modification of existing polymers is considered as one of the most efficient and inexpensive routes to design new functional materials endowed with improved performances. Notably, the modification can be achieved by free-radical grafting reactive monomers onto a given polymer backbone (Al-Malaika, 2012). Maleic anhydride was chosen as a grafted monomer for its high double reactivity. From one side, the unsaturated double carbon bond serves as a free radical reactive site for the grafting process. From the other side and after grafting, MA possesses a functional succinic anhydride group that is likely to react with the chemical compounds of the nClays surfaces and enhances the delamination of the platelets (Trivedi, 2013). To make possible the free radical grafting during melt processing, benzoyl peroxide was used as an initiator. BPO is typified by its reactive phenyl and benzoyloxyl radicals that have an outstanding ability to abstract the hydrogen atom with respect to the C−H bond of the concerned polymer backbone and ensure the grafting of the MA monomer (Pulat et Babayiğit, 2001).

Chemical anchoring of the reactive monomer on the NBR backbone can be examined by identifying the grafting sites using FT infrared spectroscopy (Sclavons et al., 1996; Sclavons et al., 2000). In the beginning, absorptions made by the major bonds in the MA structure were depicted. Figure 3-4 showed the FTIR spectrum of row maleic anhydride. The plot exhibited well-defined peaks at 1856 cm^{-1} and 1780 cm^{-1}. Those signals were assigned to the asymmetric and symmetric stretching of carbonyl (C=O) groups located at the cyclic anhydride, respectively (Sclavons et al., 2005). Asymmetric and symmetric ring stretching of the groups (=C−O−C=), unique to the cyclic ethers, were also clearly spotted at 1242 cm^{-1} and 1051 cm^{-1}, respectively. From the opposite side of the monomeric structure, a relatively broad peak, noticed at around 698 cm^{-1}, was identified as the stretching of the olefinic bond (C=C) (Nakason, Kaesaman et Supasanthitikul, 2004).

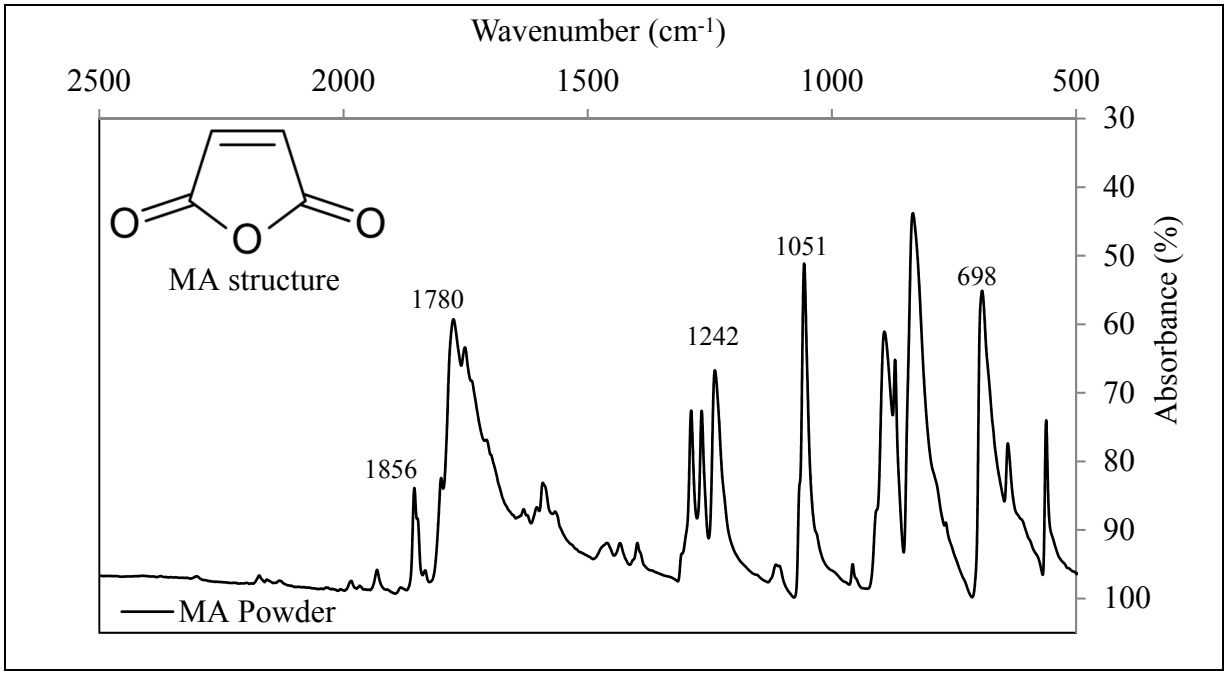

Figure 3-4. FTIR spectrum of maleic anhydride

In order to properly investigate Ma-grafting on the NBR structure, it is mandatory to figure out the mechanism of grafting and understand the transformations that the MA monomer undergoes after the process. It was reported in the literature that the grafting of maleic

anhydride may either occur on the polyacrylonitrile or the poly-butadiene segments of a given rubber containing these elements (Rao, Rao et Sreenivasulu, 1999).

Figure 3-5 represents plots of IR spectrum of the rubber/clay nanocomposite grafted with MA compared to the spectrum of the Pure NBR.

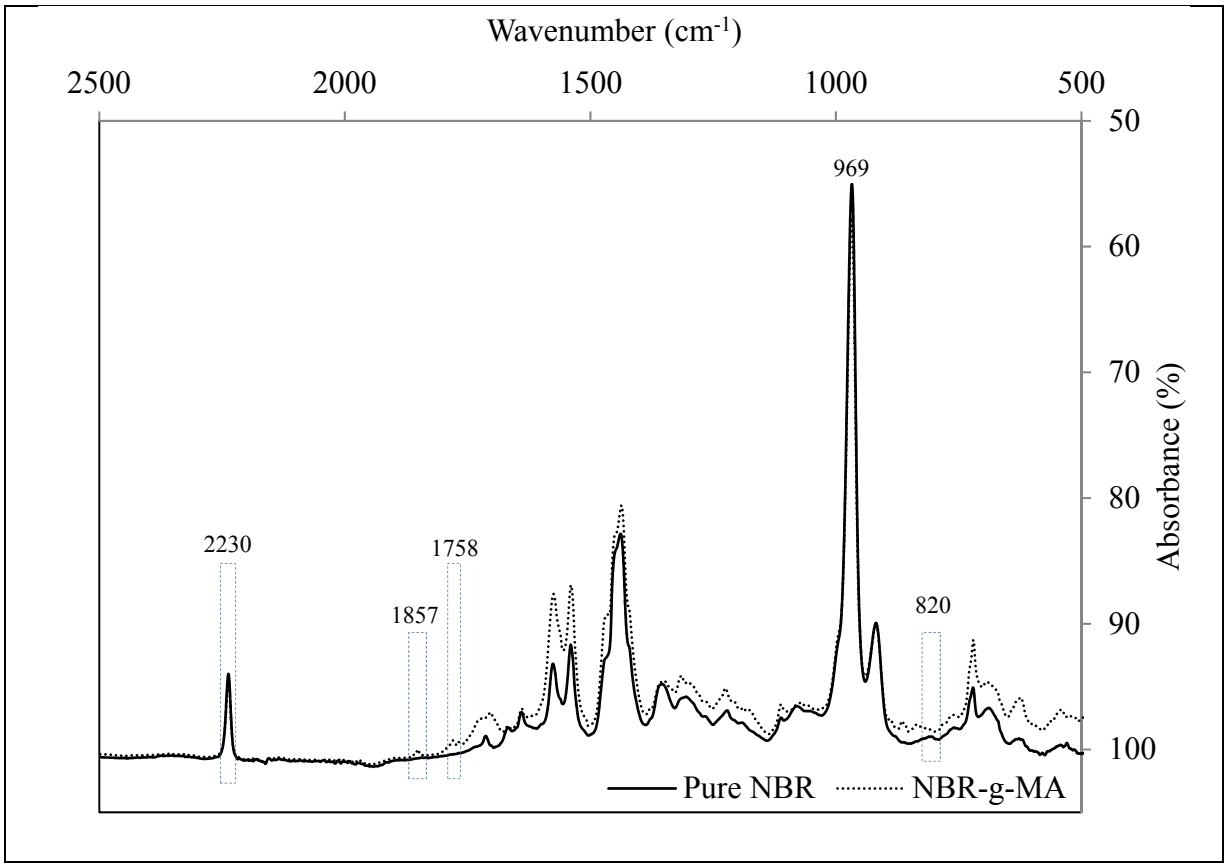

Figure 3-5. FTIR spectra of Pure NBR and NBR-g-MA

First of all, it could be noticed that new absorption peaks at around 1782 and 1857 cm^{-1} were observed. These signals were assigned to the strong symmetric and weak asymmetric stretching absorption of the carbonyl group (C=O) characteristic of the cyclic succinic anhydride (Yang et al., 2003). Moreover, the grafting of MA is achieved by the creation of a free radical in the position of the double carbon bond of the monomer. Indeed, it can be seen that the absorbance of the (C=C) signal considerably reduced in the NBR-g-MA spectrum

giving place to (C−C) bond. It should be mentioned, however, that the peak didn't completely disappear which suggested the presence of some unreacted MA present in the blend (Nakason, Kaesaman et Supasanthitikul, 2004; Sclavons et al., 2000). The MA was thus successfully introduced as a graft onto the rubbery structure. Must be kept in mind that relatively weak signal of the peaks is due to the low concentration of MA in the compound (2%). For grafting on the acrylonitrile segment of the copolymeric backbone, MA monomer would occur by addition on the unsaturated triple bond of the cyano group (C≡N). However, by inspecting the FTIR spectrum of the NBR-g-MA and compare it to the NBR signal, no decrease was noticed at the absorbance site of the cyano group located at 2230 cm^{-1} and the triple bond was unaffected. This result is suggesting that grafting would rather happen on the butadiene part of the backbone. Besides, anchoring of MA in the butadiene region could take place either by the formation of a vinylic radical monomer through abstraction and substitution of a hydrogen atom from a vinylic position or by an addition of this monomer to the carbon double bond as a result of an Ene-reaction (Huang et Sundberg, 1995; Lawson, Hergenrother et Matlock, 1990). By examining the IR spectra, it was noticed that the absorbance represented by the strong and sharp peak located at 969 cm^{-1} remained unchanged after addition of MA to the rubber. This signal corresponds to the absorbance caused by the (C−H) out of plane bending vibrations. Thus, the result reduced the probabilities that the monomer could be grafted by substitution of vinylic hydrogen in the polybutadiene (PB) segment (Rao, Rao et Sreenivasulu, 1999). On the other hand, a slight decrease in intensity was spotted on the absorbance above 820 cm^{-1}. Aforementioned peak matches with the vibrations of the carbon double bond (C=C) on the polybutadiene section. Therefore, it can be deduced that there are high chances that MA grafting could occur on the double bond of the PB (Huang et Sundberg, 1995).

Accordingly, grafting reaction during melt processing would possibly take place according to the reaction portrayed in Figure 3-6.

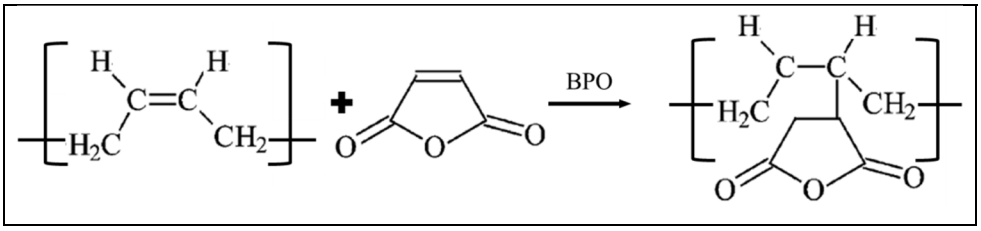

Figure 3-6. Possible grafting reaction product of polybutadiene and maleic anhydride

3.5.3 X-ray diffraction analysis of the nClay dispersion

Chemical treatment of nClay layers by cation exchange results in an enlargement of the interlayer spacing. X-ray diffraction measurements of the nClays investigated in this study were plotted as Intensity versus 2θ curves in Figure 3-7. XRD spectrum of the untreated montmorillonite nanoclay showed a broad peak located at the diffraction angle 2θ=6°. This diffraction corresponds to a basal spacing (d-spacing) of 14.73 Å according to Bragg's law applied to a diffraction emitted from a copper source. This spacing is caused by the presence of moisture attracted by the cationic charges located in the interlayers as previously described in the thermal analysis section. nClay/1, treated with dimethyl dialkyl quaternary ammonium surfactant, exhibited a well-defined reflection at 2θ=3.71° corresponding to a d-spacing of 23.82 Å. A second less noticeable peak was spotted at 2θ=6.9° (d-spacing 12.81 Å). Both signals were related to the scattering of the (001) and (002) plans of the layered stacks, respectively (Das et al., 2008). Regarding nClay/2 which is treated with methyl tallow di-hydroxyethyl quaternary ammonium surfactant, a single peak positioned at a diffraction angle of 2θ=4.79° (d-spacing 18.45 Å) was identified and assigned to the reflection of the plan (001). It can be deduced then that surface treatment in nClay/1 and nClay/2 increased the basal spacing of the first plan by about 60% and 25% respectively. The variation in the d-spacing could be related to the extent of the nano-layers surface area occupied by the organic surfactants. In fact, authors like Younghonn and al. (Kim et White, 2005) attempted to estimate the organic surface area based on calculations of the cation exchange capacity of the

nClays, which is 92 meq/100g for sodium MMT, and molecular dimensions of the surfactants. It was deduced that the quaternary ammonium cations of nClay/1 and nClay/2 covers about 120% and 70% of the layers surface, respectively. In addition, the number of long alkyl chains in the surfactants was found to affect the interlayer space in the nClays (two in nClay/1 versus one in nClay/2) (Kim et White, 2005; Williams-Daryn et Thomas, 2002).

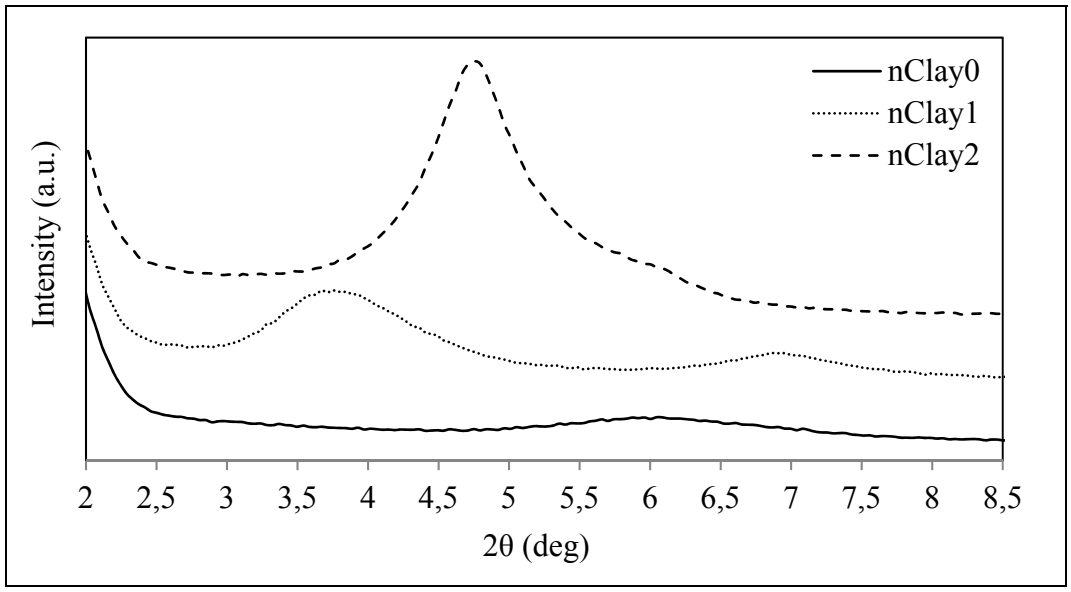

Figure 3-7. XRD patterns of MMT Bentonite Na+ (nClay/0), MMT treated with dimethyl dialkyl quaternary ammonium (nClay/1) and MMT treated with methyl tallow bis-2-hydroxyethyl quaternary ammonium

In the next step, shape and position of the basal reflections in the XRD spectra were investigated to probe the nanocomposites morphology and occasionally to monitor the extent of dispersion of the nano-platelets in the rubbery matrix. Diffraction patterns of various rubber/nClays hybrids based on nClay/1 were portrayed in Figure 3-8. It should be mentioned that the marked peaks in the figure refer to the basal reflection of the plane (001) of the nClay/1. Peaks appearing at higher diffraction angles were found to be caused by some crystalline structures located in the pure nitrile rubber as mentioned in a previous study (Zemzem, Vinches et Hallé, 2019a). Regarding the unmaleated nanocomposites RCN/11-5% and RCN/12-5%, the position of the nClay/1 scattering was slightly shifted to the lower angles suggesting an expansion of the montmorillonite layers of about 1.07 Å and 0.72 Å,

respectively. The variation of the nClay/1 layers d-spacing inside the NBR matrix was barely noticeable. The hypothesis of polymeric chains intercalation in the inter-lamellar voids is very unlikely. The literature rather attributed a small increase of basal spacing to a rearrangement of the surfactants long alkyl molecules located in the interlayer spaces (Zhou et al., 2007). As an additional note, a small difference was spotted between the effects of both described processing techniques. A comparable observation was reported in our previous work with similar nanocomposites (Zemzem, Vinches et Hallé, 2019a). From another standpoint, definitely more significant increase in d-spacing was seen with nClay/2 over fabrication with both described processing methods. From Tableau 3-1 (curves not shown), an expansion of the order of 5.76 Å and 5.43 Å were reported with RCN/21-5% and RCN/22-5% respectively. As a consequence, the incorporation of nClay/2 nanoparticles in nitrile rubber with both chemical casting and melt compounding procedures seemed to result in the penetration of the polymeric chains in between the silicate layers. Accordingly, the change in the peaks positions implies that a pronounced inclusion of the rubbery macromolecules within the nClay/2 galleries. Therefore, this inclusion led to the formation of an intercalated nanocomposite (Alex et Nah, 2006; Gatos et al., 2004). As a matter of fact, the quaternary ammonium surfactant used for the surface treatment of nClay/2 contains hydroxyl groups (O−H) rendering the hydrophilic silicate layers more organophilic (Ko, 2000). On the other side, the highly polar cyano groups (C≡N) located at the acrylonitrile segment of the nitrile rubber are very likely to establish stable hydrogen bonding with the similarly-polar hydroxyl groups (Gatos et al., 2004; Gatos et al., 2005). It might be thought then that the enhanced polarity of the silicate layers facilitated the intercalation of the acrylonitrile section, representing 34% of the overall rubber, within the inter-lamellar voids. Note however that as long as the reflection peaks were still present in the XRD spectra, a complete separation of the layers and an entire delamination of the tactoids were far from being achieved (Teh et al., 2004). For nClay/0, it was quite difficult to distinguish the peak associated to the nanoparticle from the wavy background associated to the matrix. Unfortunately, no obvious conclusions could be made about it.

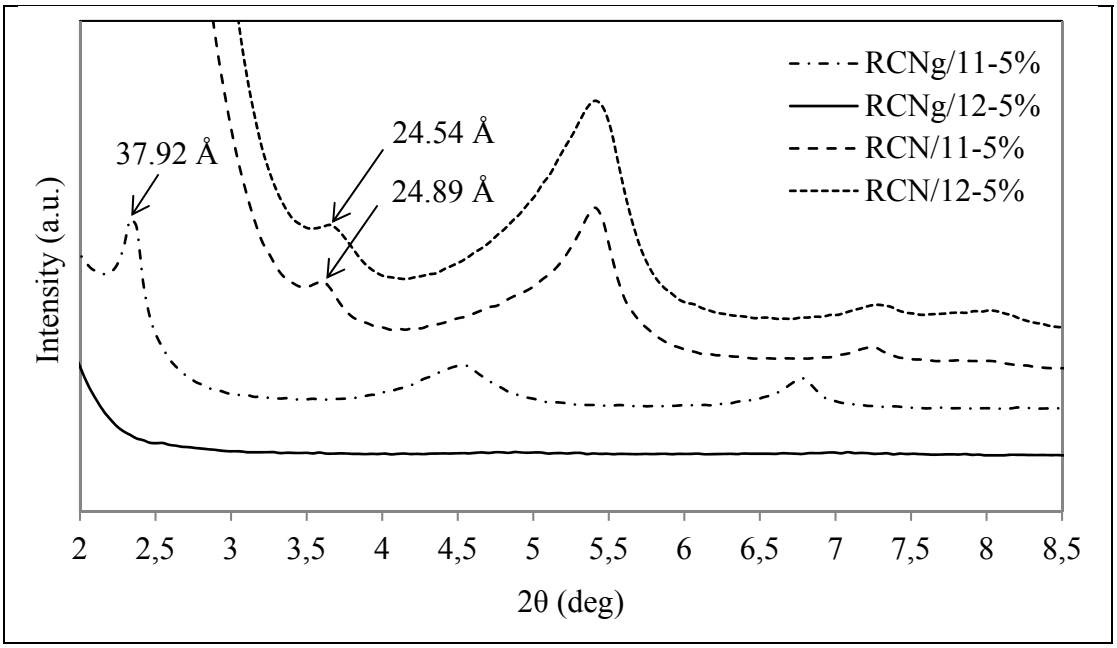

Figure 3-8. X-ray diffraction patterns of nanocomposites based on nClay/1 at 5% processed either with chemical casting and melt processing, before and after MA grafting

A common note was observed in melt processed nanocomposites grafted with maleic anhydride with all three nClays under investigation; a clear absence of scattering peaks corresponding to the reflections of nClays interlayer spacing (Figure 3-8 and Tableau 3-1). It might be assumed, allegedly, that a considerable amount of the layered stacks lost their crystallographic ordering and orientation within the nanocomposites structure (Lim et Park, 2001). Similar profiles were observed with the nanocomposites from chemical casting, except for RCNg/11-5% for which a prominent increase of d-spacing of 14.1 Å was recorded. Subsequently, it was deduced that the layered silicates reached a state of near-exfoliation regardless of the surface treatment of the nClays and independently of the chemical nature and the size of the surfactant. By consequence, it was presumed that the presence of grafted MA played the major role in the delamination of the silicate layers. As a point of fact, authors working on maleated polyolefins and organophilic nano-clay systems (Hasegawa et Usuki, 2004) reported a similar conclusion. They showed that the driving forces for polymeric chains penetration in the galleries were hydrophilic interactions in the form of strong hydrogen bonds between −COOH groups located in the MA structure and the

structural oxygen present in the silicate layers. The same deduction was stipulated with maleated EPDM and organoclays nanocomposites (Zemzem, Vinches et Hallé, 2019a).

Tableau 3-1. Basal spacing corresponding to the (001) plane reflexion of nClay/0 and nClay/2 within the nitrile nanocomposites

Nanocomposite	d-spacing (Å)	Nanocomposite	d-spacing (Å)
RCN/01-5%	N/A	RCN/21-5%	23.88
RCN/02-5%	N/A	RCN/22-5%	24.21
RCNg/01-5%	No peak	RCNg/21-5%	No peak
RCNg/02-5%	No peak	RCNg/22-5%	No peak

That being said, it could be thought at the first sight that XRD technique would be considered as the perfect tool to probe nClays exfoliation within the nanocomposites. Just by notifying the disappearance of pre-existed peaks of d-spacing reflections a conclusion could be made about the extent of exfoliation of the nClays stacks. Nevertheless, it turns out that the result of having a flat XRD spectrum wouldn't systematically mean getting homogeneous nanocomposite of well dispersed individual layers. Indeed, by looking at the mechanism of the platelets separation, two things happen to a given piling of layers. First of all, since the intercalated macromolecules penetrate randomly inside the galleries, a loss of the platelets stacking order occurs. This, hence, leads to a reduction in the size of the stuck and causes a broadening of the corresponding reflection peak in the spectrum (Vaia et al., 1996). Second, following a fairly wide extent of intercalation, multiple basal d-spacings arises giving birth to a whole distribution of broad and weak diffraction peaks for a given platelets stack (Reichert et al., 1998). Those factors contribute to the appearing of what it looks like smooth flat curve as seen with the maleated nanocomposite in Figure 3-8. Taking into account these considerations, the morphology rather tends to look like clusters of well expended and disordered few-numbered platelets piles. Single layers might also be present as a result of delamination mechanism following shear stress applied during melt processing.

3.5.4 SEM observations and EDX assessment of the nClays state of dispersion

Despite the capabilities of the X-ray diffraction analysis to provide convenient understanding about the inter-lamellar spacing of the nClays layers before and after inclusion in the rubber, little can be said about the state of dispersion and the spacial distribution of the nClays in the elastomeric matrix. Crosschecking with electronic imaging technique would provide a better understanding of the nanocomposite morphology. It should be admitted that SEM is not widely used as a reliable method to investigate layered silicate nanocomposite structures. The major reason is that the micrographs resulted from the electron scattering cannot provide enough contrast to distinguish the nClays from the elastomeric matrix. For the nanoparticles to be perceived in the micrographs, chemical etching could be applied to the observed fracture surface in order to remove the surrounding rubber, pop up the nClays to the surface and create a topology. Chemical etching is quite challenging in itself; considering the lamellar form of the nClays, surface tension forces tend to flatten the nanoparticles on the surface. This matter could easily be recognized in the following observations. Figure 3-9 (a.1) and (b.1) displayed SEM micrographs of RCN based on the untreated nClay/0 before and after MA grafting, respectively. Magnification was set in such a way that the expected size (lateral dimension) of the fillers could be detectable. Well defined profiles could readily be spotted in both images but no obvious conclusions could be made as to their nature.

Based on the SEM setups, silicate entities could be indirectly sensed through elemental analysis of the characteristic X-rays backscattered electrons after a primary electron bombardment of the sample surface. The measurements were conducted using an energy dispersive X-ray spectrometer coupled to the electron microscope and tuned to the mapping mode.

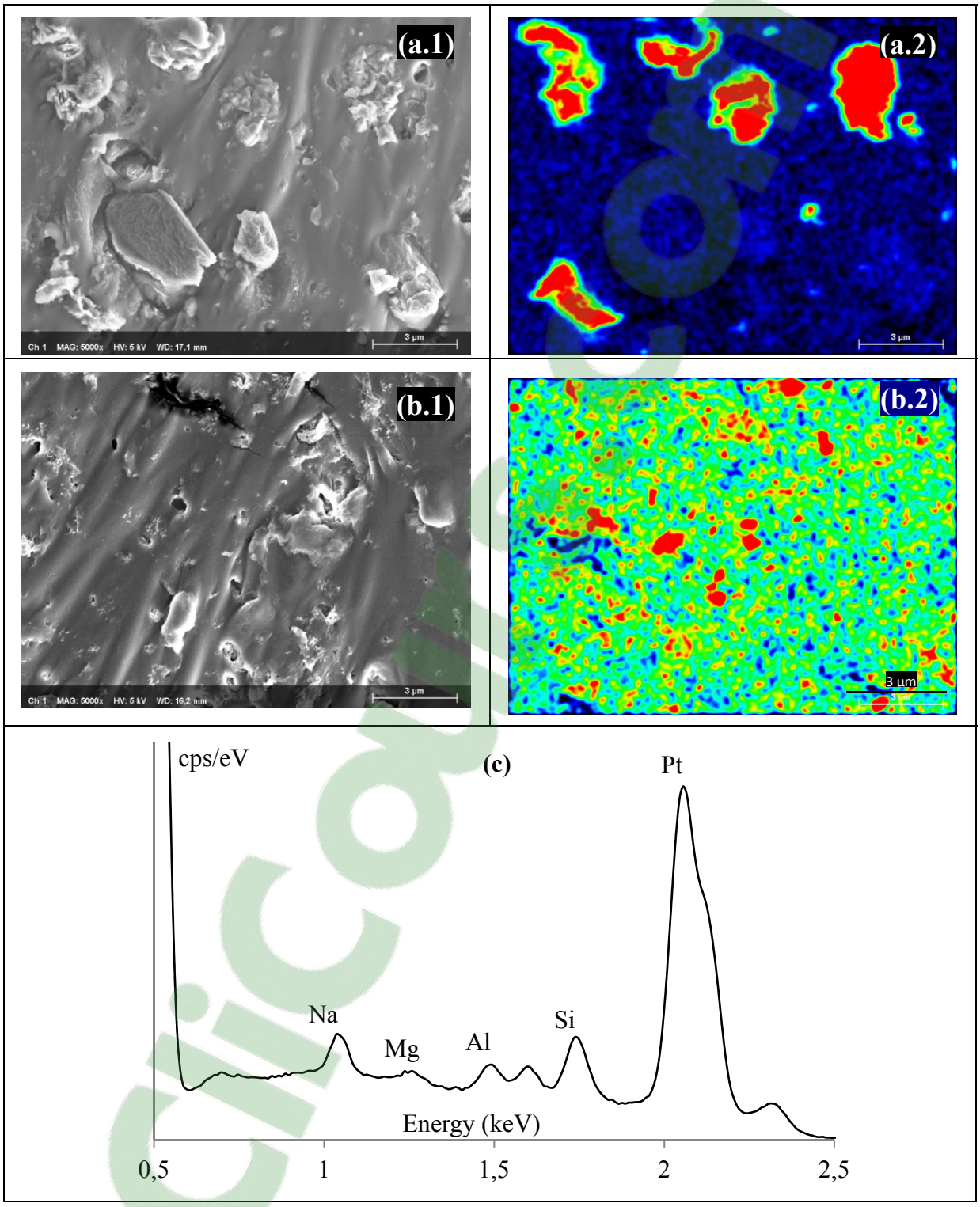

Figure 3-9. SEM micrographs of nitrile nanocomposites based on nClay/0 before (a.1) and after (b.1) maleic anhydride grafting as well as their associated EDX element mapping images (a.2) and (b.2), respectively. EDX spectrum of RCN/01-5% (c)

From a chemical point of view, it should be highlighted that the nClays under investigation are synthetic minerals composed of an alumina octahedral layer sandwiched between two tetrahedral silica layers in a the ratio of 2:1 (García-López et al., 2010). Given the difference in their ionic valence, trivalent aluminum cations are very often partially substituted by bivalent magnesium cations within the silicate layers (Paul et Robeson, 2008). Accordingly, Si, Al and Mg are substantial elements present in the structure of the investigated nClays regardless of the organic surface modification. Those elements are thus characteristics of the nClays and were used as markers to detect the presence of the nanoparticles in the micrographs. Figure 3-9 (c) portrayed the elemental EDX spectrum of the RCN/01-5% and labeled peaks in the curve confirmed the presence of the three outlined elements. As a side note, the platinum signal was originated from the conductive coating applied to the sample and sodium was the exchangeable cation located on the platelets surfaces. The best contrast to distinguish the nClays was achieved when elemental mapping of all the three structural elements (Si, Al and Mg) were superposed in a single image. Such mapping images of nitrile/nClay/0 hybrids before and after MA grafting were jointly showed in Figure 3-9 (a.2) and (b.2).

At first glance, it could be seen in the mapping image of the non-grafted nanocomposite the omnipresence of relatively large sizes of well-defined nClays clusters. Smaller separated agglomerations could also be spotted in the same image. The cold (blue) contrast in-between represents the surrounding rubbery matrix. On the other hand, maleated nanocomposite exhibited a homogeneous pattern of much smaller and uniform nanoparticles agglomerations. Also, it could be noted that the intermediate space showed a brighter contrast compared to the non-grafted material. This is suggesting either the presence of even smaller silicate entities which were barely detected by the device, or the existence of agglomerations located few microns beneath the probed surface. Either way, this observation connotes an enhancement of the nClays distribution within the nanocomposite. For further investigation, quantitative analysis of size distributions of the agglomerations was conducted. In each nanocomposite, counting was based on data collected from a sum of five mapping images at the same magnification. Since no regular shape was discerned for the agglomerations,

assessed size was set to denote the surface area of the entities. A protocol was developed on image editing software (ImageJ) to identify the agglomerations based on their brightness and their contrast in the mapping images. Automated counting was then executed. The formerly described size distribution histograms were depicted in Figure 3-10. In the first place, counting results showed that the number of agglomerations entities in the nanocomposites, for the same inspected area, increased by more than 2.5 times after the grafting of MA (from 43 to 111 entity). Additionally, the histogram of the RCN/01-5% revealed a near-flat distribution. More specifically, almost every size range of 0.05 μm^2 from 0.01 to 1 μm^2 contains up to five agglomeration entities. After MA grafting, RCNg/01-5% exhibited a clear asymmetric peak shifted to the left of the graph and showing that over 30% of the nClays assemblies have a surface area of about 0.05 μm^2. This finding helped to throw some light on the effects of MA grafting on decreasing the size of the agglomerations and homogenizing the morphology of the RCNs.

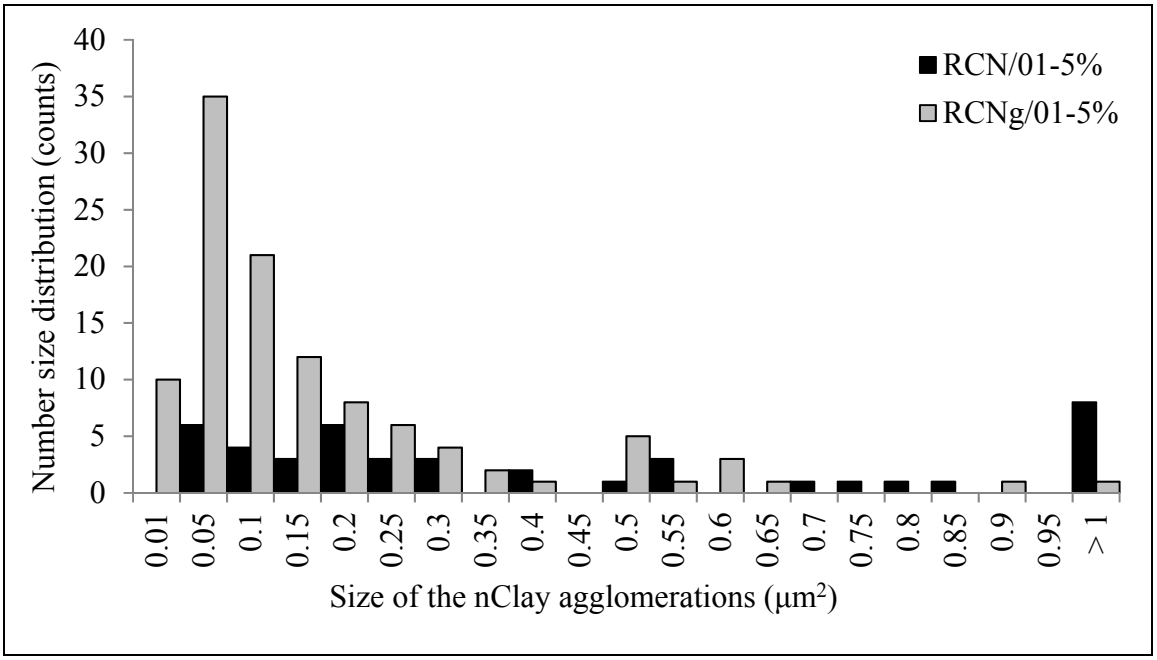

Figure 3-10. Grafting effect on size distribution of nanoclay agglomerations in nitrile rubber nanocomposite

3.5.5 TEM experiments

Further characterization support was provided from transmission electron microscopy. Through direct visualization, TEM allows, indeed, a localized understanding of the internal morphology of the nClays as well as views of the defect structure (Ray et Okamoto, 2003). Figure 3-11 (a) and (b) portrayed TEM bright field micrographs at a magnification of 200K representing nitrile nanocomposites cross-sections before and after grafting of maleic anhydride, respectively. The image corresponding to the non-grafted nanocomposite exhibited a region of about dozen of alternating narrow dark and light bands. The described multilayered feature was definitely assigned to a piling of parallel silicate nano-platelets. The thickness of the dark layers was measured in post-treatment and found to be around 1 nm. The result is in agreement with the structural thickness of a silicate monolayer documented in the literature (Alexandre et Dubois, 2000). Accordingly, the adjacent bright band would correspond to the interlayer gallery. Interestingly, the width of this gap measured at ten different positions in the layered structure was equal to 23.65 Å ± 0.5 Å. This measurement is in perfect agreement with the basal d-spacing previously assessed with XRD (24.54 Å). Similar TEM micrographs in the literature support the findings (Gilman, 1999). It is worth mentioning also that rather than polymeric intercalation process, dispersion of the layered silicate was additionally undertaken by delamination mechanism. This phenomenon is reflected in micrographs by the onset separation of small stacks of 2-5 nano-platelets (white arrows) from the external surface of the tactoids. The delamination aspect was repeatedly appearing in several micrographs taken for this nanocomposite. After MA-grafting (Figure 3-11 (b)), the existence of separated monolayers was clearly visible in the micrographs being assigned to the single dark hair-like bands.

It is to note though that the overall micrograph was majorly occupied by a bright area corresponding to the rubbery matrix. It must be kept in mind that at this level of magnification, a noticeable inhomogeneity was expected rather than a monolithic morphology.

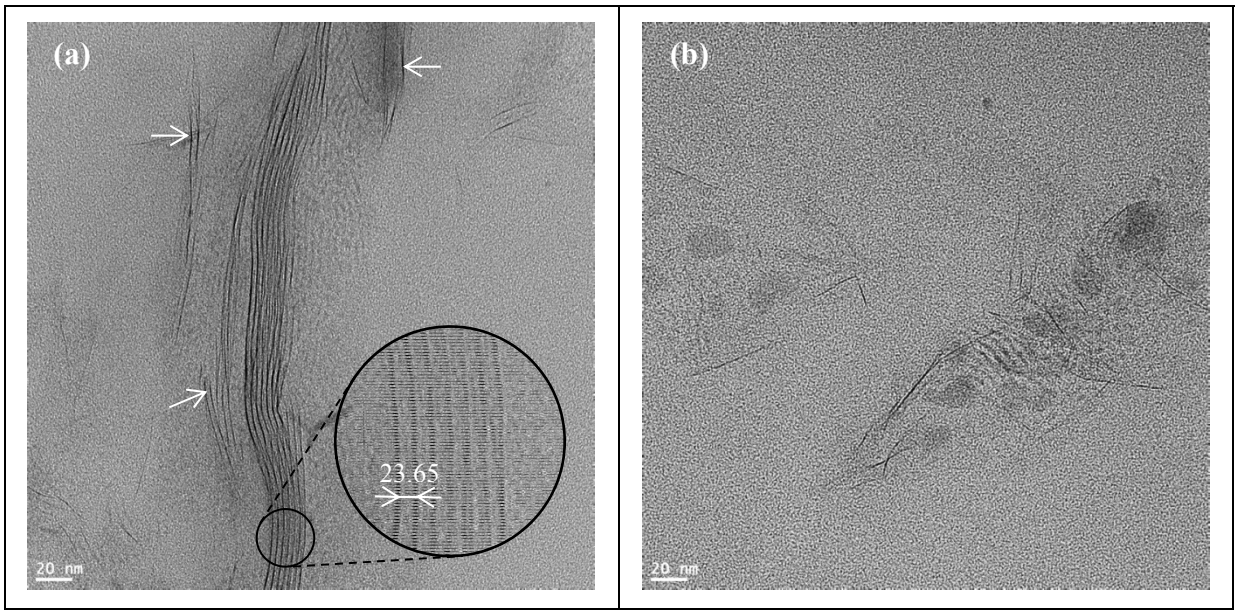

Figure 3-11. TEM micrographs of NBR nanocomposites loaded with 5% before (a) and after (b) grafting of maleic anhydride

3.5.6 SAXS experiments for nClay orientation

Even if it was assumed that a state of total exfoliation of layered silicates could be reached, the performance of a nanocomposite would still be far from being at its best for some applications. In fact, numerous studies highlighted the pronounced effect of the orientation and the alignment of the nClays platelets within the polymeric matrix on enhancing efficiency in several fields involving barrier and mechanical properties (Kim et al., 2001; Osman, Mittal et Lusti, 2004). The small angle X-ray scattering technique is considered one of the most commonly used methods to sense the orientation of crystalline forms embedded within polymeric systems (Kamal et al., 2012; Schnablegger et Yashveer). SAXS concept is based on probing X-ray reflections from the layered structure of a population of nClays tactoids, which provides a reliable understanding of the platelets orientation distribution.

The orientations of layered silicates in four nanocomposites based on nClay/1 at 5% were examined in this study. Since the processing methods were shown to considerably affect the nClays alignment, solution cast and melt processed nanocomposites were compared (RCN/11-5% and RCN/12-5%). The maleated nanocomposite (RCNg/12-5%) was also tested. Even though grafted RCN was shown to exhibit a high state of delamination, which is

expected to reduce the amount of diffraction and thus is likely to provide poor information about the nClays arrangement. The fourth sample was prepared exactly as the extruded RCN/11-5% except that it was quenched with liquid nitrogen right after the pressing step. Fast cooling was thought to freeze the morphology and ensure more orientation of the nano-layers (RCNq/12-5%).

To get a global overview of the alignment within a tested sample, a technique was adopted to build a three-dimensional representation of the nClays orientation starting from the 2D SAXS patterns. Diffraction results were acquired from the three different directions of a cubic sample. These directions correspond to the machining (MD), tangential (TD) and normal (ND) directions as portrayed in Figure 3-12 (a). It should be noted that each one of these directions is perpendicular to its associated plan of diffraction represented by the 2D SAXS stereographs. For the solution casted sample presented in Figure 3-12 (b), the 3D scattering spectrograms displayed well defined concentric circles around the primary incident beam. The ring-like dark spots at the first order counting from the center were associated to the 2θ diffraction of the nClays basal d-spacing. Their diffractions were in agreement with the position of the inter-layers peak reported with XRD. Nearly isotropic patterns in all the directions indicate the existence of randomly orientated nClay platelets within the RCN system (Prasad et al., 2001). The spectrograms associated to the RCNq/12-5% and presented in Figure 3-12 (c) also showed the reflected intensity of the nClay/1 within the nanocomposite. However, concentric blob-like circles were only spotted from the normal direction. Seen from (MD) and (TD), scattered patterns revealed a lack of diffracted intensities on either sides of the central spot. Anisotropic diffraction is the signature of an obvious orientation of the nano-platelets (Alonso et al., 2009). According to the three dimensional portrayal, the face and side alignment would suggest an orientation following the line of extrusion during processing. Finally, diffraction patterns of the maleated nanocomposite RCNg/12-5% were expressed in Figure 3-12 (d). As expected, the stereographs exhibited broad diffraction near the central blind spot. No specific scattering could be obviously attributed to the basal d-spacing of the layered silicates.

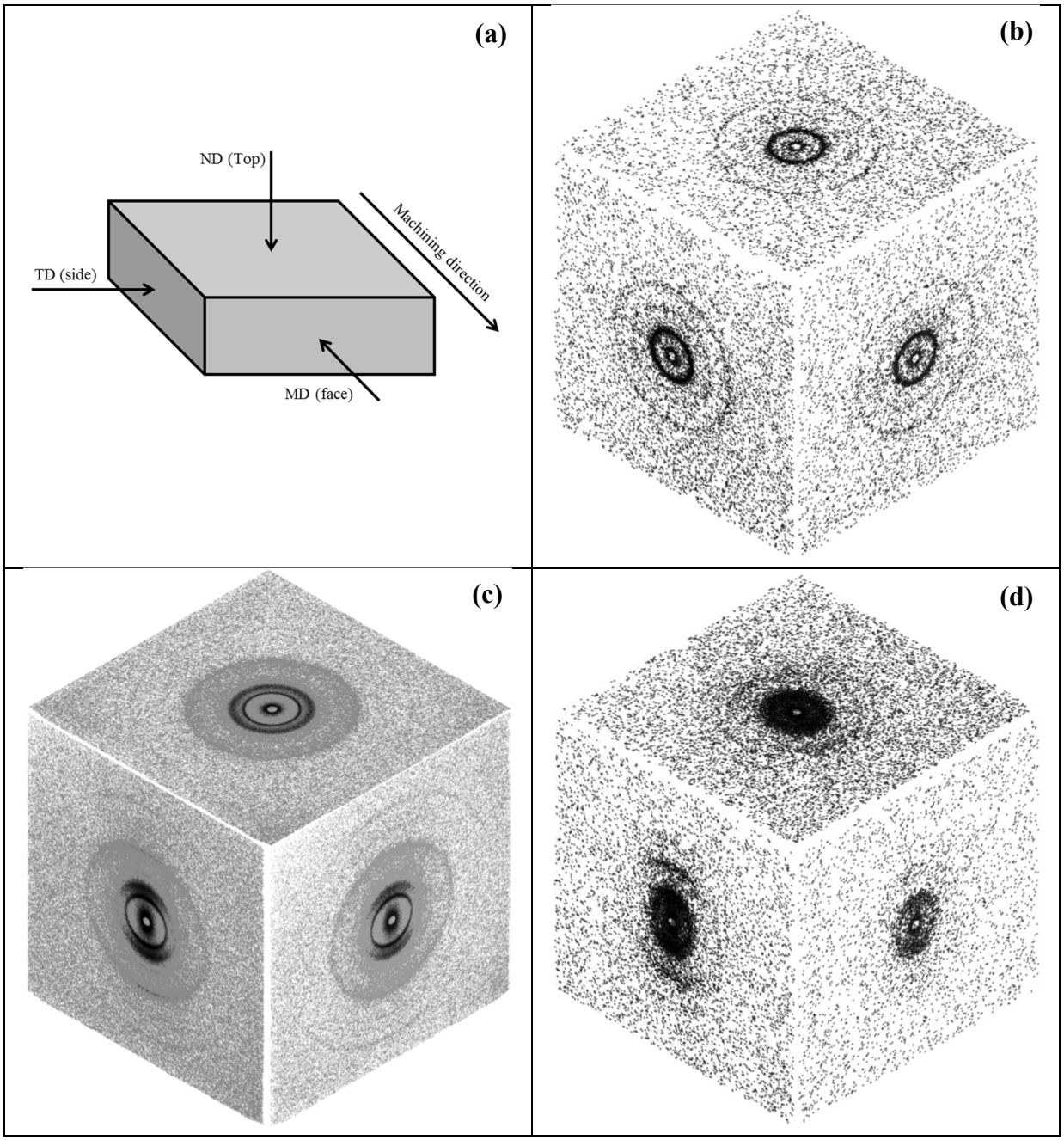

Figure 3-12. Three-dimensional representation of nClays orientation using 2D-SAXS patterns

A very convincing approach for determining the three-dimensional orientation of various hierarchical organic and inorganic structures in polymeric systems was described by Bafna and al (Bafna et al., 2003). This approach was adopted to conduct a more in-depth quantitative investigation of the layered silicate alignment within the nanocomposite

samples. As could be deduced from the previous discussion, the presence of periodic lamellar structure such the nClays was manifested by the appearance of a characteristic ring of scattered intensity at a specific range of diffraction angle 2θ. A curve of intensity versus the azimuthal angle (φ) ranging from 0 to 360° could be plotted for each radial position (2θ). In such a curve, the more sharp and intense azimuthal peaks are, the more orientation there is in the structure. For each one of the three previously identified directions, an average cosine square value could be calculated using equation (3.1) (Bafna et al., 2001) in order to provide a reasonable assumption of the state of alignment distribution of the population of nClays present in the examined nanocomposite sample:

$$\langle cos^2(\varphi_i)\rangle = \frac{\int_0^{360} I(\varphi_i) cos^2(\varphi_i) d\varphi_i}{\int_0^{360} I(\varphi_i) d\varphi_i} \tag{3.1}$$

The letter i stood for directions M, T and N.

The obtained average cosine square value was then used, for each direction i, to assess a so-called Herman's orientation factor (f) given by equation (3.2) (Vainio, 2016):

$$f_i = \frac{1}{2}(3\langle cos^2(\varphi_i)\rangle - 1) \tag{3.2}$$

A convenient presentation of the average three-dimensional orientation direction based on Herman's factor data would be by using Wilchinsky triangle which is a ternary plot that displays the extent of orientation by a single dot (Roe, 2000). By definition, a complete randomly oriented structure relative to a given direction would have a null Herman's factor, which corresponds to an average cosine square value equal to 1/3. In this case, the three-dimensional orientation would be represented by a point on the center of the Wilchinsky triangle (unfilled circle in Figure 3-13). On the other hand, the orientation assessment of a structure along a given direction corresponds to the distance of its representative point from the axis of interest for the particular orientation. In other words, for a structure perfectly orientated in the MT plane, the associated normal direction must be pointed towards the N

direction and therefore it would be represented by a point at the ND corner (see Figure 3-13). While an orientation of a structure perpendicularly to the MT plane would be represented by a point on the MT axis opposite to the ND corner.

This approach was adopted to assess the three-dimensional orientation of the four formerly described nanocomposites. The respective Wilchinsky triangle was portrayed in Figure 3-13. First, it was deduced from the cubic representation of the SAXS stereographs, the chemically casted nanocomposite RCN/11-5% exhibited an almost totally random 3D orientation within the rubbery system. In fact, its associated point was located very close to the center of the ternary plot. Second, the melt-processed RCN/12-5% sample showed a point positioned right at the normal to the (MD, MT) axe. That is already meaning that there was the same extent of orientation in the machining and tangential directions. In addition, this point was located between the center of the triangle and the ND corner. This is suggesting that the layered silicates had an obvious orientation parallel to the MT plane. Third, it could be noticed that the quenched RCNq/12-5% nanocomposite expressed the same orientation trends compared to RCN/12-5% but with a corresponding point closer the ND corner. This was implying more pronounced orientation parallel to the MT plane. Finally, a point of 3D orientation was associated with the maleated nanocomposite RCNg/12-5%. The sample followed the same former alignment tendency. However, it is noteworthy that since no well-defined rings were spotted in its corresponding stereographs, the azimuthal curve was constructed from averaging a relatively large range of radial intensity along the 2theta axis. Therefore, the observed orientation could match with the alignment of other ordered structures present in the material than the layered nanoparticles.

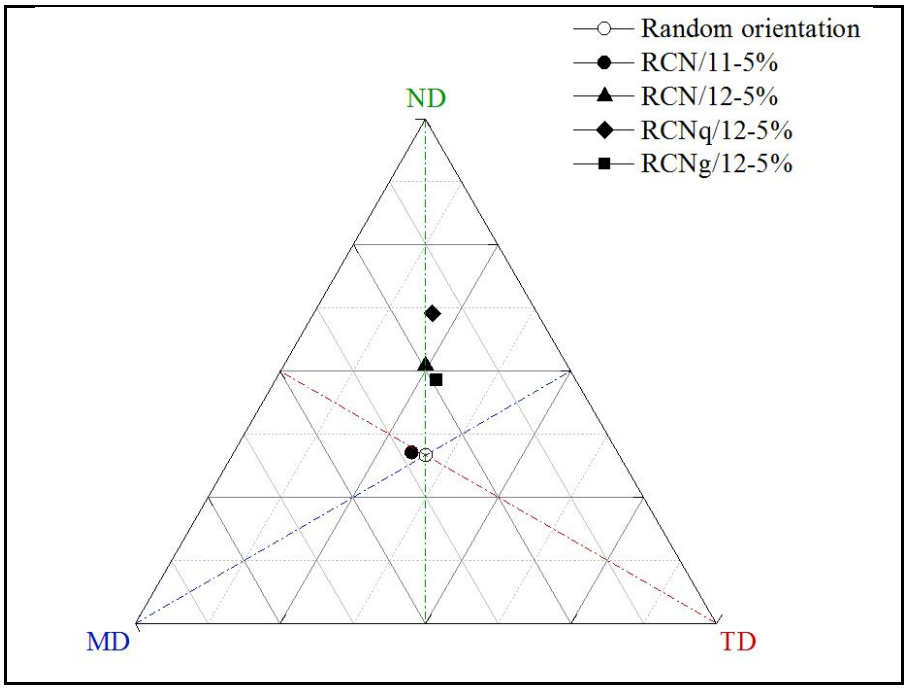

Figure 3-13. Wilchinsky triangle for three-dimensional orientation of RCN/11-5%, RCN/12-5%, maleated RCNg/12-5% and quenched RCNq/12-5%

3.6 Conclusions

In summary, the undertaken study was an attempt to design a nitrile-based nanocomposite filled with clay nanoparticles at a high level of dispersion and conducted in a preferred orientation. Layered silicates with organic surface modifications were used in order to enhance the rubber/filler compatibility. Besides, the rubbery matrix molecules were chemically grafted with maleic anhydride, a highly polar monomer that was expected to improve the affinity between the components and helps polymeric chains to intercalate within the nClays galleries. TEM, XRD and EDX/UHR-SEM characterization techniques were combined to build a state of understanding about the homogeneity of the nanocomposites. Grafting with MA was found to provide an astounding improvement to the dispersion of the layered silicates and a state of near-exfoliation has been witnessed. On the other hand, processing the nanocomposites with melt compounding through extrusion was shown to ensure an alignment of the nanoparticles following machining and tangential directions. This particular arrangement was made clearly noticeable through a 3D orientation

approach based on data collected from SAXS. Conclusively, the desired nanocomposite was successfully designed at some extent. Afterwards, it would be of great interest to know if the enhanced structural properties will guarantee improved industrial qualities.

Préface du chapitre 4 :

Le dernier chapitre constitue l'objet de l'étude menée dans l'article 3. L'objectif de ce chapitre est d'évaluer les propriétés barrières des nanocomposites dont la marphologie a été améliorée. La modélisation par les lois de Fick est adoptée pour décrire le phénomène de transport moléculaire à travers les membranes nanocomposites. Les propriétés barrières sont évaluées à travers la détermination des paramètres du mécanisme de transport ainsi que ceux de la cinétique de pénétration. L'effet de la température et de la taille des molécules pénétrantes sur la résistance aux solvants est également investigué.

CHAPITRE 4

ARTICLE 3 : MOLECULAR SORPTION AND DIFFUSION OF ORGANIC SOLVENTS THROUGH MALEATED RUBBER/LAYERED SILICATE NANOCOMPOSITES

Mohamed Zemzem, Ludwig Vinches, Stéphane Hallé

Département de génie mécanique, École de Technologie Supérieure,
1100 Notre-Dame Ouest, Montréal, Québec, Canada H3C 1K3

Article soumis à :
Journal of Polymer Testing, en date de mars 2019

4.1 Abstract

The aim of the present study is to investigate the barrier properties of a nanocomposite material against organic solvents. Molecular transport phenomena of three alcohols, namely methanol, ethanol and isopropanol, through a nitrile rubber-based nanocomposite, were carried out in temperatures ranging from 23 to 70°C. For each configuration, mass transfer kinetics were investigated for three different types of clay nanoparticles using mass uptake experiments. The state of exfoliation of the lamellar filler was expected to affect the barrier properties of the resulting material. Hence, maleated nanocomposites with enhanced dispersion morphology were also examined. Sorption tests were conducted on neat nitrile rubber to outline the clay nanoparticles' effect. Results show that all molecular transport parameters are generally susceptible to temperature variations. Sorption, diffusion and permeability coefficients noticeably increased as temperatures increased. Polymer/solvent interaction seems similarly affected. Molecular volume of the penetrant is observed to have an influence on molecule migration. The required immersion time to reach saturation and values of sorption at equilibrium both drop with the increase in molecular volumes. Diffusion and permeation coefficients are likewise affected and decrease logarithmically with the linear

increase of molecular volume. The diffusion mechanism is slightly altered by this factor and the Fickian mode is maintained. When filling the rubbery matrix with layered silicates, sorption decreased at equilibrium. Its level dropped even lower with the maleation of the nanocomposite. However, the diffusion coefficient exhibits a less systematic trend. Randomly filled nanocomposites appear to have higher diffusivity than neat rubber, but the parameter considerably decreases after maleation, which emphasizes the nanoclay's dispersion effect. Finally, the evolution of the penetrant concentration within the rubber material is portrayed with different solvents at four temperatures, based on Fick's analytical modeling of the mass transfer phenomenon.

KEYWORDS: Nitrile rubber, layered silicate nanocomposites, maleic anhydride, mass transfer kinetics, swelling.

4.2 Introduction

Molecular transport phenomena through polymeric systems play an important role in several areas of engineering and have a considerable impact in many industrial sectors (Greenkorn, 2018). Structural integrity, chemical stability and dimensional invariance in the presence of aggressive substances are qualities of great importance when applications such as food packaging, controlled drug release, filtration and electronic encapsulation are concerned (Baker, 2012). The sorption and transport properties of small organic molecules in a wide range of polymers have been extensively investigated. For instance, there are several studies on the molecular transport of most of the thermoplastic polymers, thermosets, elastomers, and geomembranes (Rao et al., 2007; Sridhar et al., 2007; Stephen et al., 2006). The barrier properties of these materials were probed in the presence of the majority of commercial chemicals, such as n-alkanes, halo-alkanes, aliphatic esters and aromatic hydrocarbons (Kumar, 2005; Swamy, 2003). The molecular transport behavior was found to be deeply affected by the structural properties of the penetrant/polymer system. In fact, studies demonstrate the influence of the segmental mobility of the polymeric matrix, the size and shape of the penetrant as well as the chemical affinity in the diffusion system (George et

Thomas, 2001). It was also found that the mass transfer phenomena closely depend on the environmental conditions surrounding the sorption process, namely temperature and humidity (Joseph, Mathai et Thomas, 2003).

Polymers reinforced with inorganic nanostructured and layered silicates have attracted substantial attention due to their unique and attractive characteristics even at low concentrations (Bhattacharya, 2016). These materials, also called nanoclays, combine the simplicity of polymer processing with the resistance of the platelet-like nanoparticles. In addition, clay nanoparticles possess two particular characteristics. First, the constitutive platelets can be dispersed on individual layers. Second, they can functionalize the surface of these layers and apply chemical modifications that allow better interactions with the hosting polymers (Azeez et al., 2013). In previous works, their high aspect ratio was stated to contribute to the reduction of fluid permeability by creating a tortuous pathway to the penetrant substance (Tan et Thomas, 2016; Zemzem, Vinches et Hallé, 2019a). The ideal state would be having a complete separation of the nano-platelets leading to a maximum of interfacial surface in the rubber/clay system. However, total delamination is technically difficult to achieve due to the non-compatibility between the components and the hydrophilic nature of the bare clay nanoparticle surface. Therefore, the successful synthesis of nanocomposites depends on the chemical affinity between the polymeric matrix and the hosted nanoparticles that ensure the thermodynamic stability of the nanocomposite system. Over the years, new techniques are continually being developed to enhance the nanoclay/polymer compatibility. The most commonly adopted method consists of modifying the surface chemistry of the nano-platelets with aliphatic organic structures to reduce the surface tension and facilitate polymeric chain intercalation (Kotal et Bhowmick, 2015). Rather than achieving intercalation via ion exchange, other methods to increase the interfacial adhesion were adopted, such as ion dipole bonding of bulk molecules to the metallic cation on the nanoclay surface and nano-platelet edge treatment with silane coupling agents (Beall et Powell, 2011). It was also found that some studies used maleic anhydride monomers as compatibilizers due to their polarity and their highly reactive nature (Issaadi et al., 2015).

Both in its solid and latex states, acrylonitrile butadiene rubber is considered to be one of the most mass produced and widely commercialized elastomers, also known as nitrile rubber. Mainly manufactured using the emulsion polymerization method, this elastomer exhibits low mechanical and barrier properties without reinforcing fillers. Attempts were made to incorporate clay nanoparticles to enhance its barrier properties, but this yielded a low state of dispersion of the nanoclays within the elastomeric matrix, resulting in poor chemical resistance quality. In our previous work (Zemzem, Vinches et Hallé, 2019b), a clay nanocomposite based on nitrile rubber was developed. Combining the grafting of nitrile rubber backbones with maleic anhydride and the organic modification of the nanoclay surfaces led to a successful synthesis of the nanocomposite with a satisfactory state of nanoclay dispersion and orientation of the nano-platelets within the elastomeric structure. Thus, the aim of the present study is to investigate the barrier properties and better understand the sorption behaviour of this material against organic solvents by probing the kinetic molecular transport parameters of the penetrant/nanocomposite system.

4.3 Reagents and materials

The nanocomposites of the present study are based on an acrylonitrile-butadiene rubber (NBR) matrix. Baymod N34.52 NBR powder was used, complements of Matexion, ON, Canada. This nitrile rubber elastomer is 34% acrylonitrile. Its Mooney viscosity is 45±5 at 100°C and its specific gravity is 0.98.

For the grafted nanocomposite samples, maleic anhydride (MA) was used as a reactive monomer and benzoyl peroxide (BPO) as an initiator of the grafting process. Both substances were purchased from Aldrich Chemical with a purity level of over 98%.

The nanocomposites were filled with three different commercial-grade clay nanoparticles (Sigma-Aldrich, Oakville, ON, Canada), one unmodified and two organically treated. The nClays were labelled as follows:

- nClay/0: a natural inorganic hydrophilic sodium montmorillonite (Na^+MMT) with no surface modification;
- nClay/1: Surface modified MMT containing 35-45 wt. % of dimethyl dialkyl (C14-C18) amine;
- nClay/2: Surface modified MMT containing 25-30 wt. % methyl dihydroxyethyl hydrogenated tallow ammonium.

High purity grade (over 98%) methanol, ethanol and isopropanol (propan-2-ol) from Fisher scientific (Hampton, NH, U.S.A.) were used as penetrant solvents in the sorption experiments. The properties of the solvents are presented in Tableau 4-1.

Tableau 4-1. Physical properties of the organic solvents used as penetrants at room temperature

		Methanol	Ethanol	Propan-2-ol
Chemical formula		CH_3OH	C_2H_5OH	C_3H_7OH
Molar mass	$g \cdot mol^{-1}$	32.04	46.07	60.10
Molecular volume	$cm^3 \cdot mol^{-1}$	40.45	58.37	76.46
Density	$g \cdot cm^{-3}$	0.792	0.789	0.786

4.4 Experimental

4.4.1 Preparation of the nanocomposites

Nitrile rubber-based nanocomposites containing the formerly described nanoclays were prepared. For every batch, a virgin nitrile rubber sample was prepared using the same processing protocol as for the nanocomposites for comparison purposes. It is worth noting that prior to every preparation, all powders were oven-dried at 65°C for 24h. To set the optimized loading for reinforcement, the first batch of nanocomposites was prepared with different nanoclay concentrations: 1, 3, 5, 10 and 15%. The nanocomposite with optimum loading will be retained and used to investigate the barrier properties using the three

aforementioned solvents at various temperatures. A HAAKE Polylab OS – RheoDrive 4 co-rotating twin screw extruder (Rheomex OS PTW16) was used to prepare the conventional and maleated nanocomposites. A detailed description of the nanocomposite process is available in our previous work (Zemzem, Vinches et Hallé, 2019b). After this, all the obtained compounds were press-molded into sheets for mass transfer experiments.

4.4.2 Mass uptake experiment

Mass uptake experiments were performed at 25, 40, 55 and 75°C. Rectangular samples (60 × 10 mm) were cut from the press-molded nanocomposite sheets using a steel die. Screw-tight test bottles containing about 10 mL of the penetrant solvent were placed in a bath of silicone oil heated to the desired temperature within an accuracy of ± 1.0°C. Dry weights of the cut samples were then placed in the bottles. At predefined time intervals, the samples were withdrawn from the solvent containers. The surface-adhered liquid was removed by gently pressing the samples between filter paper wraps and the samples were weighed on a digital balance (accuracy ± 0.01 mg). The overall process was performed within a maximum of 20 seconds to minimize errors. The sorption tests were performed until equilibrium was reached, i.e. solvent was no longer being absorbed despite continued immersion. Each test was replicated three times to obtain statistically valid data.

The percent mass uptake during solvent sorption was given by (Vinches et al., 2015):

$$\%Mass\ uptake(t) = \left(\frac{m_t - m_0}{m_0}\right) \times 100 \tag{4.1}$$

The output from a sorption experiment could also be expressed relatively to the total mass uptake of a given sample during an immersion test. The dynamic mass variation was then given by the following:

$$Dynamic\ mass\ variation(t) = \frac{M_t}{M_\infty} = \frac{m_t - m_0}{m_\infty - m_0} \tag{4.2}$$

where, M_t is the mass uptake at instant *t*, M_∞, the mass uptake at equilibrium, m_0, the initial weight of the sample, m_t, the sample's weight at instant *t* and m_∞, the sample's weight at equilibrium.

4.5 Theory

4.5.1 Sorption behavior

Even though nitrile nanocomposites are dense and nonporous materials, they can be permeated to some extent by liquids, gases and vapours of liquids at a molecular level (Mathai, Singh et Thomas, 2002). Liquid absorption in a given polymeric membrane is best expressed by Fick's theory. Hence, absorption is governed by a concentration-independent diffusivity (Baker, 2012). Based on Fick's second law, the dynamic mass variation over time of an absorbing polymer can be analytically described by a polynomial of degree *n* (equation (4.3)). An effective way to predict the diffusion mechanism in a given system is to establish a relationship between the sorption data from mass uptake experiments and the analytical approach (Stephen et al., 2006).

$$\frac{M_t}{M_\infty} = K \cdot t^n \tag{4.3}$$

K is a constant closely related to the diffusion coefficient of the system as well as to the sample thickness, and n is a real number, indicating the type of diffusion mechanism.

Depending on the relative mobility in the polymer/penetrant system, three modes of diffusion are considered. The diffusion is Fickian, or Case I, when the mobility of the polymeric chains highly exceeds the diffusion rate of the penetrant. The dynamic mass variation is expected to be proportional to the square-root of time, accordingly, *n*=1/2. This mechanism is usually found in systems involving polymers, especially elastomers, whose glass transition temperature is well below the ambient temperature in which the diffusion process is taking place. On the other hand, diffusion is non-Fickian, or Case II, when *n*=1. In this case, the

diffusion rate of the penetrant exceeds the mobility of the polymeric macromolecules. A diffusion mechanism is considered anomalous when the exponent *n* is between 1/2 and 1 and when the mobility of both polymer chains and penetrant molecules are comparable (Tan et Thomas, 2016).

4.5.2 Kinetics of mass transfer

Molecular transport through polymeric systems is admitted to be a diffusion process (Masaro et Zhu, 1999). The diffusion coefficient of the molecular flow through a given polymeric membrane can be calculated using the thin-film solution with Fick's second law of mass transfer:

$$\partial C/\partial t = D(\partial^2 C/\partial x^2) \tag{4.4}$$

where, C refers to the liquid concentration within the membrane at a given time *t* and at depth *x* within the sample. An analytical solution of this differential equation defines the liquid concentration during sorption through a given rubber sheet of thickness h, at time *t*, and at distance x. Resolution of the second law of Fick's equation leads to an expression of the mass of the penetrant absorbed by the film as a function of time, previously defined as the dynamic mass variation. A fair approximation at short durations, where $M_t/M_\infty \leq 0.6$, is given by the following expression (Karimi, 2011).

A detailed development of the resolution of Fick's second law can be consulted in our previous works (Zemzem, Vinches et Hallé, 2017b):

$$\frac{M_t}{M_\infty} = 4\left(\frac{D}{\pi}\right)^{1/2} \cdot \left(\frac{\sqrt{t}}{h}\right) \tag{4.5}$$

Therefore, the diffusion coefficient can be graphically deduced from the slope of the reduced sorption plot overlaying the experimental data of sorption. Interestingly, the reduced sorption

plot connects the dynamic mass variation with the normalized square root of time, which is expected to be linear for short time periods.

The solubility, *S*, of the studied materials is related to the chemical nature of both penetrant and polymer; it is the capacity of the polymer to uptake the solvent. The permeability coefficient, *P*, is defined as the volume of the penetrant that has past through a unit area of the membrane per unit time on a normalized thickness, all within a unit pressure difference across the system. This parameter depends on both solubility and diffusion coefficients of the process (Joseph, Mathai et Thomas, 2003); it is therefore defined as:

$$P = D \times S \tag{4.6}$$

4.5.3 Concentration profile

From a practical point of view, knowing the depth of penetration of a given diffusing substance into a structure is valuable information, especially when considering the storage of liquids in containers made of polymers. It was previously explained that liquid penetration through polymeric systems is a diffusion process governed by Fick's second law.

Solving the differential equation under the described conditions gives (Aminabhavi, Harlapur et Ortego, 1997):

$$\frac{C(x,t)}{C_\infty} = 1 - \frac{4}{\pi}\sum_{n=0}^{\infty}\frac{1}{(2n+1)}\exp\left(\frac{-(2n+1)^2\pi^2 D}{h^2}\cdot t\right)\times\sin\left(\frac{(2n+1)\pi}{h}\cdot x\right) \tag{4.7}$$

where $C(x,t)$ is the concentration of the penetrant liquid at a fixed time *t* and at a distance *x* from the membrane surface, C_∞, also labelled C_{inf} in the figures, is the liquid concentration at equilibrium and *D* is the approximated diffusion coefficient, assumed to be constant for short time periods; values of *D* are calculated based on equation (4.5).

4.6 Results and discussions

4.6.1 Dynamic solvent uptake

First, it is important to assess the concentration loading effect on the barrier properties. In fact, achieving a noticeable level of enhanced chemical resistance requires the addition of a high concentration of nanoclays. However, excessive amounts of filler lead to bulkiness as well as loss of transparency, whereas moderated amounts of nanoclays are expected to enhance the chemical resistance of the nanocomposite and improve its mechanical properties and structural characteristics. The evaluation of kinetic parameters of molecular transport must take into consideration the geometric properties of the tested sample, namely its thickness. Hence, sorption data are interpreted using reduced sorption plots. In these plots, the dynamic mass variation of the immersed sample is portrayed as a function of the root of the normalized time: $M_t/M_\infty = f(t^{1/2}/h)$. For instance, Figure 4-1 represents the dynamic mass variation of RCN specimens loaded with different concentrations of nClay/1; 1, 3, 5, 10 and 15%. The mass uptake curve of pure NBR (NBR/P) is also presented in the same plot as a reference. Immersion tests are conducted in methanol. Incidentally, the average standard deviation of all sorption measurements in what follows is less than 1.8%. The resulting curves start off showing linearity up to around 60% of saturation, after which they exhibit concave behavior towards the x-axis until approaching the sorption equilibrium values. From the described plot, it is noticed that sorption behavior is proportional to the nClay content. The rate of mass uptake increases as the filler concentration increases. Comparable dependence is mentioned in the literature for different elastomers, such as ethylene propylene diene methylene rubber (Wu et al., 2018). In addition, and based on sorption data at equilibrium, sorption at saturation state is found to decrease as nClay/1 concentration increases from 1 to 15%. This observation is justifiable. In fact, sorption at equilibrium corresponds, by definition, to the maximum amount of solvent that a given sample can accommodate in its structure. On the other hand, nClays are inorganic impermeable fillers. Hence, for a given sample volume, the more nClay in the structure, the less available space there will be for absorption. Under these circumstances, it was decided that the concentration

in nClay would be 5%. Furthermore, reduced sorption plots were used with approximations using Fick's law to calculate the diffusion coefficients of polymer/penetrant systems.

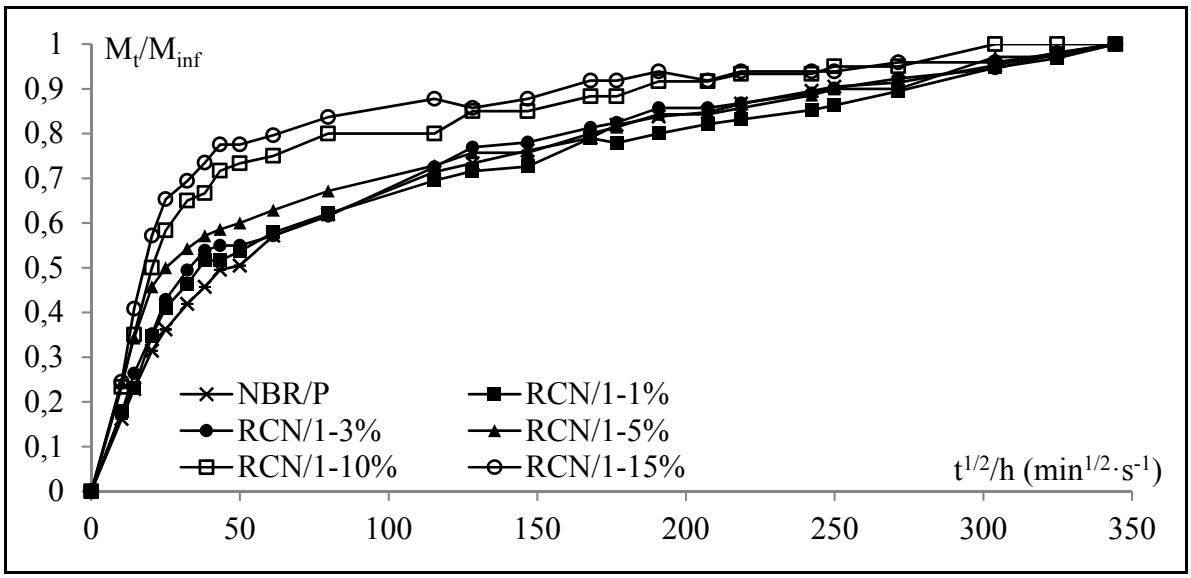

Figure 4-1. Dynamic mass variation in methanol of NBR/P and RCNs at 1, 3, 5, 10 and 15% of nClay/1 as function of normalized time

Molecular transport through dense rubber/clay nanocomposite membranes is suspected to be sensitive to the molecular size of the penetrant substance (George et Thomas, 2001). Therefore, sorption experiments were conducted using three solvents, methanol, ethanol and isopropanol (see Tableau 4-1), each differing by a constant molecular volume of 18 $cm^3 \cdot mol^{-1}$. As the molecular diffusion is a temperature-activated process, sorption data is considered as an excellent guide to study the effect of temperature on the mass transport behavior. Hence, sorption experiments with each solvent are performed at 23, 40, 55 and 70°C. Associated data are presented in Tableau 4-2. Parts of these results are illustrated in Figure 4-2 and Figure 4-3.

Mass uptake occurs when solvent is adsorbed. As a general observation, one can notice that all curves exhibit the similar characteristic behavior of polymeric materials. Due to the high concentration gradient of the solvent in contact with the surface of the specimen at first exposure, the rate of mass uptake is observed to be relatively high. The polymeric sample

was instantaneously exposed to intense solvent stress and the polymeric macromolecules are expected to respond elastically to the presence of the penetrant particles. Over the duration of exposure, the small penetrant molecules cause the polymeric chains to relax, producing more space for the solvent to occupy (Haseeb et al., 2011). As the immersion time increases, the rate of mass uptake gradually decreases until it reaches a plateau corresponding to a state of equilibrium in which no more solvent is being absorbed.

Figure 4-2 illustrates the sorption data of NBR/P, RCN/0, RCN/1 and RCN/2 in isopropanol at 23, 40, 55 and 70°C. At first sight, mass uptake behavior over time is almost identical for all temperatures. Nevertheless, sorption attains the equilibrium state more quickly as the temperature increases. In fact, steady state is not achieved before 540 min of immersion at 23°C, while it is reached in 310 min at 70°C. The same trend occurs with intermediate temperatures therefore not all data was graphically represented to avoid redundancy. A reduced sorption plot associated to the above sorption data confirms this finding; curves exhibit linearity up to around 60 to 65% of mass uptake. Also, it was remarked that the slope of the linear segment is steeper the higher the temperature. These findings are directly related to the kinetic of mass transfer that will be discussed in the following sections. From another perspective, the proportion of sorption at saturation exhibits a systematic increase as the temperature regularly increases. It was noticed that for all temperatures, the nature of the nanoclay does not seem to have a substantial effect on the value of sorption at saturation. In what follows, RCN/1 is considered to illustrate the effect of temperature. From 23 to 55°C, the maximum of solubility rises from around (12.5 ± 1.1) % at regular intervals of about 6 to 7%. For the immersion test at 70°C, the maximum sorption value rises by a factor of almost twice the mass uptake percent interval observed with the intermediate temperatures and sorption at equilibrium was reached at (43.6 ± 1.3) %. The temperature effect is also investigated with methanol and ethanol. To reduce the number of figures, associated sorption data curves are not portrayed. The same trend is observed with both alcohols and the regular increase of temperature results in an augmentation of the sorbed amount of solvent at equilibrium. The augmentation of solubility as the temperature increases is a straightforward deduction in thermodynamics. Indeed, for a liquid to dissolve in a polymeric structure, the

total free energy of mixing should be negative, and the more negative it is, the higher the solubility. Since solvent molecules in their liquid state exhibit a highly chaotic arrangement, the associated entropy ΔS tends to be positive. In addition, the effect of temperature on the process is embedded within the entropy term of Gibbs' free energy of mixing, an increase in temperature is generally followed by an increase of solubility (Poon, Castellino et Cheng, 2007). Yet interestingly, temperature has a lesser effect on the sorption of methanol. The values of sorption at saturation vary more systematically with the increase of temperature, but with an interval of mass uptake barely exceeding 5%. No particular jump of sorption was noted at 70°C as with isopropanol.

Figure 4-3 portrays the mass percent uptake data of NBR/P, RCN/0, RCN/1 and RCN/2, at 23°C, in methanol, ethanol and isopropanol. Homologous results at 40, 55 and 70°C are also examined although not graphically represented. Here again, sorption plots of all solvents follow the same tendency as the typical mass uptake curve of a liquid/polymer system. However, the nature of the penetrant seems to have a substantial influence on the extent of sorption at equilibrium. Indeed, the methanol pattern of mass gain starts with a high rate then levels off at about 495 min. The same behavior was noted for the isopropanol curve except that equilibrium state was reached at around 540 min of immersion time. A more significant effect is observed on the solubility coefficient. Indeed, while methanol attains saturation at (20.7 ± 1.7) % of mass uptake in RCN/1, isopropanol does so at (13.4 ± 0.9) %, for the same nanocomposite and same immersion time of 850 min. An intermediate value is exhibited by ethanol. Similar conclusions are reported in a study involving solubility and diffusion of a number of hydrocarbons through poly(dimethyl-siloxane) (Cocchi, De Angelis et Doghieri, 2015). The authors state that the molar solubility is inversely proportional to the penetrant's chain length. And as the solubility is governed by entropic effects, polymeric chain segments exhibit higher affinity to smaller molecules. A related point to consider is that the solubility is clearly affected by the presence of nanoclays, namely in the case of methanol. Further inspection of this will be provided in upcoming sections. Let us consider the evolution of the gap of sorption between the solvents as a function of temperature. Starting with ethanol and isopropanol, it is noted that isopropanol molecules are less taken up by about 4% by the

RCN/1 sample than the ethanol molecules at room temperature. This gap lessens as temperature increases until almost vanishing at 70°C within the interval of measurement error. Surprisingly, methanol seems to exhibit a less systematic behavior. The associated solubility coefficient increases as temperature increases as expected, but at a lower rate (around 5% per 15°C) compared to the other solvents. As a result, the sorption of methanol attains saturation at 32.8%, which is more than 10% lower than isopropanol.

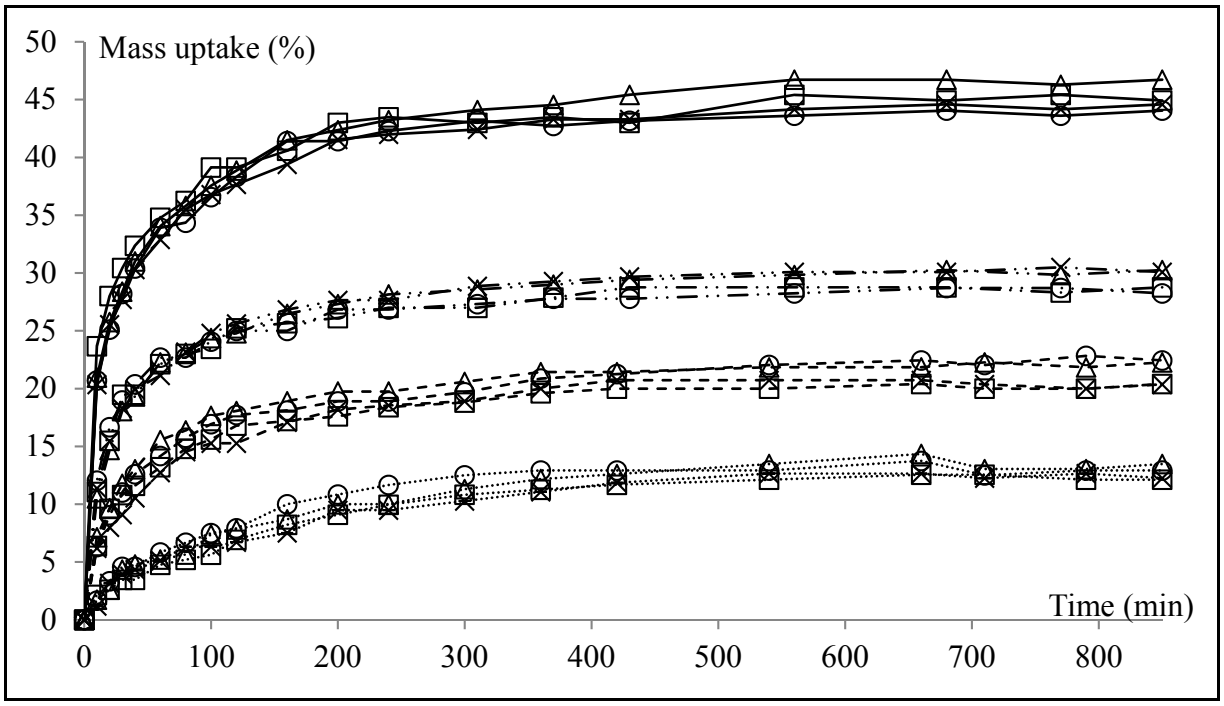

Figure 4-2. Mass uptake of NBR/P and RCN for different nClays in isopropanol at different temperatures.
Line styles refer to Temp.: (⋯) 23°C, (− −) 40°C, (− ··) 55°C and (——) 70°C
Legend :(×) NBR/P, (□) RCN/0, (○) RCN/1 and (△) RCN/2

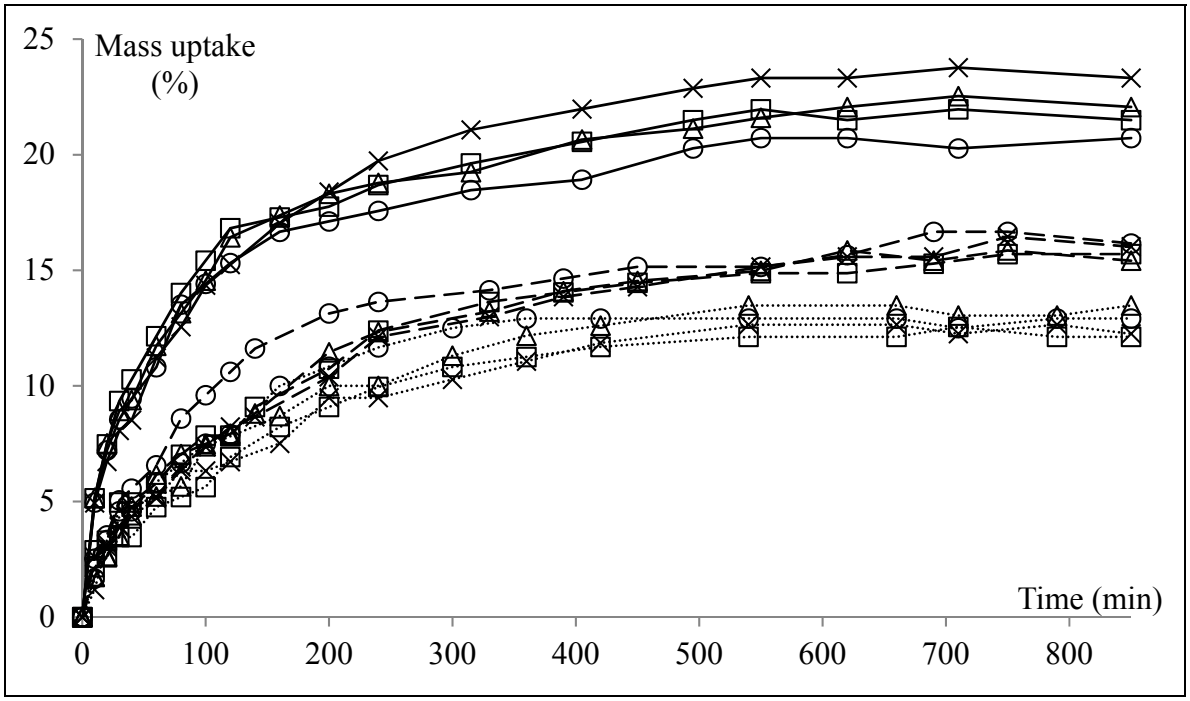

Figure 4-3. Mass uptake of NBR/P and RCN for different nClays in different solvents at 23°C. Line styles refer to: (···) isopropanol, (− −) ethanol and (−−) methanol
Legend :(×) NBR/P, (□) RCN/0, (○) RCN/1 and (△) RCN/2

Tableau 4-2. Solubility coefficients (S) of NBR/P and RCNs in methanol, ethanol and isopropanol at four different temperatures (23, 40, 55 and 70°C)

Solvent	T°	NBR/P	RCN/0	RCN/1	RCN/2
Methanol	23°C	20.63	21.03	18.47	19.25
	40°C	27.36	26.46	24.62	26.54
	55°C	34.42	32.45	29.15	31.34
	70°C	39.81	36.26	32.82	34.85
Ethanol	23°C	12.99	13.64	14.14	13.22
	40°C	22.47	21.63	22.27	23.04
	55°C	33.19	33.47	36.97	36.84
	70°C	47.20	45.63	46.46	47.48

Tableau 4 2. (Suite)

Isopropanol	23°C	10.28	10.82	12.50	11.30
	40°C	18.91	18.80	19.69	20.59
	55°C	30.08	28.76	28.24	29.83
	70°C	44.16	45.41	43.61	46.72

The permeability of low molecular weight substances through a membrane structure involves matter migrating from one side to the other. For organic dense elastomeric matrices, a conceptual understanding of the phenomena is to say that this transport process combines the sorption of the small penetrants into the membrane's surface followed by the diffusion by concentration gradient through the structure. Permeability is thus intrinsically linked to the ratio of the total path length travelled by the penetrant molecules over the thickness of the specimen. Diffusion and solubility are expected to be affected by the addition of inorganic and impermeable fillers in the polymeric matrix, such as clay nanoparticles. In effect, fillers act as obstacles forcing the penetrant molecules to work around them, increasing the tortuousness of available pathways. In addition, the presence of lamellar structure fillers, as is the case with nanoclays, is believed to modify the alignment of the adjacent polymeric macromolecules. This morphological modification results in an indirect alteration of the permeation mechanism (Manias, 2007). From a phenomenological perspective, a high degree of tortuosity is reached by increasing the specific surface of the filler capable of creating a maze path that slows down molecular penetration. In the case of nanoclays, specific surface enhancement, while keeping low filler loading, is only possible by increasing the extent of dispersion. RCNg/1 is a maleated nanocomposite that was synthetized in our previous work. It exhibited a higher state of dispersion compared to conventional RCN/1. In what follows, molecular transport characteristics are investigated according to the structural properties of the nanocomposite. In every case, results are compared to the unfilled rubber matrix.

Figure 4-4 displays percent mass uptake curves of NBR/P, RCN/1 and RCNg/1 in methanol at 40°C and 70°C. For both temperatures, a consistent trend can be observed; solubility

coefficient in methanol decreases with the presence of layered silicate fillers (RCN/1), the coefficient is even lower with maleated nanocomposite (RCNg/1). At 40°C, sorption of methanol is reduced from 30.2% to 26.6% with the addition of nClay/1 in the conventional nanocomposite. Mass uptake at saturation drops by an additional 4% after maleation of the nanocomposite. At 70°C, the effect of the nanoclay is more pronounced. The difference in mass percent uptake between NBR/P and RCN/1 decreases twofold compared to sorption data at 40°C. However, sorption is slightly reduced during maleation.

For all three materials, the effect of the penetrant's nature is also examined and the associated sorption data in methanol and isopropanol at 55°C are displayed in Figure 4-5. The same previously observed tendency appears preserved. For methanol, sorption data for the three materials follow the same behavior observed at 40 and 70°C. It can even be observed that the sorption pattern follows the trend of high temperatures and is closer to that examined at 70°C. The solubility coefficient values lay in the intermediate zone between the coefficients associated to 40 and 70°C. Interestingly, higher molecular volume penetrants deviate from the previous bias. In actual fact, sorption at equilibrium in isopropanol barely decreased while loading with nClay/1. Nevertheless, a drop of about 5% is clearly spotted with the maleated nanocomposite. Not shown in the figure but worth mentioning, ethanol sorption data exhibit intermediate values.

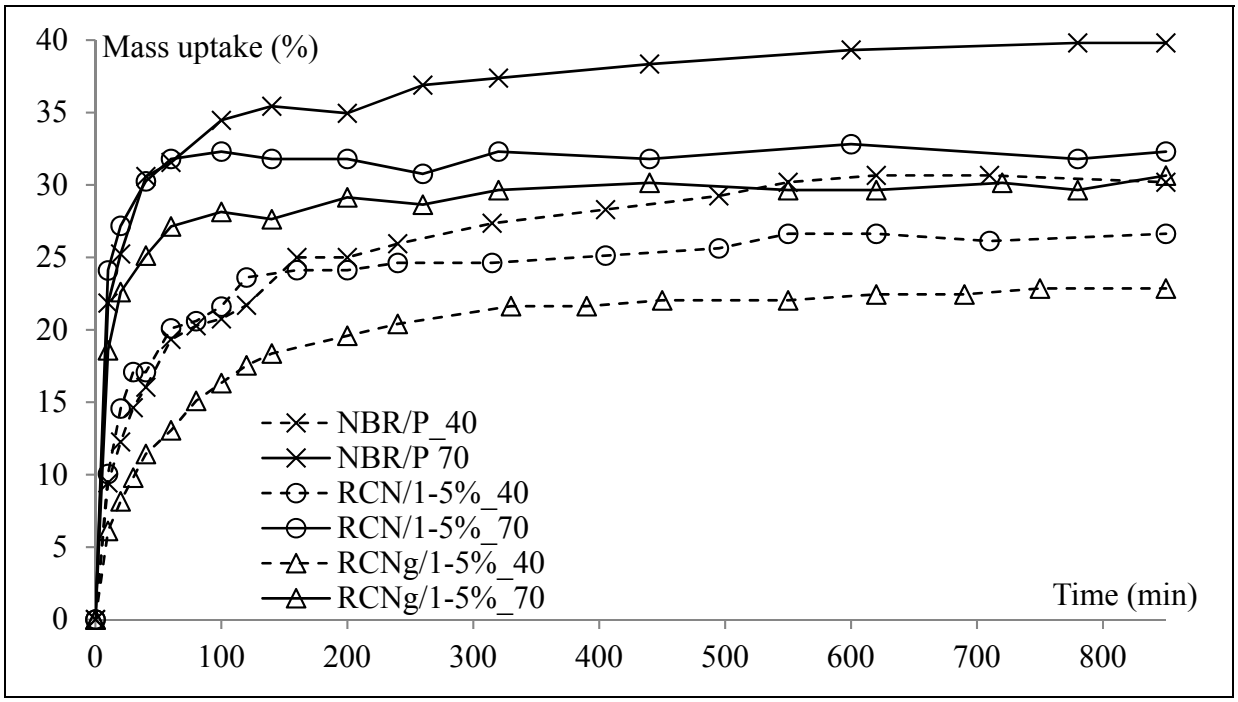

Figure 4-4. Comparison of mass uptake of NBR/P, RCN/1 and RCNg/1 in methanol at 40°C and 70°C

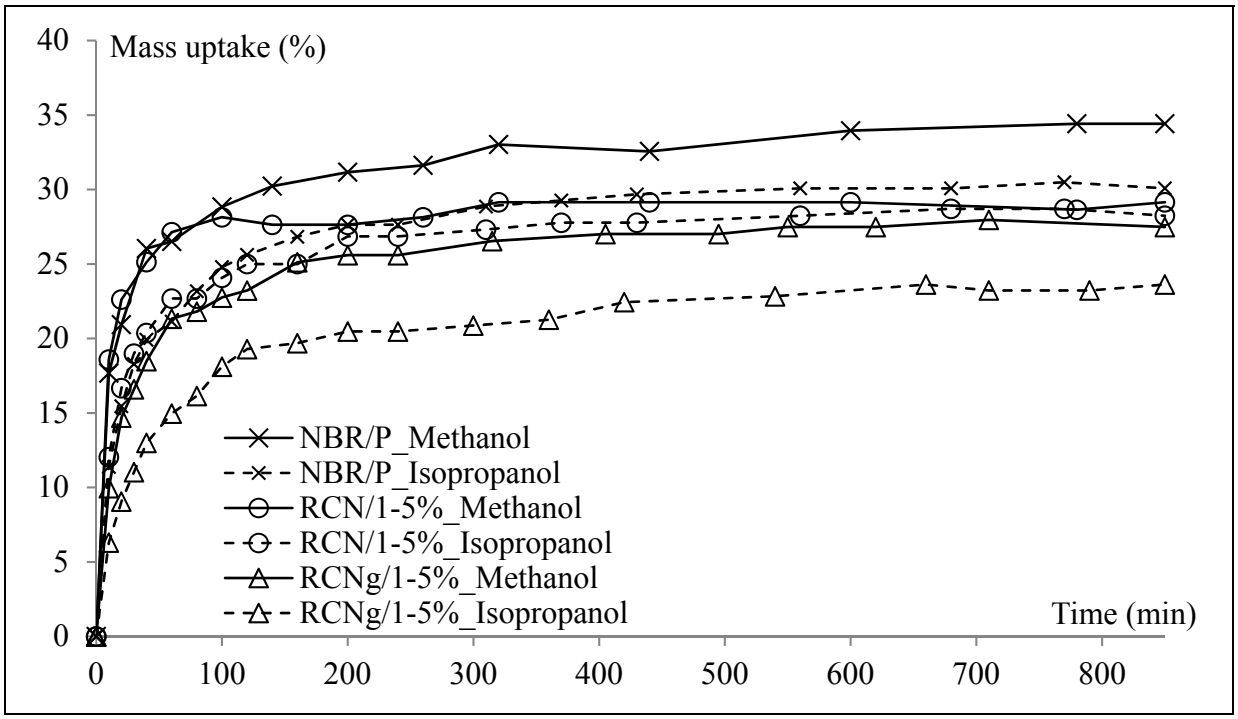

Figure 4-5. Comparison of mass uptake of NBR/P, RCN/1 and RCNg/1 in methanol and isopropanol at 55°C

4.6.2 Mass transfer mechanism

Let us investigate the molecular transport phenomenon from a mesoscopic point of view and let us only consider the diffusion phase of the process. It was stipulated that a net mass transport within a polymeric medium takes place from the high to low concentration spot. In this statistical approach, only the mean displacement of all involved penetrant molecules from their starting to ending positions is considered. But when considering individual molecules, the diffusion of each particle consists of a random constant motion from one free volume to another with no privileged direction. Free volumes are the result of polymeric chain entanglement. These tiny holes appear and disappear at the same rate as the penetrant molecule displacements. Diffusion is thus dictated by the redistribution of the unoccupied volume (Baker, 2012). Thus, the diffusion mechanism of a penetrant/polymeric system is classified depending on the molecular penetration rate compared to the mobility of the polymeric macromolecules. Being thermo-dependent, the diffusion behavior is expected to vary as the temperature varies. In addition, the diffusion process relies on the relaxation of the polymeric segment, which consequently, is believed to be affected by the molecular volume of the penetrant.

The empirical relation expressed by equation (4.3) was chosen to numerically estimate the diffusion mode of the systems investigated in this study. A very good correlation is obtained for all regressions ($R^2 > 0.98$). Tableau 4-3 summarizes the entire set of diffusion mechanism index *n*, as well as interaction factor *K* of NBR/R and the three RCNs with all three solvents at the four previously listed temperatures. A few key observations are worth pointing out. It may be noted that the values of the factors exhibit systematic increase as temperature increases. This supports the premise of increased polymer/solvent interaction. The same trend is confirmed for all the solvents. As indicative information, the interaction factor of the RCN/1/isopropanol system goes from (52 ± 4) to (213 ± 17) $\times 10^{-3}$ $g \cdot g^{-1} \cdot min^{-n}$ within the [23, 70°C] temperature interval. Furthermore, the *K* factor varies linearly along with the temperature with a slope of about 54×10^{-3} $g \cdot g^{-1} \cdot min^{-n}$/15°C. An exception was observed with methanol, *K* rises with the temperature until 55°C then drops slightly at 70°C. When

investigating the solvents in this regard, no obvious correlation is noted between the magnitude of *K* and the nature of the penetrant alcohol. This result is understandable since all three solvents exhibit similar chemical structures and no different interactions are expected with the polymeric materials. This tendency is also noticed with all conventional nanocomposites (RCN/0, RCN/1 and RCN/2), but nothing can be said about the influence of the nature of the nanoclay on this parameter. To emphasize the influence of nanoclays in conventional and maleated nanocomposites, the associated least-square estimations of *K* with methanol are depicted in Figure 4-6 from 23 to 70°C. It clearly shows that the presence of the nanoparticles intensifies *K* up to 55°C suggesting an increase of the matrix/solvent interaction due to the presence of the filler. Thereafter, a substantial drop in the interaction parameter is witnessed after the maleation of the nanocomposite. The data at 70°C are an exception.

Let us shed light on the diffusion mechanism index under the described considerations. Still from data presented in Tableau 4-3 and starting with the effect of temperature, a general remark can be made. Factor *n* diminishes slightly as temperature increases. The deduction is valid for all solvents except for methanol at 70°C. The index varies in a general way from around 0.5 at 23°C up to values approaching 0.3 at 70°C. Although below 0.5, this mechanism is still classified as Fickian and it is generally termed as sub-Fickian behavior. In Fickian mode, the rate of chain-segment relaxation is higher than the rate of the penetrant diffusion. The drop of the diffusion behavior index involves an increase in macromolecule mobility. According to the results, this mobility is induced by the elevation of the temperature. Considering data from the perspective of the penetrant's nature, not much can be said and there is no systematic evolution with the change in solvent. It is noteworthy, however, that the diffusion mechanism is Fickian with all the penetrants and *n* index laying between sub-Fickian and Fickian thresholds. Truthfully, it was expected that the increasing molecular volume from methanol to isopropanol would reduce the diffusion rate of the penetrants and result in a systematic drop of the mechanism index, which is not the case. Indeed, the previous hypothesis was not validated, because the temperature effect was omitted. In other words, temperature is the most influential parameter in the mass transfer

process. When increasing the temperature, the effect observed is a rise in the segmental mobility of the chains, but also an increase in the diffusivity rate of the molecular penetrants. At a particular range of temperature, this fact overcomes the effect of the molecular size of the penetrant. This conclusion is even more pronounced when the results that follow are investigated. To demonstrate the impact of nanoclay fillers on the diffusion mechanism, *n* index of NBR/P, RCN/1 and RCNg/1 is estimated with all solvents at all temperatures. An example of the data is shown at 40°C with the three solvents in Figure 4-7. The neat nitrile rubber exhibits the lowest diffusion mechanism index. The associated values are (0.37 ± 0.01), (0.45 ± 0.02) and (0.41 ± 0.02) with methanol, ethanol and isopropanol, respectively. With the addition of clay nanoparticles, there is no noticeable change. The *n* index barely increased and diffusion still obeys Fick's law. This applies to all present solvents. Interesting behavior was observed with the maleated nanocomposites: associated diffusion indexes show substantial increases. The *n* values reach a maximum of (0.58 ± 0.05) with ethanol and isopropanol. Therefore, the diffusion mechanism deviates from Fickian to anomalous behavior. In fact, over the delamination of the layered silicate nanoparticles and the dispersion of the inorganic nano-platelets in the polymeric structure, a restriction of the segmental chain mobility in the polymeric medium occurred. In this configuration, lamellar silicates have a similar effect to crystals in glassy polymers. Finally, it should be noted that the described pattern only occurs within a restricted temperature range: 40 to 55°C.

Tableau 4-3. Diffusion mechanism index and constant *K* of NBR/P and RCNs with methanol, ethanol and isopropanol at four different temperatures (23, 40, 55 and 70°C)

		n				*K* ($\times 10^{-3}$)			
Solvent	T°	NBR/P	RCN/0	RCN/1	RCN/2	NBR/P	RCN/0	RCN/1	RCN/2
Methanol	23°C	0.47	0.45	0.46	0.43	69	82	88	94
	40°C	0.38	0.41	0.39	0.43	137	145	170	143
	55°C	0.36	0.36	0.38	0.39	211	251	255	230
	70°C	0.35	0.61	0.62	0.61	227	167	175	167

Tableau 4 3. (Suite)

Ethanol	23°C	0.51	0.45	0.59	0.57	42	62	38	34
	40°C	0.46	0.43	0.46	0.47	88	98	94	95
	55°C	0.34	0.30	0.32	0.30	171	190	194	203
	70°C	0.30	0.29	0.32	0.33	195	237	216	198
Isopropanol	23°C	0.46	0.54	0.51	0.52	59	42	52	45
	40°C	0.42	0.37	0.44	0.44	110	144	108	119
	55°C	0.41	0.42	0.42	0.44	149	152	159	128
	70°C	0.32	0.32	0.32	0.32	210	235	213	204

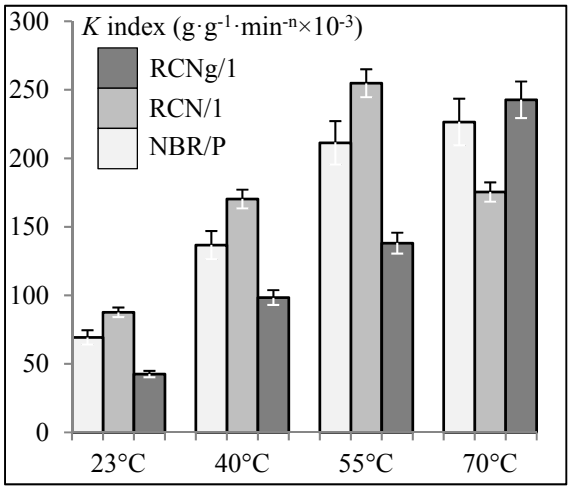

Figure 4-6. Constant *K* of NBR/P, RCN/1 and RCNg/1 with methanol at 23, 40, 55 and 70°C

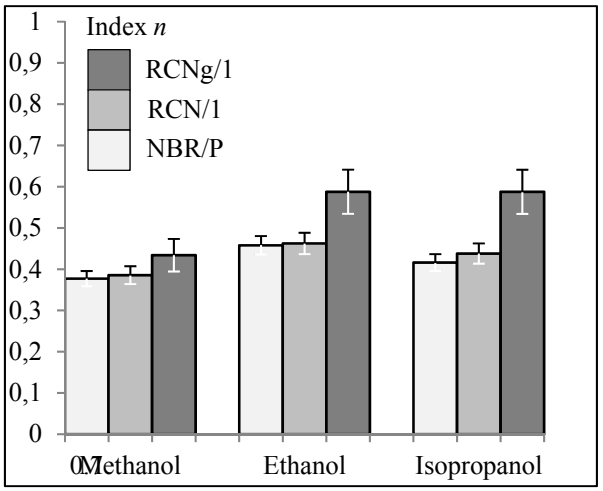

Figure 4-7. Diffusion index of NBR/P, RCN/1 and RCNg/1 with all solvents at 40°C

4.6.3 Diffusion coefficient and permeability

The diffusion mechanisms of the systems under investigation are demonstrated to be more or less Fickian. Dynamic solvent uptake is therefore expected to exhibit linear dependence, for short durations, to the normalized square root of time. Hence, a fine approximation of the diffusion coefficient can be estimated based on Fick's second law of mass transfer. Figure

4-8 shows histograms of the overall diffusion coefficients of NBR/R and the three RCNs with methanol, ethanol and isopropanol at the four formerly designated temperatures. Several comments can be made based on the data presented. Firstly, a clean and concise augmentation of the diffusion coefficients appears as the temperature increases from 23 to 70°C. The trend is observed with all polymer/solvent systems. Temperature seems to intensify every aspect related to the molecular migration process. The most pronounced variation is associated to the smallest molecular penetrant. For instance, the *D* coefficient of RCN/1/methanol surges from $(2.7 \pm 0.3) \times 10^{-8}$ $cm^2 \cdot s^{-1}$ at 23°C to $(28.2 \pm 1.1) \times 10^{-8}$ $cm^2 \cdot s^{-1}$ at 70°C. A similar tendency is observed with ethanol and isopropanol, but the rate of variation is smaller. For example, when the temperature rises from 23 to 70°C with isopropanol, the diffusion coefficient increases from $(1.6 \pm 0.2) \times 10^{-8}$ $cm^2 \cdot s^{-1}$ to $(7.5 \pm 0.3) \times 10^{-8}$ $cm^2 \cdot s^{-1}$, respectively. Consequently, a systematic behavior is deduced with the variation of the penetrant size. Indeed, Figure 4-8 clearly shows a strong reduction of coefficient *D* as the molecular volume of the penetrant increases. The diminution appears to follow a logarithmic pattern and the observation remains valid for all temperatures. The findings are in agreement with research carried out on aromatic hydrocarbons (Rusina, Smedes et Klanova, 2010). The same observations are reported in the work of Moller et al. on the diffusion of phenols (Möller et Gevert, 1994) and the logarithm of *D* was found to linearly decrease as the molecular size increased. This results from the geometric requirements of the penetrant molecule based on the penetration process governed by a "jump to a free volume" mechanism. It should be noted that the molecular size of the penetrants is assimilated to the molecular volume since there is no significant variation of bond angles or chain conformations between the molecules of the investigated solvents. Isopropanol shows the lowest *D* values. A related point to consider is that isopropanol has a branched structure. Previous studies show that linear molecules exhibit higher diffusivity and any ramification in the structure is expected to restrain movement and decrease their diffusion coefficient (Aminabhavi et Khinnavar, 1993). Incidentally, diffusivity can also be correlated to the penetrant solvent's viscosity. In alcohols, viscosity systematically increases as the amount of atom carbons in the structure increases. Studies by Vahdat et al. establish a reciprocity

between the diffusion coefficient and the viscosity of solvents in elastomeric systems (Aminabhavi et Phayde, 1995).

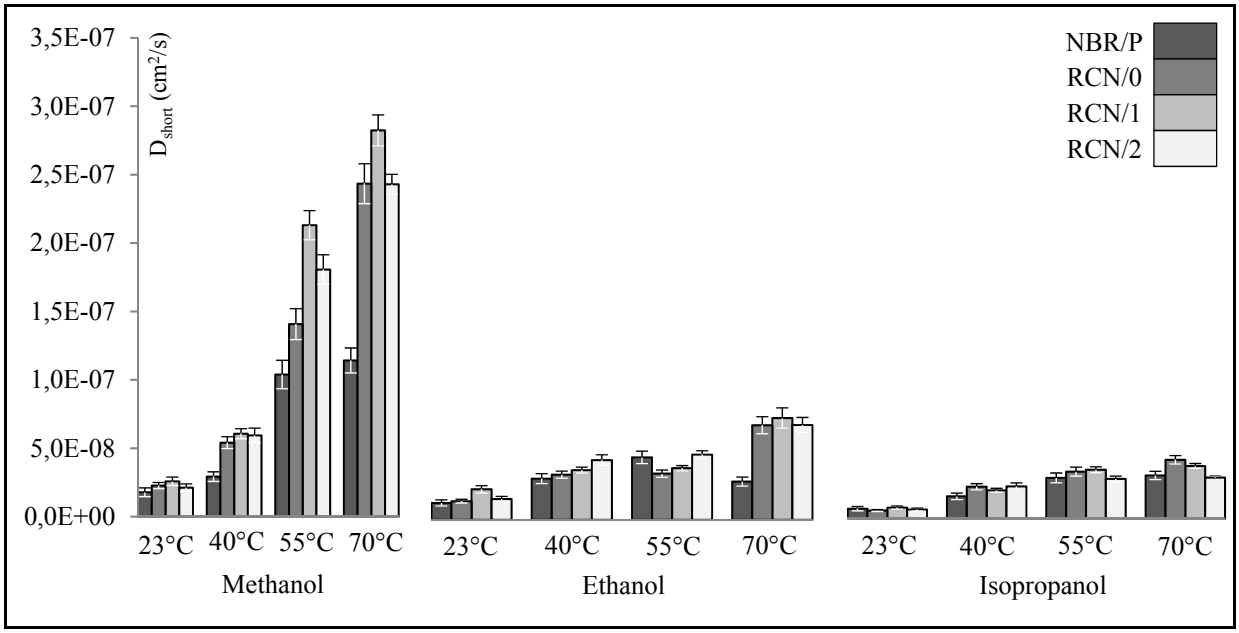

Figure 4-8. Diffusion coefficients of methanol, ethanol and isopropanol in NBR/P, RCN/0, RCN/1 and RCN/2 at 23°C, 40°C, 55°C and 70°C

The following section investigates the effect of the presence of nanoclays on the diffusion coefficients. Since the early works of Nielsen, filled polymeric matrices with inorganic layered silicates are suggested to increase the tortuous path of the diffusing molecules. The proposed model is supposed to result in filled materials having enhanced barrier properties (Tan et Thomas, 2017). This theoretical approach is only valid when considering nanoclay fillers as impermeable and as having perfectly separated nano-platelets that are totally aligned perpendicularly to the diffusion direction. In Figure 4-9, the diffusion coefficients of NBR/P, RCN/1 and RCNg/1 with methanol are compared at four temperatures. The diffusion coefficients of the same materials in methanol, ethanol and isopropanol at 23°C are presented in Figure 4-10. In general, temperature and molecular volume have the same previously-described effects on all three materials. *D* increases exponentially as temperature increases with respect to Arrhenius' relation and decreases in logarithmic fashion as the penetrant molecular volume linearly increases. Interestingly, randomly filled nanocomposites exhibit higher *D* coefficients compared to the unfilled nitrile rubber. The same can be seen with all

solvents and at all temperatures. For instance, the diffusion coefficient of methanol in RCN/1 at 70°C doubles with NBR/P in the same conditions. This observation is directly associated to the poor state of dispersion of the nanoclays in the matrix. In fact, it was shown in our former work that RCN/1 exhibited weak interfacial interaction with the rubber chains due to chemical incompatibility and lack of affinity. During the diffusion process, penetrant molecules are believed to accumulate in the nanoclay/polymer interfacial zone. From there, the penetration mechanism is established through the communication of the charged cavities, which is thought to cause the increase in the rate of diffusion. More interestingly, the diffusion coefficient with the three solvents and at the four temperatures is witnessed to encounter a substantial drop during maleation of the nanocomposite.

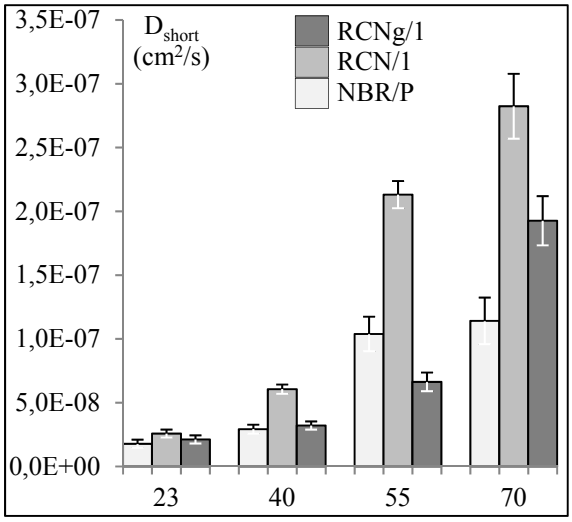

Figure 4-9. Diffusion coefficient of NBR/P, RCN/1 and RCNg/1 with methanol at 23, 40, 55 and 70°C

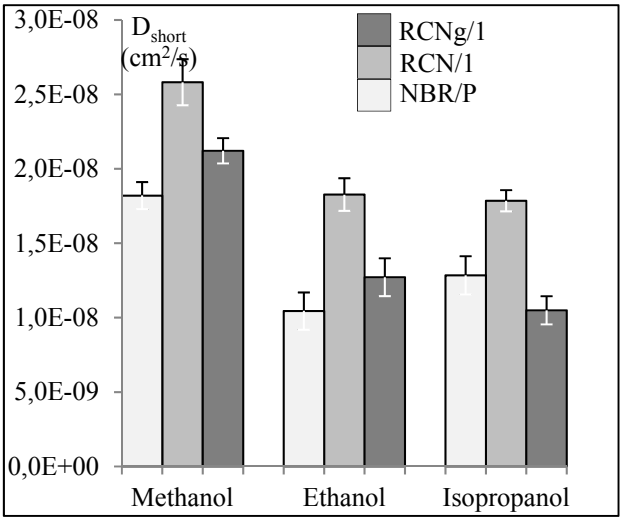

Figure 4-10. Diffusion coefficient of NBR/P, RCN/1 and RCNg/1 with all three solvents at room temperature (23°C)

To use an example from Figure 4-9, *D* in methanol at 55°C goes from $(21.3 \pm 1.0) \times 10^{-8}$ $cm^2 \cdot s^{-1}$ to $(6.6 \pm 0.7) \times 10^{-8}$ $cm^2 \cdot s^{-1}$. The reduction in diffusivity is a result of the nanoclays' improved state of dispersion, increasing the pathways of the penetrant. Moreover, the enhancement of the compatibility between the layered silicates and the rubber medium eliminates the cavities in which the penetrant tends to accumulate.

When the diffusion mechanism obeys Fick's law and the sorption process is governed by Henry's rule, the overall permeability of the solvent/membrane system can be determined by multiplying the coefficients of diffusion and solubility. As previously seen, diffusion slightly deviates from the Fickian mode under certain circumstances. Therefore, permeation coefficients calculated in this study are only considered as estimations. An obvious observation is that *P* values exhibit the same tendencies as diffusion coefficients for a given penetration system.

4.6.4 Concentration profiles

Probing the depth of liquid penetration in the membrane structure is valuable information for industrial purposes. However, sensing molecular penetration in a dense material over time is technically challenging and requires sophisticated equipment to obtain reliable data. After demonstrating that mass transfer in the systems under investigation are predominantly ruled by Fickian laws, an approximation of the penetrant concentration profile can be drawn based on the solution of Fick's second law, expressed by equation (4.7). In Figure 4-11 (a), concentration patterns of methanol in RCN/1 are displayed along the membrane's half-thickness at 23, 40, 55 and 70°C. It is noticed that at room temperature, the penetrant starts to penetrate the membrane at the exposed surface where the concentration should be at its maximum. Penetration continues until it reaches the centre at about 10 min of immersion time. Meanwhile, the concentration of methanol attains 85% of its limit at 70°C. The evolution of methanol concentration at the specimen center does not seem to follow a systematic trend. The concentration rises by a whole 55% by only increasing the temperature from 40 to 55°C.

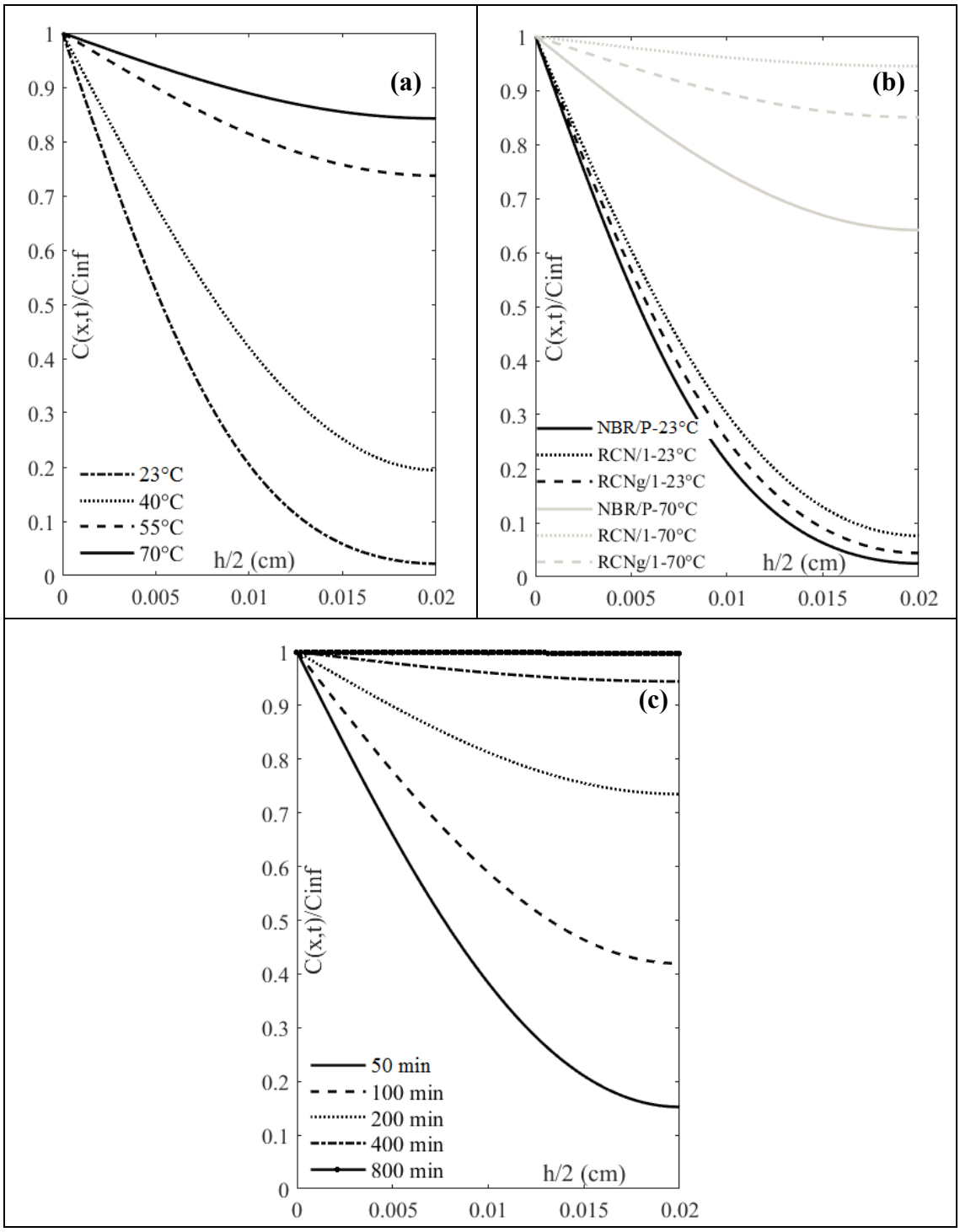

Figure 4-11. Concentration profiles of:
(a) methanol diffusion in RCN/1 at 23, 40, 55 and 70°C for 10 min of immersion time
(b) methanol in NBR/P, RCN/1 and RCNg/1 at 23 and 70°C for 30 min
(c) methanol in NBRg/1 at 23°C for a time interval ranging from 50 to 800 min

In order to visualize the effect of the nanoclays on the penetration patterns of methanol, $C(x,t)/C_{inf}$ curves associated to NBR/P, RCN/1 and RCNg/1 at 23 and 70°C are presented in Figure 4-11 (b). The graph indicates that after 30 min of immersion, less than 10% of the liquid reaches the core of the tested samples. There is no significant variation between the three materials worth reporting. However, it should be mentioned that the values of concentration follow NBR/P< RCNg/1< RCN/1. At 70°C, the same order is maintained with an enlargement of the concentration gap at the center between the three materials. For instance, when the conventional nanocomposite achieves 95% of the concentration at equilibrium, the concentration of the maleated nanocomposite is 10% lower for the same immersion time of 30 min. Lastly, the analytical modeling of the mass transfer process makes it possible to infer the evolution of the penetrant's presence at the center of the sample over time. Hence, Figure 4-11 (c) displays curves of $C(x,t)/C_{inf}$ of methanol as a function of the membrane at half-thickness at room temperature for different time lapses ranging from 50 to 800 min. The concentration of methanol in the rubber matrix increases until reaching a maximum at 800 min. At this state of saturation, the concentration of the penetrant equals its initial concentration on the interface, and this in every point of the sample structure.

4.7 Conclusions

Achieving a high level of layered silicate dispersion in a nitrile rubber-based nanocomposite is quite challenging. Physical mixing of the nanometric fillers with the elastomeric matrix does not guarantee enhanced barrier properties. In our previous work, a specially made nanocomposite with a high degree of exfoliation was developed with maleation. In the present study, the chemical resistance of this maleated nanocomposite was compared to that of a conventional filled-material at four different temperatures ranging from 23 to 70°C.

Mass uptake experiments based on a gravimetric technique were adopted to assess mass transport characteristics in three alcohols: methanol, ethanol and isopropanol. With all materials and regardless of the immersion medium, findings show a substantial increase of

molecular transport parameters with the increase in temperature. These parameters were also found to be inversely proportional to the molecular volume of the penetrant, the only exception being methanol at 70°C. When it came to filling the rubber matrix with nanoclays, the sorption at equilibrium decreased proportionally with the concentration of filler. The decrease was seen to be intensified with the nanoclays' enhanced state of dispersion. Conversely, diffusivity was clearly noticed to be more sensitive to the morphological properties of the nanocomposite. The presence of bulky fillers within the elastomeric system seemed to negatively affect the diffusion coefficient, which was observed to increase with the addition of 5% of nanoclays, after which, a substantial decrease in diffusivity was witnessed during maleation. The permeation coefficient behaved in the same way and followed the *D* coefficient pattern. Although slightly altered by the presence of nano-fillers, the diffusion mechanism in all solvents kept behaving in a Fickian mode, which gives more credibility to our calculation of mass transfer kinetics, using approximations from models of Fick's law.

The maleated nanocomposite succeeded in enhancing the barrier properties of the native nitrile rubber to some extent. However, more work must be done to optimize the developed material. In addition, more sophisticated techniques must be used to accurately probe molecular migration characteristics through the polymeric structure. Moreover, temperature was seen to have a substantial effect on all parameters of mass transport. Therefore, a thermodynamic study should be carried out on the molecular migration phenomena.

SYNTHÈSE DES RÉSULTATS ET CONCLUSIONS

Réussir la synthèse, la délamination, la dispersion et l'orientation des nanoargiles dans la structure polymérique est un facteur clé pour améliorer les propriétés d'un nanocomposite. Cette thèse a consisté à développer des matériaux nanocomposites, à base de caoutchouc nitrile, chargés par des nanoargiles lamellaires, avec des propriétés barrières optimisées. La démarche suivie est divisée en trois phases. D'abord, les procédures expérimentales permettant de synthétiser les nanocomposites ont été établies, étapes qui seront suivies par le contrôle de leur morphologie en termes de dispersion et d'orientation des nanoargiles au sein de la matrice polymérique. Ensuite, il s'agit d'optimiser la morphologie des nanocomposites par application de modifications chimiques sur la structure des chaines élastomères ainsi que sur les surfaces des lamelles nanoargile afin d'augmenter l'affinité chimique entre les nanoparticules et la matrice. Enfin, les propriétés barrières des nanocomposites optimisés à la pénétration de solvants organiques ont été évaluées.

L'ajout de nanoargiles dans la structure du caoutchouc nitrile par un simple mixage mécanique ne garantit pas l'obtention d'un nanocomposite. Cela est dû aux forces de Van der Waals qui relient les lamelles silicates au sein d'une particule ainsi qu'à la tendance des nanoargiles elles-mêmes à s'agglomérer. Trois techniques parmi les plus répandues dans la littérature ont été testées pour la synthèse de nanocomposites étudiés : i) mélange en solution, ii) mise en forme par mixage et iii) mise en forme par extrusion. Des nanoargiles de grade commercial traitées par un surfactant organique sont utilisées comme charge de renfort. La diffractométrie aux rayons X a montré que les lamelles silicates se sont espacées de près de 6 Å dans la matrice ce qui prouve l'intercalation des chaines élastomères dans l'espace interlamellaire. La mise en forme par extrusion produit une intercalation légèrement plus étendue que les autres techniques. Les observations par TEM confirment la morphologie décrite et montrent en plus une certaine délamination qui se traduit par la présence de lamelles individuelles. En outre, des analyses par diffusion des rayons X aux petits angles ont montré une orientation aléatoire des nanoargiles dans les nanocomposites produits par mixage et par solution. Toutefois, un alignement des nanoargiles selon les directions latérales

de la membrane est observé dans le nanocomposite extrudé. L'apparition d'un tel ordre est due aux forces de cisaillement appliquées sur l'échantillon par la buse de l'extrusion. Une analyse plus fine a montré que l'orientation est non homogène dans la structure de l'extrudat et l'alignement est privilégié sur les surfaces du matériau. Les propriétés barrières des nanocomposites obtenus ont été évaluées afin de les corréler aux modifications morphologiques observées. Les résultats ont montré que la prise de masse à l'équilibre a diminué de 13% avec un nanocomposite mixé et de 17% avec un nanocomposite extrudé. Les échantillons produits par mélange en solution ont présenté des valeurs intermédiaires. Afin de comprendre l'effet des paramètres de mise en forme dans le mixeur sur les propriétés barrières, les coefficients de cinétique de transport ont été mesurés pour des temps de résidence allant de 5 à 25 min et pour des contraintes de cisaillement allant de 25 à 155 N·m. Il a été montré que la diffusivité ainsi que la perméabilité au sein du nanocomposite décroit en fonction de l'augmentation du temps de mixage. De même, ces coefficients diminuent en augmentant la contrainte appliquée jusqu'à atteindre un maximum à 95 N·m.

Selon les résultats présentés au chapitre 2, les paramètres de la mise en forme ne sont pas suffisants pour exfolier les nanoargiles dans la structure nanocomposite. Dans le chapitre 3, la compatibilité entre la matrice en caoutchouc nitrile et les nanoargiles a été optimisée afin de favoriser l'intercalation. Plus des deux tiers de la macromolécule associée est hydrophobe à cause de la structure chimique du polybutadiène, ce qui limite sa diffusion dans l'espace interlamellaire des nanoargiles. L'idée consiste à rendre la section décrite plus hydrophile en greffant un monomère à polarité élevée comme de l'anhydride maléique. D'autre part, deux types de nanoargiles organiquement modifiées, en plus des nanoargiles non traitées, ont été utilisées. L'ensemble des nanocomposites produits sont mis en forme par extrusion afin de maintenir l'orientation des nanoargiles. Avant la synthèse, une étude thermogravimétrique a été menée afin de s'assurer de la stabilité des agents tensioactifs qui sont soumis aux contraintes thermiques de la mise en forme. Les courbes TGA et celles de leurs dérivées ont montré que les tensioactifs ne se dégradent pas en dessous de 200°C et que les nanocomposites sont stables dans les conditions d'extrusion à 160°C. De plus, une analyse FTIR a été effectuée pour s'assurer du greffage du MA sur la chaine élastomère. Les spectres

obtenus ont montré des indices prouvant la présence du monomère greffé sur la section polybutadiène. Ensuite, l'effet des modifications chimiques sur la morphologie des nanocomposites a été examiné en croisant les résultats de trois techniques. En premier lieu, des analyses XRD ont montré que les tensioactifs terminés par des groupes hydroxyles assurent l'intercalation la plus étendue. En outre, la présence du MA a causé la quasi-disparition des pics de réflexion avec toutes les nanoargiles. Un résultat qui montre que les nanoargiles ont perdu leur structure empilée et qu'une morphologie exfoliée est susceptible d'être présente. En second lieu, une analyse EDX couplée à un MEB de haute résolution a été menée afin d'avoir un aperçu plus clair sur l'état de dispersion des nanoargiles. La représentation cartographique a prouvé la réduction de la taille des agglomérations et l'amélioration de l'homogénéité de la dispersion des nanoargiles en présence de MA. En dernier lieu, une observation localisée par TEM a permis la distinction d'une morphologie combinée intercalée/exfoliée. En effet, les micrographes ont montré d'une part la présence de lamelles individuelles et ont confirmé d'autre part les données de XRD sur la distance interlamellaire. L'orientation des nanoargiles est aussi discutée dans le chapitre 3 à travers une approche tridimensionnelle en se basant sur des résultats stéréographiques de SAXS. L'alignement est privilégié dans le sens de l'extrusion ainsi que le sens qui lui est tangentiel.

Dans le chapitre 4, les nanocomposites conçus avec un état d'exfoliation amélioré sont repris pour évaluer leurs propriétés barrières face à des solvants organiques. La résistance chimique des nanocomposites greffés en MA est comparée à celle d'un nanocomposite conventionnel à quatre températures différentes allant de 23 à 70°C. Des tests de prises de masse basés sur une technique gravimétrique ont été réalisés pour évaluer le transfert de masse à travers les échantillons, de trois alcools : le méthanol, l'éthanol et l'isopropanol. Avec tous les matériaux et quel que soit le milieu d'immersion, les résultats ont montré une augmentation substantielle des paramètres de transport moléculaire avec l'augmentation de la température. Ces paramètres se sont également révélés inversement proportionnels au volume moléculaire du pénétrant, la seule exception étant le méthanol à 70°C. Il a été montré également que la sorption à l'équilibre a diminué proportionnellement avec l'augmentation de la concentration des nanoargiles dans le système. Il est à constater que la diminution de la sorption s'est

intensifiée avec l'amélioration de la dispersion des nanoargiles. Sur le côté opposé, la diffusivité est clairement plus sensible aux propriétés morphologiques du nanocomposite. En fait, la présence de nanoargiles en tactoïdes au sein de la matrice semble affecter négativement le coefficient de diffusion, dont l'augmentation a été observée avec l'ajout de 5% de nanoargiles. Ensuite, une diminution substantielle de la diffusivité a été observée au cours de l'ajout de MA. Le coefficient de perméation se comporte de la même manière et suit le coefficient de diffusion. Bien que légèrement modifié par la présence de charges nanométriques, le mécanisme de diffusion avec tous les solvants reste Fickien, ce qui permet un calcul de la cinétique de transfert de masse basé sur des approximations de la seconde loi de Fick. Le nanocomposite greffé améliore les propriétés barrières du caoutchouc nitrile.

Pour conclure, la modification chimique de la structure élastomère par anhydride maléique combinée avec la fonctionnalisation des nanoargiles a permis l'obtention d'une morphologie homogène du nanocomposite. La dispersion des nanoargiles est améliorée, et les états exfolié et intercalé coexistent dans la structure. D'autre part, l'optimisation des paramètres de mise en forme a assuré un certain alignement des lamelles nanoargiles dans la membrane. Les modifications apportées aux nanocomposites ont des répercussions directes sur ses propriétés barrières. Des améliorations significatives ont été mesurées sur les paramètres de la cinétique de transport des solvants organiques.

LIMITATIONS, RECOMMANDATIONS ET PERSPECTIVES

L'objectif de la thèse est d'optimiser les propriétés barrière d'un nanocomposite en caoutchouc nitrile à travers l'optimisation de la dispersion et de l'orientation des nanoargiles dans sa matrice. L'exfoliation n'est pas optimale, mais un état combiné entre exfolié et intercalé est bel et bien obtenu. Certains paramètres auraient pu être mieux optimisés comme par exemple la vitesse de rotation des vis en extrusion afin d'améliorer l'exfoliation des nanoargiles.

Cependant, une augmentation de la température dans le baril d'extrusion risque de dégrader le matériau et les tensioactifs. La présence du MA fait augmenter la viscosité du nanocomposite ce qui le rend difficile à extruder et augmente la pression dans l'extrudeuse. Une teneur plus élevée en MA fait perdre à l'élastomère son intégrité et la mise en forme est rendue impossible à une concentration au-delà de 2,5%.

Des limitations technologiques sont apparues lors de la caractérisation morphologique du nanocomposite. En effet, l'analyse TEM est un outil assez puissant pour observer directement la microstructure et identifier la configuration morphologique des nanoargiles dans la matrice. Cependant, l'analyse est très localisée et les observations effectuées ont seulement servi pour confirmer les constatations des analyses XRD. Une étude quantitative basée sur un échantillonnage représentatif des zones observées permettrait un complément d'information sur la morphologie des nanocomposites.

Des informations complémentaires sur les propriétés de transfert de masse auraient pu être apportées à l'aide d'une cellule gravimétrique respectant la norme ASTM F 1407. Cette norme consiste à évaluer la perte de masse causée par l'évaporation du solvant pénétrant dans une cellule spécialement conçue est capable de fournir des informations additionnelles comme le temps de claquage de la membrane et le taux de perméation. Toutefois, des problèmes majeurs d'étanchéité n'ont pas permis d'aboutir et les résultats obtenus se sont avérés non exploitables.

Les résultats obtenus ainsi que les interprétations fournies dans cette étude laissent entrevoir plusieurs recommandations. D'autres paramètres de mise en forme peuvent avoir un effet direct sur l'orientation des nanoargiles dans la matrice. Certains peuvent être optimisés (la température de pressage, la pression appliquée et le temps de maintien). En outre, il est vivement conseillé d'optimiser l'épaisseur de l'orifice de la buse rectangulaire d'extrusion. En effet, un orifice trop large risque de ne pas produire assez de contraintes de cisaillement pour agir sur l'orientation des lamelles et un profil d'alignement sera seulement obtenu sur les surfaces, un orifice trop mince conduit à l'obtention d'un extrudât qui s'épaississe à la sortie. La caractérisation de la morphologie des nanocomposites peut être grandement enrichie par une étude rhéologique. La réponse rhéologique du nanocomposite est susceptible de montrer un comportement pseudo-solide dans la région des basses fréquences, ce qui reflète l'élasticité du réseau des lamelles nanoargiles. La quantification de l'étendue de l'exfoliation peut s'évaluer à travers la contrainte seuil qui découle de l'intensité du comportement d'élasticité. De plus, on a constaté que la température avait un effet important sur tous les paramètres du transport de masse. Par conséquent, une étude thermodynamique des phénomènes de migration moléculaire mérite d'être menée. En dernier lieu, plus qu'une recommandation peut être fournie à l'égard de l'évaluation des propriétés barrières. D'abord, il est préconisé de suivre les tests de prise de masse par des mesures de désorption. Après avoir atteint son équilibre de sorption, l'échantillon nanocomposite se place à l'air libre sur une balance et la variation de sa masse est suivie en fonction du temps. La technique permet d'évaluer le taux d'évaporation et ainsi déterminer le coefficient de désorption du matériau. En outre, et par corrélation avec la méthode de prise de masse, l'évaluation de la variation du volume d'un échantillon à son immersion dans le solvant pénétrant permet d'aboutir à une approximation des paramètres de la cinétique de transport. L'avantage de cette méthode réside dans la possibilité de l'automatiser. En effet, le suivi de l'évolution volumique peut s'effectuer par l'acquisition au fil du temps des données d'une caméra numérique. Enfin, le phénomène de diffusion peut être sondé de plus près par spectroscopie infrarouge à réflectance totale atténuée. L'idée consiste à détecter dynamiquement des groupes fonctionnels caractéristiques du pénétrant en suivant son évolution dans la membrane testée au fil du temps.

Suite à ce projet, certaines perspectives peuvent être envisagées. Dans la présente thèse, l'approche adoptée pour améliorer les propriétés barrières du nanocomposite consiste à créer un chemin tortueux qui ralentit la diffusion du pénétrant. Une autre approche est à explorer. Il est connu que la majorité des polymères sont immiscibles les uns dans les autres. Mélanger le caoutchouc nitrile avec un deuxième polymère dans des proportions soigneusement choisies est susceptible de créer une morphologie co-continue. Une telle morphologie assure la présence d'une interface continue entre les deux phases. Arriver à loger et aligner les lamelles nanoargiles dans la zone interfaciale est susceptible de s'opposer à la pénétration d'un solvant. Dans cette optique, la rhéologie sera un outil puissant pour vérifier la formation d'un réseau tridimensionnel de percolation des nanoargiles. Cette idée fera l'objet d'un article de revue qui sera soumis ultérieurement. Plus loin, réussir à disperser et aligner les lamelles nanoargiles dans une matrice polymérique pourra servir à améliorer d'autres propriétés du matériau. À titre d'exemple, les minéraux argileux réduisent le transfert de chaleur maximal et minimisent la propagation de la flamme. Un nanocomposite à base de nanoargile peut substituer en partie un retardateur de flamme tout en maintenant une protection adéquate contre les incendies pour une charge ignifuge inférieure et moins couteuse.

Les nanocomposites d'argile polymère sont déjà utilisés dans de nombreuses applications. Dans le futur, les efforts de recherche devraient se concentrer sur le développement de matériaux multifonctionnels. Certes, ces nanocomposites continueront d'être utilisés pour améliorer les propriétés mécaniques, d'inflammabilité et de barrière contre les solvants. Cependant, les limites fondamentales de la chimie des argiles empêchent leur utilisation dans des applications relatives à la conductivité électrique, thermique ainsi que dans les applications optiques. Dans le même ordre d'idées, combiner les nanoargiles avec d'autres charges nanométriques pour obtenir un matériau multifonctionnel sera probablement envisageable dans l'avenir. La combinaison des lamelles argileuses avec des nanotubes de carbone, du graphène, ou des points quantiques, pourrait résulter à un nanocomposite intéressant doté de propriétés physico-chimiques, thermiques et électriques améliorées, lui permettant ainsi de remplacer une multitude de matériaux dans une pièce complexe.

CHAPITRE 5

ARTICLE DE JOURNAL : SORPTION AND DIFFUSION OF GOLD AND SILVER NANOPARTICLES IN SOLUTION THROUGH NITRILE RUBBER MEMBRANE

Mohamed Zemzem, Ludwig Vinches, Stéphane Hallé

Dept. of Mechanical Engineering, École de Technologie Supérieure
1100 Notre-Dame West, Montreal (QC) H3C 1K3 Canada

Article publié dans :
Journal of Applied Polymer Science, volume 134(39), juin 2017
https://doi.org/10.1002/app.45350

5.1 Abstract

Mechanical and physical properties of the rubber material may be affected by swelling when brought into contact with solutions of engineered nanoparticles (ENP). As the rubber swells in the liquid carrier of the ENP, the polymeric chains of the network expand and the ENP can penetrate the structure being carried by the diffusion of the liquid. The aim of this work is to assess the influence of ENP and evaluate the effect of additives present in the solutions on the diffusion process through a rubbery structure. Swelling of membrane material specimens was evaluated by measuring mass gain and liquid diffusion was then deduced. The present study focuses on the contact of nitrile rubber membranes with commercial gold ENP (5 nm and 50 nm in diameter) and silver ENP (50 nm) in MilliQ water. Swelling tests were also conducted with MilliQ water and filtrates (the solutions from which the ENP were extracted). Results show that the diffusion coefficients of all the solutions of ENP are slightly different and are around 1.2 × 10-10 $cm^2.s^{-1}$. However, it should be noted that these coefficients are notably higher for the filtrates and reach 2.4 × 10-10 $cm^2.s^{-1}$ for the filtrate of the silver ENP. This result underscores the effect of the ENP on the liquid penetration process. We also found that the ENP has a noticeable effect on the Fickian diffusion mechanism of the penetrant; it was noticed that the presence of these nanoparticles lowers the diffusion mechanism index. Moreover, the size of the nanoparticles was found to have an impact on the diffusion coefficient of the solutions as well as their solubility. These findings help to better understand the diffusion phenomenon of the ENP through nitrile membrane materials.

Keywords: Engineered nanoparticle solutions • Nitrile rubber • Swelling • Sorption • Fickian diffusion mechanisms.

5.2 Introduction

Day after day, the field of nanotechnology offers unprecedented opportunities for progress. A broad variety of nanomaterials has been developed, produced and studied. These materials are currently used in numerous products and industrial applications. In particular, gold and silver engineered nanoparticles have attracted great attention due to their potential application in several fields, especially in medical sciences and electronic components (Alex et Tiwari, 2015; Haider et Kang, 2015). Gold ENP (AuNP) are already an essential component of numerous clinical processes, being used for drug delivery (Kumar, Zhang et Liang, 2013), radiotherapy (Hainfeld et al., 2012), biosensing (Hutter et Maysinger, 2013) as well as to detect and identify infectious diseases (Lin et al., 2013). Besides, silver ENP (AgNP) are well known for their anti-microbiological and anti-infective properties (Griffith et al., 2015) and are being incorporated into products ranging from biological sensing and catalysts (Li et al., 2013) to optics (Tagad et al., 2013). In their solid phase, ENP are more likely to become aerosolized than in their liquid phase, in suspension or in colloidal solution form. To overcome the inherent problems relating to their dispersion in the air, these ENP are increasingly used in suspension in liquids (Ostiguy et al., 2006). On the other hand, a wide range of common applications are currently wholly dependent on synthetic rubber. It is a material of countless uses. The potential application areas include filtration, transportation, and confection industries (Bhowmick et Stephens, 2000). In many of these applications, for example in filtration processes or in the production of packaging, ENP in solution come in contact with rubbery membranes. Unfortunately, it is well known that the presence of such contact affects the physical and chemical properties of the elastomeric products (Candau, Bastide et Delsanti, 1982; Miller-Chou et Koenig, 2003; Starmer, 1993). In fact, when placed in contact with the liquid carrier of the ENP, a polymeric structure will absorb a portion of the substance and subsequently swell. The swelling of elastomeric materials is a complex chemical process, which can be affected by many factors such as liquid and elastomer nature, size and shape of the penetrant, and polarity of the polymeric structure (George, knörgen et Thomas, 1999; George et Thomas, 2001). In addition, to overcome agglomeration and low packing density issues in the ENP suspensions, steric stabilization is performed by adding a polymer dispersant to the suspension (Polyvinylpyrrolidone-PVP); polymer chains are adsorbed by particle surfaces, extend in water, and physically repel one another (Kraynov et Müller, 2011; Shi, 2002). The presence of these additives can affect the swelling phenomena.

The study of the sorption phenomena and transport properties of liquids in elastomers has been the object of intensive investigations. An exceptional summary of the earlier theoretical research on the molecular transport of liquids into solid polymeric materials can be found in a volume by Crank and Park (Crank, 1979; Park et Crank, 1968). More recently, there has been pioneering research efforts to find procedures by which transport coefficients of given systems can be determined accurately through experiment (Balik, 1996b; George et Thomas, 2001; Masaro et Zhu, 1999). Several experimental techniques have been used to study the solvent transport properties of a polymeric matrix (Hui et al., 1987; Möller et Gevert, 1994; Turner et Abell, 1987; Vrtis et Farris, 1996). Of these, the gravimetric method, although simple, has been shown by many to yield reliable data (Aminabhavi, Munnolli et Ortego,

1996; Joseph, Mathai et Thomas, 2003; Stephen et al., 2006; Zhu et Vesely, 2007). Regarding nitrile elastomers, Stamer et al. (Starmer, 1993) studied the sorption and diffusion of various liquids through commercial nitrile rubber to determine how its transport behavior is affected by the choice of solvent as well as the nature of the polymer. The team shows that the swelling curves of the Acrylonitrile-Butadiene Copolymer mainly depend on the molar volume of the penetrant. Gravimetric technique also provides valuable information about kinetic parameters of the transport process. Aminabhavi et al. studied the transport behavior of numerous organic solvents and proposed numerical schemes to calculate diffusion, solubility and permeability coefficients as well as the concentration profile of the penetrant through rubbery membrane structures (Aithal et Aminabhavi, 1990; Shanthamurthy et Aminabhavi, 1990). Furthermore, Perron et al. applied the gravimetric technique on nitrile materials used to make disposable protective gloves to assess the kinetics of penetration of certain solvents and related mixtures through these nitriles (Perron et al., 2000; Perron, Desnoyers et Lara, 2002a). A recent project led by Vinches et al. (Vinches et al., 2015; Vinches et al., 2013) was conducted to assess the permeability of nitrile materials used in protective gloves to certain ENP in solution. The results validated the penetration of gold and titanium dioxide nanoparticles through some nitrile membranes. Up to this point, studies have been made on the penetration of these nanoparticle suspensions through nitrile membranes, but there is rare knowledge about the transport kinetics of these solutions and the effect of their properties on the penetration phenomenon.

The main objective of the present paper is to evaluate the kinetic parameters of commercial gold and silver ENP solutions penetration through nitrile glove material using the gravimetric method. The effect of the presence of the nanoparticles as well as additives on these parameters will also be assessed.

5.3 Materials

5.3.1 Nanoparticle solutions

A total of three commercial ENP suspensions were used in this study. Namely, 5 nm and 50 nm gold ENP as well as 50 nm silver ENP (labeled as AuNP-5, AuNP-50 and AgNP-50 respectively) were in suspension in MilliQ water. All solutions were purchased from NanoComposix, Inc. (San Diego, CA, USA). The concentration for both gold suspensions was 0.05 mg/mL. On the other hand, the initial concentration of AgNP-50 was 5 mg/ml. For this, the solution was diluted in MilliQ water (18.2 MΩ.cm at 25°C and TOC < 2 µg C L^{-1}) to be used at 0.05 mg/mL. Finally, all the solutions were coated with PVP to ensure their stability. Solutions were stored at 4°C away from any light. A part of the nanoparticle solutions were filtered to separate the nanoparticles from the liquid carried by ultrafiltration (Amicon Ultra-4, 3kDa, Millipore) using 70 mL centricons at 3500xG for 40 min. In this paper, filtrates will be designated by a /f symbol in front of the associated nanoparticle solution label.

5.3.2 Nitrile rubber material

The elastomer chosen for this study is a material from disposable protective glove. The commercial model of the glove is Nitri-Care® 3005PF purchased from Showa (Georgia, USA). This model is oil resistant and entirely made of nitrile rubber. In this paper, the disposable glove material is identified as NBR. The average thickness of the rubber sample, performed in triplicate, is 117 ± 6.5 µm. The measurements were made using a micrometer (±0.1 µm).

5.4 Experimental

5.4.1 Nanoparticle suspension characterization techniques

A series of experiments were performed to characterize the ENP solutions. Size distributions were evaluated using Transmission Electron Microscopy (TEM, JOEL JEM-2100F) and Dynamic Light Scattering techniques (DLS, Mobius-Wyatt). An energy-dispersive X-ray spectroscope (EDX) coupled to the TEM was retained to confirm the chemical composition of the ENP. For DLS and XRD, triplicate measurements were performed for each colloidal solution.

5.4.2 Swelling experiment and sorption data

Experimental evaluation of the swelling was carried out by monitoring the amount of absorbed penetrant as a function of time. Mass uptake measurements were performed on rectangular specimens cut from the palm section of the glove (10 mm × 60 mm). After having been weighed, samples were placed in screw-tight bottles containing about 10 ml of the described solutions. At periodic intervals, samples were removed, gently dried with filter paper wraps and weighed on a digital balance (± 0.1 mg). The experiments were stopped when the samples had attained equilibrium saturation and no further change was recorded over an immersion period of two days (Aithal et Aminabhavi, 1990). Three replicates were measured for each test in order to obtain statistically valid data.

5.5 Theory

5.5.1 Diffusion mechanism

Data obtained from the mass uptake were used to examine more closely the behavior of the penetrating solutions within the membrane structure and determine their diffusion mechanism.

The experimental results of dynamic mass variation (M_t/M_∞) were compared to the pace of the empirical equation of the power law given by equation (Stephen et al., 2006):

$$M_t/M_\infty = K \cdot t^n \quad (5.1)$$

M_t and M_∞ are defined as the mass uptake at instant t and at the saturation state. Their expressions are given by:

$M_t = m_t - m_0$
$M_\infty = m_\infty - m_0$

where m_t, m_0 and m_∞ are the weights of the sample at a given time t, at the initial and equilibrium states respectively.

K is a characteristic constant of the elastomeric material. K depends on the structural characteristics of the polymer and its interaction with the solvent (Masaro et Zhu, 1999); n indicates the nature of the transport mechanism. If n = 0.5, the transport mechanism follows the Fickian mode, which occurs when the rate of polymer chain relaxation (R_{relax}) is greater than the rate of the penetrant diffusion (R_{diff}). If n = 1, the transport mechanism is non-Fickian, it occurs when R_{relax} is small compared to R_{diff}. In many cases, the transport mechanism falls between the two previous configurations ($0.5 < n < 1$). This occurs when penetrant diffusion and polymer relaxation have comparable rates. Then, diffusion shows an "anomalous" behavior (Karimi, 2011; Masaro et Zhu, 1999).

This adaptation is applied for short periods at which the mass uptake values do not exceed 60%. The adjustment data on the nonlinear curve of this relationship was made on MATLAB through a regression of the Leveberg-Marquardt algorithm (Kwan Jr, 1998).

5.5.2 Kinetic parameters of mass transport

5.5.2.1 Diffusion

In the literature, several methods have been developed to estimate the diffusivity of a liquid through a polymeric membrane (Hui et al., 1987; Möller et Gevert, 1994; Turner et Abell, 1987; Vrtis et Farris, 1996). Most of these methods use Fickian diffusion theory to predict the diffusion coefficient of the penetrant. In this study, reduced sorption plots of the swelling data show an initial quasi-linear trend. This behavior fits very well with the solutions of Fick's second law of diffusion given by (Crank, 1979; Park et Crank, 1968):

$$\frac{\partial C}{\partial t} = D\left(\frac{\partial^2 C}{\partial x^2}\right) \quad (5.2)$$

with *C* being the concentration of the penetrant, *x* the transport depth of the penetrant into the membrane and *D* the constant value of diffusion considered as independent of the concentration. Thus, for the sake of simplicity, diffusion through the membrane is considered to be unidirectional and penetration from the edge of the sample was neglected. Initial and boundary conditions for a membrane of thickness h are as follows (Balik, 1996b):

$$\begin{array}{lll} for\ t = 0 & 0 < x < h & C = 0 \\ for\ t \geq 0 & x = 0, x = h & C = C_\infty \end{array} \quad (5.3)$$

Under these conditions, the total mass uptake of the penetrant by either of the equations listed below is (Balik, 1996a):

$$M_t/M_\infty = \frac{4}{h}(\frac{Dt}{\pi})^{0.5} + \frac{8}{h}(Dt)^{0.5}\sum_{n=1}^{\infty}(-1)^n \text{ ierfc}(\frac{nh}{2(Dt)^{0.5}}) \quad (5.4)$$

$$M_t/M_\infty = 1 - \frac{8}{\pi^2}\sum_{n=0}^{\infty}\frac{1}{(2n+1)^2}\exp(\frac{-(2n+1)^2\pi^2 Dt}{h^2}) \quad (5.5)$$

These two equations converge rapidly at short and long time intervals respectively. It is worth noting that immersion time is considered to be short if M_t/M_∞ is lower than 60%. In order to avoid analytical complications, diffusion coefficient can be obtained by considering only the first few terms of the equations described above (Karimi, 2011).

For short times ($M_t/M_\infty \leq 60\%$), *D* is determined as the initial slope of the relation:

$$M_t/M_\infty = \frac{4}{h}(\frac{Dt}{\pi})^{0.5} \quad (5.6)$$

For long times ($M_t/M_\infty > 60\%$), *D* is determined as the limiting slope of the relation:

$$\ln(1 - M_t/M_\infty) = \ln(\frac{8}{\pi^2}) - \frac{\pi^2 Dt}{h^2} \quad (5.7)$$

This diffusion coefficient can be optimized. It should be noted that the swelling of the nitrile in aqueous solutions is generally significant (Choi et Ha, 2009). Thus, a correction is made to the diffusion coefficient, which takes into account the elongation and volume changes of the swelled sample. The new intrinsic diffusion coefficient involves the rate of volume variation φ and is given by relation (Brown, Jenkins et Park, 1973; Unnikrishnan et Thomas, 1997):

$$\overline{D} = D/\phi^{7/3} \quad (5.8)$$

ϕ corresponds to sample volume ratio before and after inflation.

5.5.2.2 Sorption and permeation

The ability of the membrane to dissolve the solution in its structure is a characteristic parameter of the interaction of the system solution/elastomer. This ability is given as the ratio of the mass of the absorbed solvent to that of the initial weight of the specimen and is known as the solubility parameter or sorption *S*. At equilibrium, *S* is given by (Aminabhavi et Khinnavar, 1993; Mathew et al., 1995):

$$S = \frac{m_\infty - m_0}{m_0} \tag{5.9}$$

The permeability coefficient may therefore be deduced and is given by (George et Thomas, 2001; Joseph, Mathai et Thomas, 2003):

$$P = \overline{D} \cdot S \tag{5.10}$$

5.5.2.3 Concentration profile

Penetration of the liquid throughout the rubber sheet is expressed by Fick's second law of diffusion presented in equation (5.2). The diffusion coefficient is assumed to be constant for short times. Solving equation (5.11) provides the concentration of the penetrant at a time *t* and a distance (depth) *x* within the membrane structure, under the same initial and boundary conditions previously presented:

$$\frac{C(x,t)}{C_\infty} = 1 - \frac{4}{\pi}\sum_{n=0}^{\infty}\frac{1}{(2n+1)}\exp\left(\frac{-(2n+1)^2\pi^2 D}{h^2}\ t\right) \times \sin\left(\frac{(2n+1)\pi}{h}\ x\right) \tag{5.11}$$

where $C(x,t)$ is the concentration of the absorbed solution at fixed time *t* and distance *x* from the membrane surface. C_∞ is the solution concentration at equilibrium. *D* is the approximated diffusion coefficient for short times calculated from equation (5.6).

For each nanoparticle solution, the concentration profile is evaluated for MilliQ water, nanoparticle solutions and the associated filtrates after a lapse time of 17 hours. Moreover, to see the evolution of a given solution's penetration within a membrane's structure, the concentration profile of MilliQ water will be represented over the membrane thickness for five different time lapses.

5.6 Results and discussions

5.6.1 Characterization of ENP solutions

The characterization techniques performed in this study serve to validate the size of the ENP indicated by the manufacturer and control their chemical composition. The images obtained by the TEM provide a size distribution of the ENP (Figure 5-1). These analyses were conducted for a population of over 100 nanoparticles. For AuNP-5, this distribution is centered at 5.02 ± 0.60 nm. For other ENP, their distributions are centered at 47.88 ± 4.70 nm for AuNP-50 and 50.50 ± 6.50 nm for AgNP-50. These results are amply consistent with data provided by the manufacturer.

The hydrodynamic diameter was also assessed by DLS analysis. The results showed an average of (9.2 ± 0.2) nm for AuNP-5, (67.2 ± 0.6) nm for AuNP-50 and (63.7 ± 0.6) nm for AgNP-50. Figure 5-1 and Figure 5-2 show typical images of each ENP as well as a number distribution according to the hydrodynamic diameter of AuNP-5.

TEM is a number-based observation. The technique gives an estimation of the projected area diameter of a nanoparticle. On the other hand, DLS is an intensity-based technique. The nanoparticles, in the solvated state, undergo thermal motion in the colloidal solution. Their size is determined by measuring the random changes in the intensity of a scattered light from the suspension. The hydrodynamic size was expected to be slightly larger than the TEM size. In fact, it is calculated from the diffusional properties of the nanoparticles in the aqueous media and takes into account their interactions with the surrounding molecules.

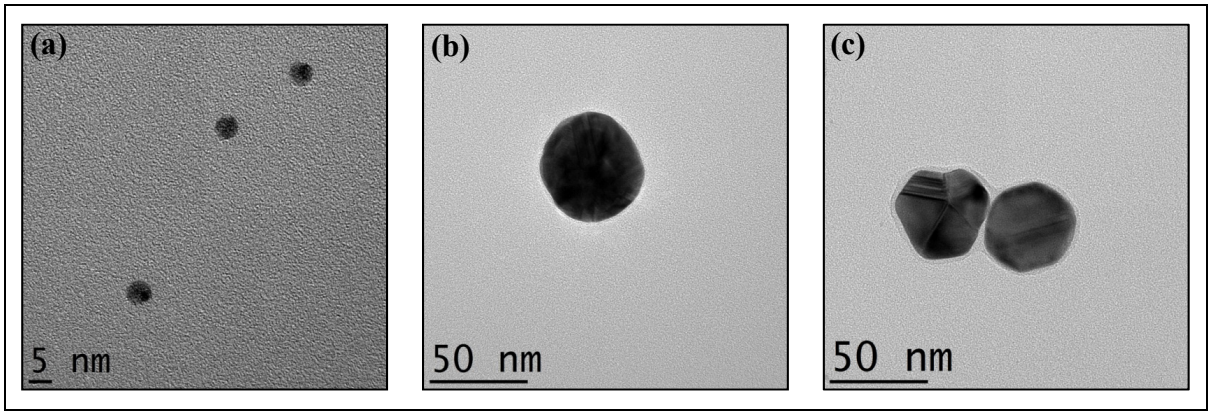

Figure 5-1. TEM images of (a) AuNP-5, (b) AuNP-50 and (c) AgNP-50

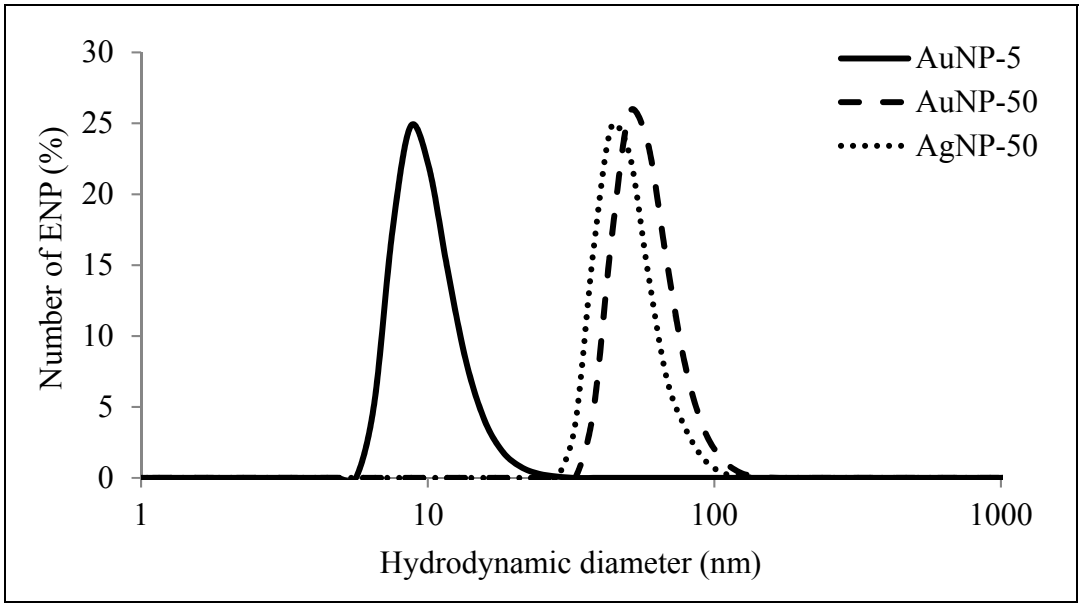

Figure 5-2. Number distribution according to the hydrodynamic diameter of AuNP-5, AuNP-50 and AgNP-50

5.6.2 Effect of ENP on the sorption of colloidal solutions

Contact between a sample of nitrile membrane and these solutions causes the material to swell, under the effect of solubility. The presence of nanoparticles in the solution may have an effect on the swelling of the material, and subsequently on the kinetics of penetration of the suspension through the structure. To determine this effect, the suspensions underwent an ultrafiltration technique to separate the ENP from the carrier liquid. Then mass uptake measurements were performed in compliance with the previously used protocol.

5.6.2.1 Sorption experiment

First, data on the relative mass gain of the sample were plotted as a function of time: $(m_t - m_0)/m_0 = f(t)$. Figure 5-3 shows the curves obtained with the NBR in contact with MilliQ water as well as the three ENP.

The curves indicate a similar behavior for the three ENP solutions within the range of experimental error. The average standard deviation of these measurements is less than 2.5%. A gradual increase in weight gain is observed and it reaches a plateau at 50% for the ENP solutions at an immersion time of around 125 hours. This plateau highlights the attainment of maximum swelling. The mass gain at equilibrium was slightly lower with the liquid carrier (around 45%).

The data obtained with the AgNP-50 solution and the corresponding filtrate is displayed in Figure 5-4. Although mass uptake is identical until approximately 30 hours of immersion, a

significant difference appears when reaching the plateau. The equilibrium is reached at (51.5 ± 2.2) % for the AgNP-50 solution and at (43.5 ± 2.4) % for its filtrate. The same behavior is noticed with the AuNP-50 solution and its filtrate; (51.25 ± 2.1) % and (44.65 ± 1.9) %, respectively. However, there is no remarkable difference between the AuNP-5 solution and its filtered solution.

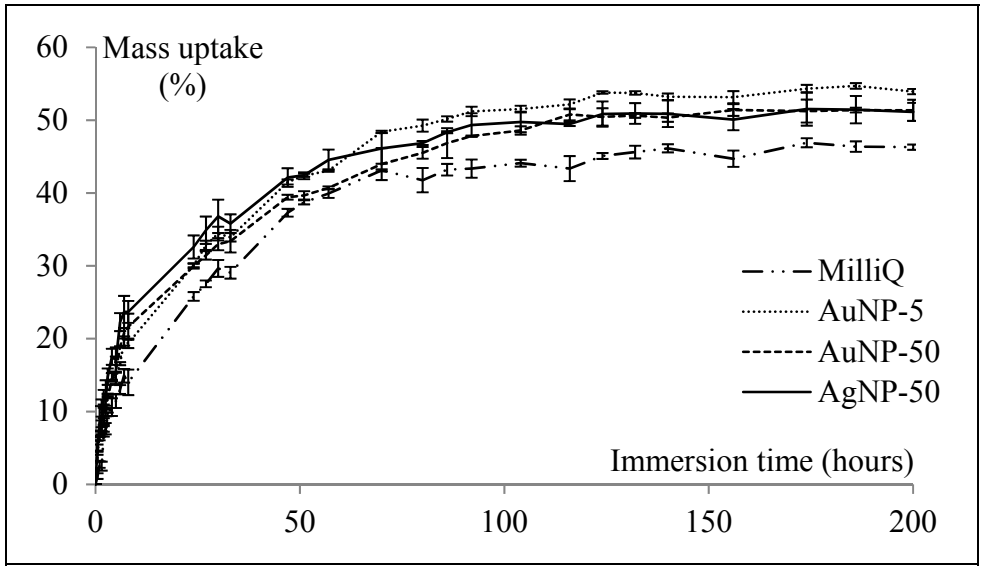

Figure 5-3. Mass uptake ratio of NBR in MilliQ water, AuNP-5, AuNP-50 and AgNP-50 as a function of time

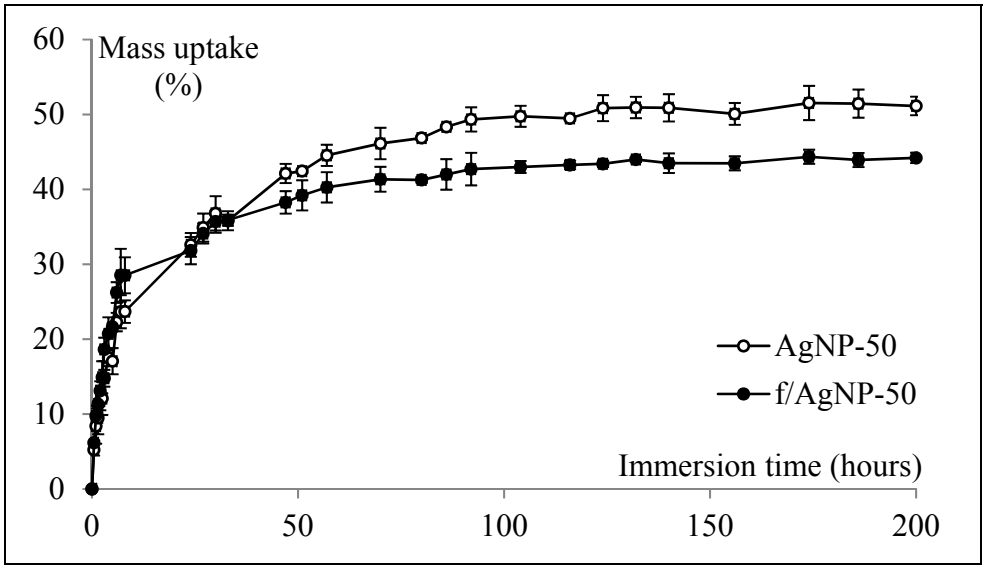

Figure 5-4. Mass uptake ratio of NBR in AgNP-50 and AgNP-50/f as a function of time

To provide a closer look at the kinetics of penetration of the different solutions through the NBR, the swelling data were shown schematically by reduced sorption curves representing mass uptake as a function of the root of the normalized time: $M_t/M_\infty = f(t^{1/2}/h)$.
Figure 5-5 shows the described curves for MilliQ water, AuNP-50 solution and the associated filtrate in contact with NBR.

The resulting curves exhibit the same characteristic swelling gait of an elastomer material. Their behavior shows linearity up to around 65% of equilibrium. They are then concave towards the x-axis and gradually approaching the sorption equilibrium values. This final state is defined by a plateau that corresponds to the saturation of the material (Kwan Jr, 1998).

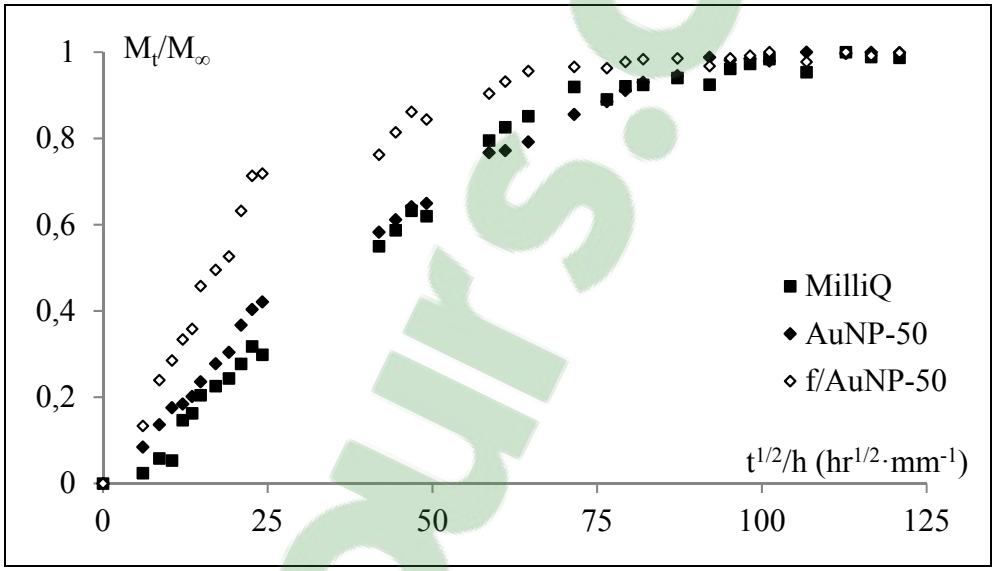

Figure 5-5. Fractional length change of NBR for MilliQ water, AuNP-50 and AuNP-50/f as a function of normalized time

5.6.2.2 Diffusion mechanism

In order to determine the influence of the presence of ENP on the transport mechanism of the colloidal solutions, equation (5.1) was applied to the mass uptake data in short terms ($M_t/M_\infty \leq 60\%$). The following figure is an example of non-linear regression obtained with MATLAB and was applied to the sorption data from the filtrate of AuNP-50 (Figure 5-6). A very good correlation was obtained for all regressions ($R^2 > 0.98$).

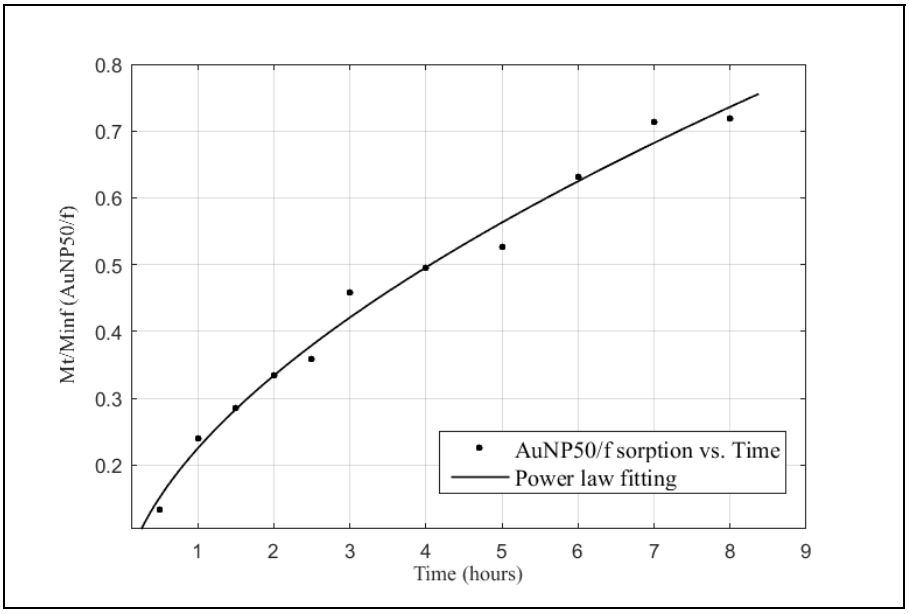

Figure 5-6. Nonlinear curve fit of the power law equation to experimental data sorption of AuNP-50/f

Figure 5-7 and Figure 5-8 compare the index *n* and the parameter *K* of all the solutions. As with MilliQ water and except for AuNP-5/f, the filtrates of ENP solutions have almost similar values of *n* which are around 0.55, a value representative of Fickian diffusion. This is due to the fact that elastomeric materials have a low glass transition temperature when compared to the ambient temperature during experiments. Thus, the macromolecular chains are highly mobile and their relaxation exceeds the mobility rate of the penetrating substance (Grinsted, Clark et Koenig, 1992; Masaro et Zhu, 1999). The notable differences between AuNP-5/f and AuNP-50/f results also indicate that regardless of the type and the size of the nanoparticles, additives of different formulations can be present in the colloidal suspensions for stability purposes.

It should also be noted that for all colloidal solutions, the presence of the ENP lowers the index *n*. Its value for the three colloids is round 0.4. Although below 0.5, this mechanism is still classified as Fickian, it is generally termed as a "sub-Fickian" behavior (Ganji, Vasheghani-Farahani et Vasheghani-Farahani, 2010; Gierszewska-Drużyńska et Ostrowska-Czubenko, 2012; Wang, Wu et Lin, 2008). This situation is encountered when the transport rate of the penetrant is lower than the relaxation rate of the chains (Gierszewska-Drużyńska et Ostrowska-Czubenko, 2012). The decrease of R_{diff} can be caused by the obstruction effect formed by the presence of the ENP. The studies of Thomas and those of Crank showed that if particles of larger sizes are compatible in form with the polymeric matrix structure, these particles occupy the free space between the chains and may decrease the mobility rate of the penetrant liquid (George et Thomas, 2001; Park et Crank, 1968).

Figure 5-8 shows that the *K* factors of AuNP-5 and AuNP-50 filtrates have almost tripled compared to MilliQ water. For AgNP-50/f, this value is more than four times that of the

liquid carrier. This increase demonstrates a strong interaction between the filtrates and the membrane material. *K* values for all the ENP solutions are more than twice the value of the factor associated with MilliQ water. It should be noted that following the ultracentrifugation process, residues of PVP not attached to the ENP remain present in the filtrate. Thus, the presence of PVP in the solutions of this study increases in the following order: MilliQ water < filtrate < colloidal solution. PVP is a polymer known for its high polarity (Baeg et al., 2008; Haaf, Sanner et Straub, 1985). The trend observed in Figure 5-8 may be due to the interaction of the PVP with the acrylonitrile compound that constitutes the nitrile membrane structure and which is also highly polar (Haseeb et al., 2011).

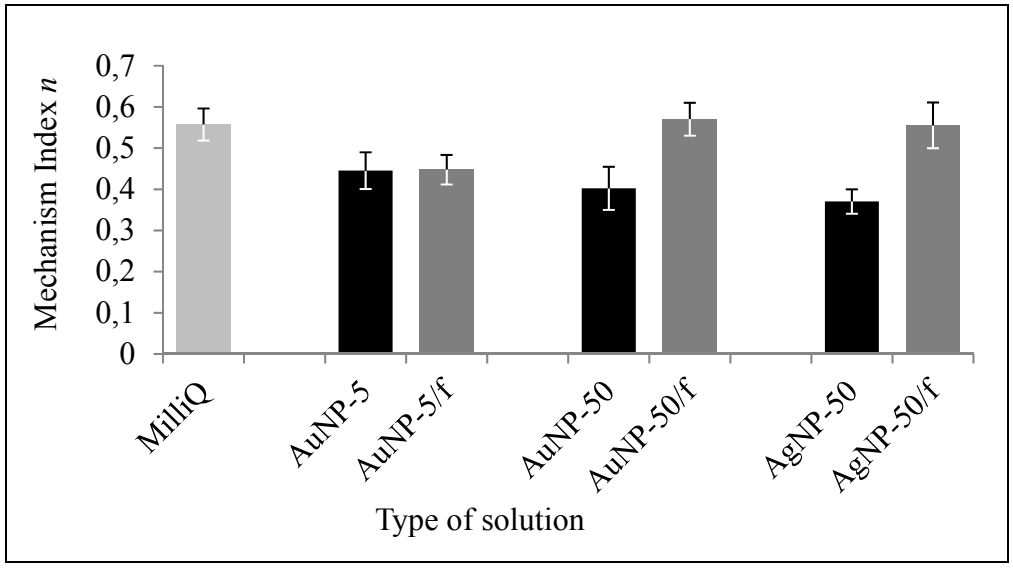

Figure 5-7. Diffusion mechanism index *n* of MilliQ water, ENP solutions and filtrates through the NBR

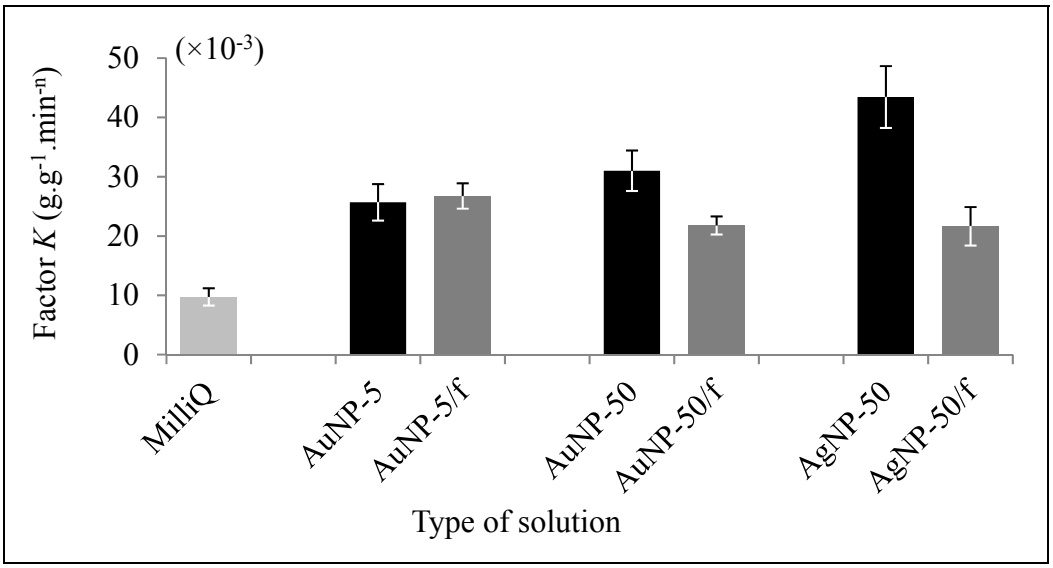

Figure 5-8. *K* index (g•g^{-1}• min^{-n}) of MilliQ water, ENP solutions and filtrates through the NBR

5.6.2.3 Kinetic parameters

Diffusion coefficients:

The Fickian nature of the process by which the liquid solutions are transported through the nitrile structures enables a good approximation of their diffusion coefficients using Fick's second law. Figure 5-9 presents the results of the diffusion coefficients calculated with equation (5.6) at short periods of time ($M_t/M_\infty \leq 60\%$).

The diffusion coefficients of MilliQ water and AuNP-5 solution are similar and approximately (1.0 ± 0.08) × 10^{-10} cm^2.s^{-1}. However, ENP solutions of 50 nm nanoparticles have slightly higher diffusion coefficients ranging from (1.21 ± 0.11) × 10^{-10} cm^2.s^{-1} for AuNP-50 to (1.46 ± 0.11) × 10^{-10} cm^2.s^{-1} for AgNP-50. The nature of the ENP seems to have an effect on the diffusivity of these solutions. This aspect can be explained by the fact that silver nanoparticles are ionic. The charged particles are capable of reacting with the highly polar acrylonitrile phase of the nitrile network (Baker, 2000). Since no substantial difference was noticed between diffusion coefficients of MilliQ water and the three colloidal solutions, an effect of the ENP on diffusivity can only be seen through the filtrates. Figure 5-9 shows that for all ENP suspensions, the diffusion coefficient of the corresponding filtered solution is significantly higher. These values are in the range of (1.4 ± 0.12) × 10^{-10} cm^2.s^{-1} for the AuNP-5/f, (2.4 ± 0.26) × 10^{-10} cm^2.s^{-1} for the AuNP-50/f and (2.1 ± 0.2) × 10^{-10} cm^2.s^{-1} for AgNP-50/f. These results reinforce the hypothesis of a barrier formed by the ENP facing liquid penetration. In addition, the filtered solutions of the gold ENP suspensions have different diffusion coefficients. This difference is probably due to different chemical compositions of the liquid carriers (additives as stabilizers).

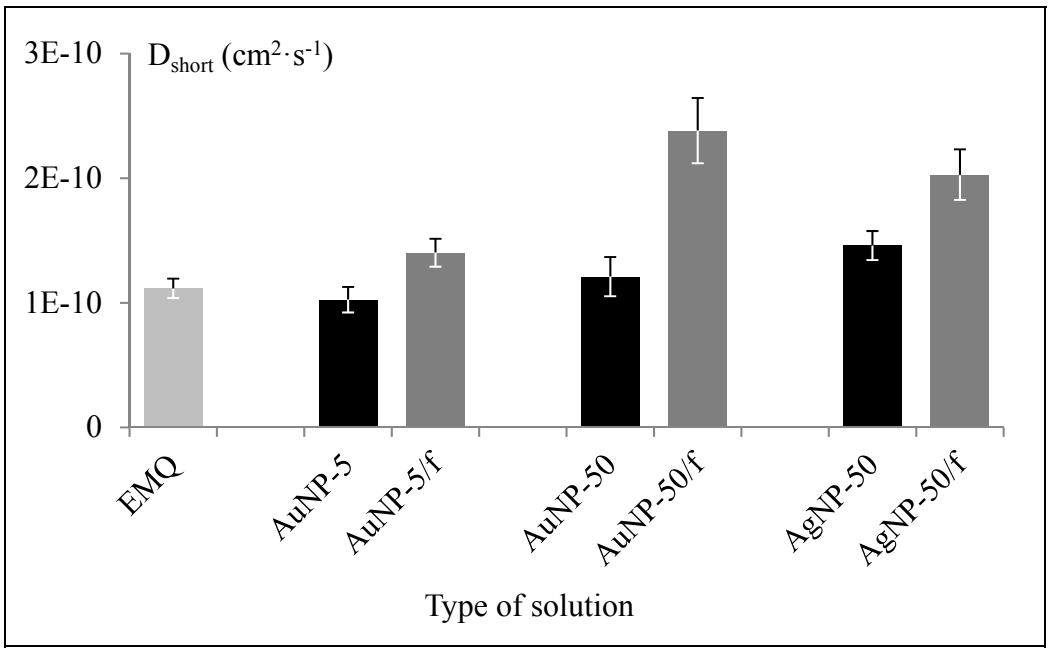

Figure 5-9. Short time diffusion coefficients of MilliQ water, ENP solutions and filtrates in NBR

Sorption and permeation coefficients:

The permeability of the studied solutions through the membrane structure depends both on their diffusivity and their solubility (sorption). The values of sorption rate and permeation coefficient were evaluated by equations (5.9) and (5.10) and are represented by the histograms of Figure 5-10 and Figure 5-11 respectively.

The results in Figure 5-10 show that MilliQ water has a sorption rate of (46.7 ± 3.2) %. All ENP solutions have somewhat higher rates ranging from (54.7 ± 5.5) % for AuNP-5 down to (51.5±4.1) % for AgNP-50. The slight difference noticed between the ENP solutions is due to the fact that the sorption rate is inversely proportional to the particle size in the penetrant (Joseph, Mathai et Thomas, 2003). The ENP and additives present in the colloids makes it more difficult to accommodate the penetrant into the polymer matrix.

The permeation results show the same trends as the diffusion coefficients (Figure 5-11). The liquid carrier shows a slightly lower permeation rate due to its relatively low solubility. ENP solutions have permeation coefficients that are close to one another and are slightly higher for the nanoparticles of 50 nm. Permeation rates for filtrates are much greater than that of the associated ENP solutions. This discrepancy may be due to the absence of ENP, which hinder the passage of the penetrant. The differences were also noted between the filtered solutions themselves. These variations are likely caused by the variation of the chemical composition and contents of additives, such as stabilizers.

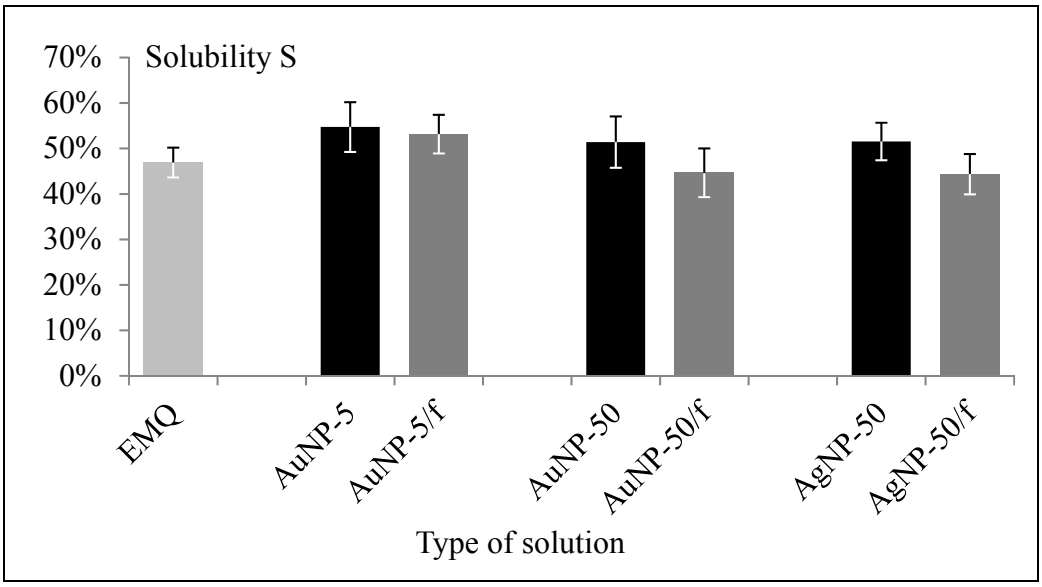

Figure 5-10. Sorption parameter *S* of MilliQ water, ENP solutions and filtrates in the NBR

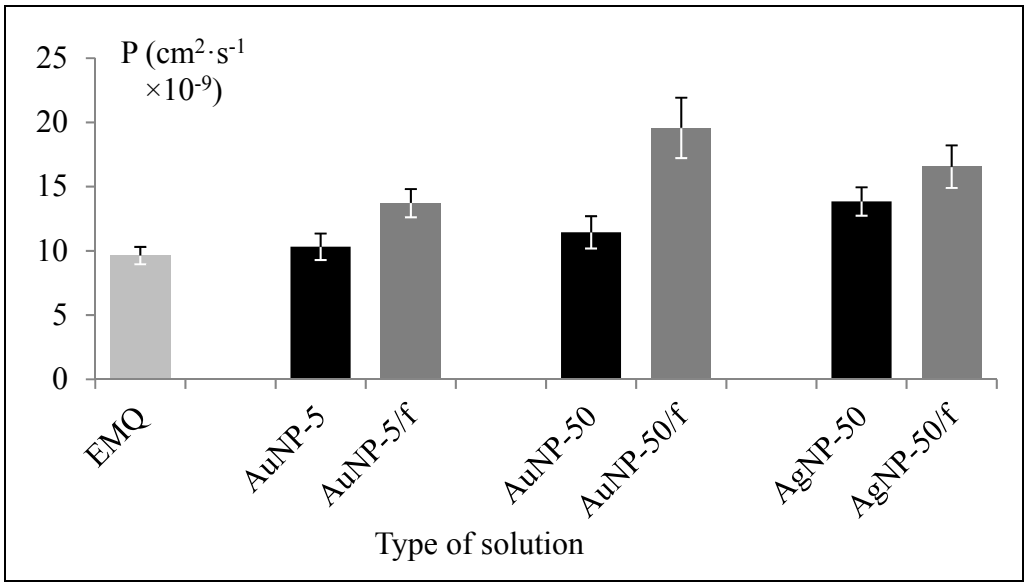

Figure 5-11. Permeation coefficient *P* of MilliQ water, ENP solutions and filtrates through the NBR

Concentration profile:

Concentration ratios $C_{(t,x)}/C_{\infty}$ of MilliQ water in the NBR structure were calculated using equation (5.12). These profiles are represented in Figure 5-12 for five different time lapses until sorption equilibrium. The curves show that during the immersion of the NBR sample, the liquid begins to penetrate the structure of the material and reaches its center after about 5

hours of immersion. The concentration of water in the matrix increases to attain a maximum, starting at 134 hours. In this state of equilibrium and in every point in the structure of the sample, the concentration of the penetrant is equal to its initial concentration on the interface.

In order to visualize the previously discussed results regarding the effect of the nanoparticles on the penetration of the carrier solution in the membrane structure, the concentration profiles of MilliQ water, AuNP-50 and its filtrate were represented in Figure 5-13. Concentrations of MilliQ water as well as the nanoparticle solution exhibit the same profile and are almost equal in the membrane structure. About 25% of the initial concentration of these two solutions is noticed in the center of the membrane structure at 17 hours of immersion. However, at the same time of immersion, the concentration ratio of the filtrate at the center of the membrane is around 55%. Therefore, the amount of the penetrant solution doubles in the core of the structure when nanoparticles are absent. This representation highlights again the obstruction effect caused by the presence of the nanoparticles in the solution.

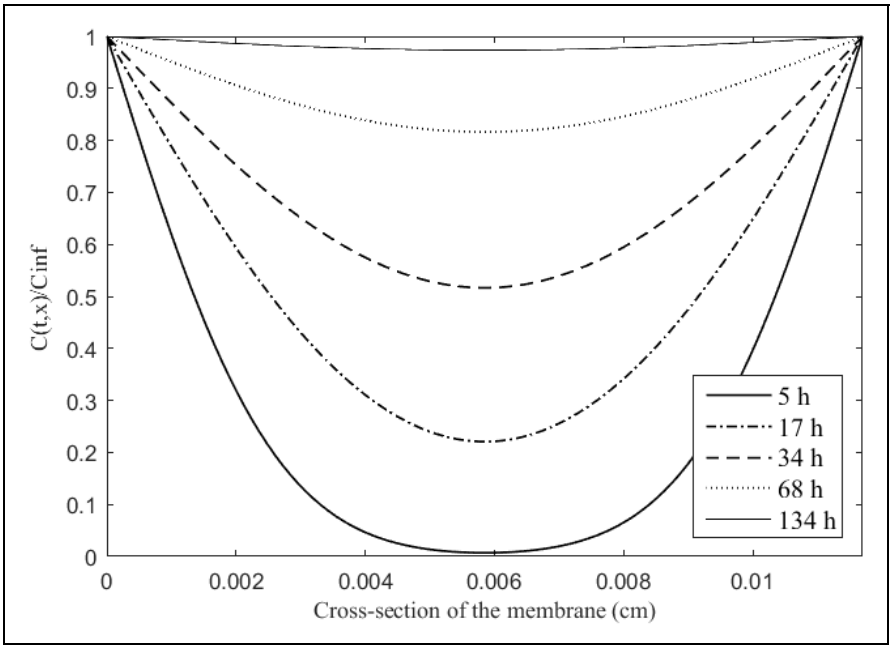

Figure 5-12. Concentration profile of MilliQ water in NBR structure for five given times (5, 17, 34, 68 and 134 hours)

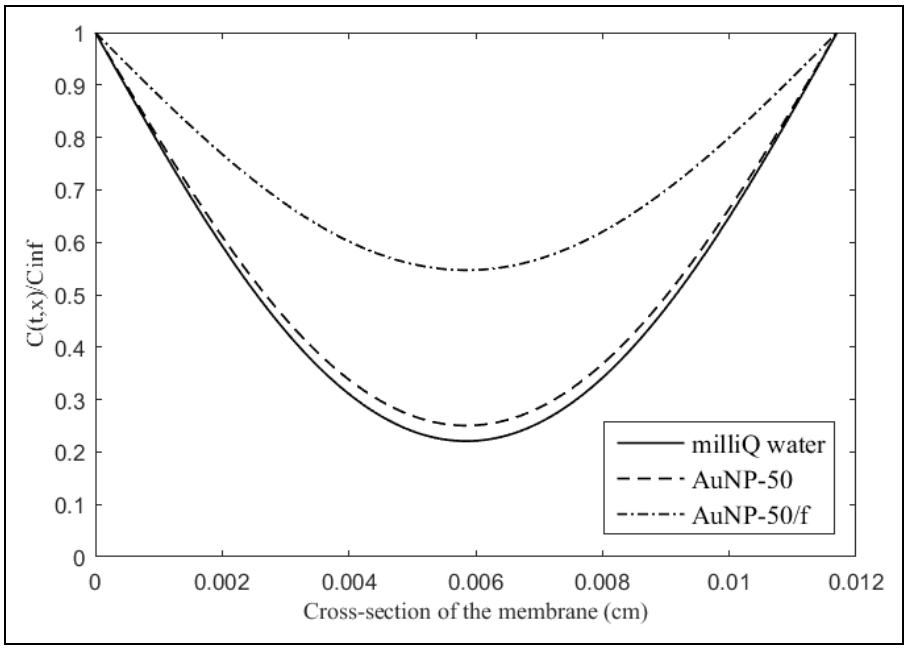

Figure 5-13. Concentration profile of MilliQ water, AuNP-50 and the associated filtrate in NBR structure after 17 hours of immersion

5.7 Conclusions

Although simple, the gravimetric method is an effective technique to study the penetration kinetics of liquid solutions through polymeric membrane structures. This paper presents an analysis of the effect of the presence of nanoparticles on the transport process of colloidal solutions through nitrile films. First, mass uptake data were used to assess the diffusion mechanism of two gold and one silver nanoparticle solutions through the matrix of the material. This mechanism was also evaluated for the associated filtrates as well as for MilliQ water. Values of the mechanism index are found to be representative of Fickian diffusion. By comparing the results of the ENP solutions and the associated filtrates, the presence of the nanoparticles in the solutions seems to lower the index *n*. This situation indicates that the transport rate of the penetrant is decreased in comparison to the relaxation rate of the chains. Hence, the nanoparticles tend to produce a barrier effect to the penetration of the carrier solution. It is also worth noting that the difference noticed in the filtrate's indexes demonstrates that regardless of the type and the size of the nanoparticles, additives of different formulations can be present in the colloidal suspensions. Second, sorption data were used to evaluate diffusion, solubility and permeability coefficients of the solutions through the membrane. It was noticed that the diffusion coefficient of the filtered solution is significantly higher when compared to the ENP solutions. This result underscores once again the barrier effect that the ENP form in the face of liquid penetration. Furthermore, the size of the nanoparticles in the solution seems to have a slight effect on the kinetics of penetration. The difference between the filtrated solution coefficients affirms the different chemical

compositions of the liquid carriers (additives such as stabilizers). Finally, the profiles of liquid concentration were calculated by the analytical solution of Fick's equation. Results show that in the center of the membrane and at the same immersion time, the amount of the penetrant solution more than doubles when nanoparticles are absent. In conclusion, kinetic parameters of ENP solution permeation through nitrile films highlighted an obstruction effect caused by the presence of the nanoparticles in the liquid. Upcoming studies will follow the penetration of these nanoparticles in the matrix of the material and evaluate the kinetics of their penetration through the nitrile membrane structure.

ANNEXE I

ACCOMPLISSEMENTS ACADÉMIQUES

Articles de revue avec comité de lecture :

Zemzem M., Vinches L. et Hallé S. *Molecular sorption and diffusion of organic solvents through maleated rubber/layered silicate nanocomposites*. Soumis à Journal of Polymer Testing en date de mars 2019.
Zemzem M., Vinches L. et Hallé S. *Morphological investigation of maleic anhydride-grafted nitrile rubber/nanoclay nanocomposites*. Soumis à European Polymer Journal en date de mars 2019.
Zemzem M., Vinches L. et Hallé S. *Influence of processing parameters on barrier properties of nitrile/nanoclay nanocomposite membrane against organic solvent*. Journal of Polymer Research, 2019. **26**(3): 64.
Zemzem M., Vinches L. et Hallé S. *Sorption and diffusion of gold and silver nanoparticles in solution through nitrile rubber membrane*. Journal of Applied Polymer Science, 2017. **134**(39): 45350.
Vinches L., Zemzem M. et Hallé S. *Effects of sweat and 3D-deformation on the mechanical behaviour of nitrile rubber gloves*. Progress in Rubber Plastics and Recycling Technology, 2017. **33**(4): 203-220.
Vinches L., Zemzem M., Hallé S., Peyrot C., Wilkinson K.J. et Tufenkji N. *Effectiveness of protective gloves against engineered nanoparticles: difficulties in evaluation*. International Journal of Theoretical and Applied Nanotechnology, 2016. **4**: 9-16.
Vinches L., Zemzem M., Hallé S., Peyrot C., Wilkinson K.J. et Tufenkji N. *An improved experimental methodology to evaluate the effectiveness of protective gloves against nanoparticles in suspension*. Journal of Occupational and Environmental Hygiene. 2017. **14**(7): 95-101.

Articles de conférence avec comité de lecture :

Zemzem M., Vinches L. et Hallé S. *Processing parameters effect on barrier properties of nitrile based nanocomposite membrane*. ANTEC Conference Proceedings, 2018.

Zemzem M., Vinches L. et Hallé S. *Diffusion of nanoparticles in solution through elastomeric membrane*. Journal of Physics: Conference Series, 2017. **829**(1): 012003.

Vinches L., Zemzem M., Boutrigue N., Hallé S., Wilkinson K.J., Lemarchand L., Peyrot C. et Tufenkji N. *Towards understanding the mechanisms and the kinetics of nanoparticle penetration through protective gloves*. Journal of Physics: Conference Series. 2014. **617**(012030).

Résumés de conférences avec comité de lecture :

Zemzem M., Vinches L., Hallé S. (2018). *Processing parameters effect on barrier properties of nitrile based nanocomposite membrane*. Proceedings of ANTEC®2018, 7-10 mai, Orlando, États-Unis.

Zemzem M., Vinches L., Hallé, S. (2016). *Diffusion of nanoparticles in solution through elastomeric membranes*. Applied Nanotechnology and Nanoscience International Conference ANNIC®2016, 9-11 novembre, Barcelone, Espagne.

Zemzem M., Hallé S., Vinches L. (2014). Évaluation expérimentale de la pénétration de l'or colloïdale à travers les gants de protection. 36ème Congrès de l'AQHSST, 11-13 mai, Mont St-Anne, Québec.

Vinches L., Zemzem M., Hallé S., Peyrot C., Wilkinson K.J., Tufenkji, N. (2016). *A rigorous protocol for evaluating the effectiveness of gloves against nanoparticles in solution*. 5th International conference Nanosafe, 7-10 novembre, Grenoble, France.

Vinches L., Zemzem M., Hallé S., Peyrot C., Wilkinson K.J., Tufenkji, N. (2015). *Effectiveness of Protective Gloves against Engineered Nanoparticules: Difficulties in the evaluation!* Proceedings of the 6th International Conference on Nanotechnology: Fundamentals and Applications, 15-17 juillet, Barcelone, Espagne.

Vinches L., Zemzem M., Hallé S., Wilkinson K.J., Tufenkji N. (2015). *Dermal protection against nanoparticles: warning on the use of gloves*. International Congress on Safety of Engineering Nanoparticles and Nanotechnologies, 12-15 avril, Helsinki, Finlande.

Vinches L., Zemzem M., Boutrigue N., Hallé S., Wilkinson K.J., Lemarchand L., Peyrot C., Tufenkji N. (2014). *Towards understanding the mechanisms and the kinetics of nanoparticle penetration through protective gloves*. 3rd International conference Nanosafe, 17-19 novembre, Grenoble, France.

Communications par affiche :

Zemzem M., Hallé S. et Vinches L. (2018). Optimisation des propriétés barrières d'un matériau nanocomposite en nitrile chargé par des nanoargiles. ASM international – Chapitre de Montréal, 28 mars, Université de McGill, Montréal, Canada.

Zemzem M., Hallé S. et Vinches L. (2017). Amélioration de l'imperméabilité aux solvants d'un film en nitrile par ajout de nanoparticules d'argile. 39ème Congrès de l'AQHSST, 16-18 mai, Victoriaville, Canada.

Zemzem M., Hallé S. et Vinches L. (2017). Optimisation des propriétés barrières d'un matériau nanocomposite en nitrile chargé par des nanoargiles. 15ème exposition HIGHTEX – Groupe CTT, 4-5 avril, Place Bonaventure, Montréal, Canada.

Zemzem M., Hallé S. et Vinches L. (2017). Évaluation expérimentale de la diffusivité des nanoparticules en solution à travers les membranes élastomères. ASM international – Chapitre de Montréal, 15 mars, Polytechnique Montréal, Montréal, Canada.

Zemzem M., Hallé S. et Vinches L. (2016). Cinétique de pénétration des nanoparticules en solution à travers la structure d'une membrane élastomère. 38ème Congrès de l'AQHSST, 18-20 mai, Shawinigan, Canada.

Rapport de recherche :

Vinches L., Zemzem M., Hallé S., Peyrot C., Wilkinson K.J. et Tufenkji N. (2016). Mesure de l'efficacité des gants de protection contre les nanoparticules dans des conditions simulant leur utilisation en milieu de travail. Rapport IRSST R-933, 80 pages.

Prix et distinctions :

Type	Compétition	Rang	Organis.	Date
Compétition	Concours description du projet de recherche	Prix de participation	ÉTS	02/2018
Bourse	Concours de la bourse interne	-	ÉTS	01/2018
Bourse	Concours de la bourse interne	-	ÉTS	01/2017
Bourse	Concours de la bourse interne	-	ÉTS	01/2016
Poster	Vulgarisation scientifique par affiche	Lauréat de la meilleure affiche	AQHSST	05/2017
Poster	Vulgarisation scientifique par affiche	Lauréat de la meilleure affiche	AQHSST	05/2016
Poster	Vulgarisation scientifique par affiche	Lauréat de la meilleure affiche	ÉREST	02/2016
Poster	Vulgarisation scientifique par affiche	Lauréat de la meilleure affiche	ÉREST	02/2015
Conférence	Soutien à la publication	-	ÉTS	04/2018
Conférence	Soutien à la publication par conférence	-	ÉREST	04/2016
Conférence	Fonds d'internationalisation de la recherche	-	ÉTS	04/2016
Résumé	Meilleur résumé - Colloque RRSSTQ/AQHSST	Lauréat du meilleur résumé	RRSSTQ/AQHSST	03/2014

LISTE DE RÉFÉRENCES BIBLIOGRAPHIQUES

Aabitha, VK, Ajay Vasudeo Rane et K Rajkumar. 2015. « Processing of Nano Fillers In Nitrile Rubber-A Novel Technique ». *journal of metals, materials and minerals,* vol. 25, n° 2, p. 45-55.

Abubakar Zauro, Sirajo, et Badalamoole Vishalakshi. 2018. « Pectin graft copolymer-montmorillonite composite: Synthesis, swelling and divalent metal ion adsorption ». *Separation Science and Technology*, p. 1-16.

Adak, Bapan, Mangala Joshi et Bhupendra Singh Butola. 2018. « Polyurethane/clay nanocomposites with improved helium gas barrier and mechanical properties: Direct versus master-batch melt mixing route ». *Journal of Applied Polymer Science,* vol. 135, n° 27, p. 46422.

Aithal, U Shanthamurthy, et Tejraj M Aminabhavi. 1990. « Measurement of diffusivity of organic liquids through polymer membranes: A simple and inexpensive laboratory experiment ». *J. Chem. Educ,* vol. 67, n° 1, p. 82.

Al Minnath, Mehar, G Unnikrishnan et E Purushothaman. 2011. « Transport studies of thermoplastic polyurethane/natural rubber (TPU/NR) blends ». *Journal of Membrane Science,* vol. 379, n° 1-2, p. 361-369.

Al-Malaika, Sahar. 2012. *Reactive modifiers for polymers*. Springer Science & Business Media.

Alex, Rosamma, et Changwoon Nah. 2006. « Preparation and characterization of organoclay-rubber nanocomposites via a new route with skim natural rubber latex ». *Journal of applied polymer science,* vol. 102, n° 4, p. 3277-3285.

Alex, Saji, et Ashutosh Tiwari. 2015. « Functionalized gold nanoparticles: Synthesis, properties and applications-A review ». *Journal of Nanoscience and Nanotechnology,* vol. 15, n° 3, p. 1869-1894.

Alexandre, Michael, et Philippe Dubois. 2000. « Polymer-layered silicate nanocomposites: preparation, properties and uses of a new class of materials ». *Materials Science and Engineering: R: Reports,* vol. 28, n° 1-2, p. 1-63.

Alonso, Rafael Herrera, Luis Estevez, Huiqin Lian, Antonios Kelarakis et Emmanuel P Giannelis. 2009. « Nafion–clay nanocomposite membranes: morphology and properties ». *Polymer,* vol. 50, n° 11, p. 2402-2410.

Aminabhavi, Tejraj M, Sujata F Harlapur et J Dale Ortego. 1997. « Transport characteristics of fluoroelastomers by ketones and nitriles ». *Polymer,* vol. 38, nº 11, p. 2725-2731.

Aminabhavi, Tejraj M, et Rajashekhar S Khinnavar. 1993. « Diffusion and sorption of organic liquids through polymer membranes: 10. Polyurethane, nitrile-butadiene rubber and epichlorohydrin versus aliphatic alcohols (C 1-C 5) ». *Polymer,* vol. 34, nº 5, p. 1006-1018.

Aminabhavi, Tejraj M, Ravindra S Munnolli et J Dale Ortego. 1996. « Molecular migration of some industrial solvents into fluoropolymer membranes ». *Waste Management,* vol. 16, nº 4, p. 277-287.

Aminabhavi, Tejraj M, et Hemant TS Phayde. 1995. « Molecular transport characteristics of Santoprene thermoplastic rubber in the presence of aliphatic alkanes over the temperature interval of 25 to 70 C ». *Polymer,* vol. 36, nº 5, p. 1023-1033.

Azeez, Asif Abdul, Kyong Yop Rhee, Soo Jin Park et David Hui. 2013. « Epoxy clay nanocomposites–processing, properties and applications: A review ». *Composites Part B: Engineering,* vol. 45, nº 1, p. 308-320.

Baeg, Kang-Jun, Yong-Young Noh, Jieun Ghim, Bogyu Lim et Dong-Yu Kim. 2008. « Polarity effects of polymer gate electrets on non-volatile organic field-effect transistor memory ». *Advanced Functional Materials,* vol. 18, nº 22, p. 3678-3685.

Bafna, A, G Beaucage, F Mirabella et S Mehta. 2003. « 3D hierarchical orientation in polymer–clay nanocomposite films ». *Polymer,* vol. 44, nº 4, p. 1103-1115.

Bafna, Ayush, Gregory Beaucage, Francis Mirabella, George Skillas et Satish Sukumaran. 2001. « Optical properties and orientation in polyethylene blown films ». *Journal of Polymer Science Part B: Polymer Physics,* vol. 39, nº 23, p. 2923-2936.

Baker, R.W. 2012. *Membrane Technology and Applications*. John Wiley and Sons.

Baker, Richard W. 2000. *Membrane technology*. Wiley Online Library.

Balik, Charles M. 1996a. « On the extraction of diffusion coefficients from gravimetric data for sorption of small molecules by polymer thin films ». *Macromolecules,* vol. 29, nº 8, p. 3025-3029.

Balik, CM. 1996b. « On the extraction of diffusion coefficients from gravimetric data for sorption of small molecules by polymer thin films ». *Macromolecules,* vol. 29, nº 8, p. 3025-3029.

Barrer, Richard M. 1951. *Diffusion in and through Solids*. Ripol Classic

Beall, Gary W, et Clois E Powell. 2011. *Fundamentals of polymer-clay nanocomposites*. Cambridge University Press.

Bee, Soo-Ling, MAA Abdullah, Soo-Tueen Bee, Lee Tin Sin et AR Rahmat. 2018. « Polymer Nanocomposites based on Silylated-Montmorillonite: A Review ». *Progress in Polymer Science*.

Benbayer, Chahinez. 2014. « Nanocomposites à base d'argile et de surfactants polymérisables (surfmers): synthèse et propriétés ». Université Nice Sophia Antipolis.

Bhadran, Bhavya, Dhanya Vijayan, Neena George, CS Julie Chandra, PM Sabura Begum et Rani Joseph. 2018. « Reinforcing effect of organoclay in nitrile rubber-Effect of mill mixing and latex stage mixing ». *Applied Clay Science,* vol. 165, p. 91-102.

Bharadwaj, Rishikesh K. 2001. « Modeling the barrier properties of polymer-layered silicate nanocomposites ». *Macromolecules,* vol. 34, nº 26, p. 9189-9192.

Bhattacharya, Mrinal. 2016. « Polymer nanocomposites—a comparison between carbon nanotubes, graphene, and clay as nanofillers ». *Materials,* vol. 9, nº 4, p. 262.

Bhowmick, Anil K, et Howard Stephens. 2000. *Handbook of elastomers*. CRC Press.

Brown, WR, RB Jenkins et GS Park. 1973. « The sorption and diffusion of small molecules in amorphous and crystalline polybutadienes ». In *Journal of Polymer Science: Polymer Symposia*. Vol. 41, p. 45-67. Wiley Online Library.

Caldona, Eugene B, Al Christopher C De Leon, Bryan B Pajarito et Rigoberto C Advincula. 2017. « A Review on Rubber-Enhanced Polymeric Materials ». *Polymer Reviews,* vol. 57, nº 2, p. 311-338.

Candau, Sauveur, Jacques Bastide et Michel Delsanti. 1982. « Structural, elastic, and dynamic properties of swollen polymer networks ». In *Polymer Networks*. p. 27-71. Springer.

Cervantes-Uc, José M, Juan V Cauich-Rodríguez, Humberto Vázquez-Torres, Luis F Garfias-Mesías et Donald R Paul. 2007. « Thermal degradation of commercially available organoclays studied by TGA–FTIR ». *Thermochimica Acta,* vol. 457, nº 1-2, p. 92-102.

Choi, Sung-Seen, et Sung-Ho Ha. 2009. « Influence of the swelling temperature and acrylonitrile content of NBR on the water swelling behaviors of silica-filled NBR vulcanizates ». *Journal of Industrial and Engineering Chemistry,* vol. 15, nº 2 (3//), p. 167-170.

Choudalakis, G, et AD Gotsis. 2009a. « Permeability of polymer/clay nanocomposites: a review ». *European polymer journal,* vol. 45, nº 4, p. 967-984.

Choudalakis, G., et A. D. Gotsis. 2009b. « Permeability of polymer/clay nanocomposites: A review ». *European Polymer Journal,* vol. 45, nº 4 (4//), p. 967-984.

Christidis, GE. 2011. « Industrial clays ». *EMU Notes in Mineralogy,* vol. 9, p. 341-414.

Chu, Qi, Pingya Luo, Qingfeng Zhao, Junxiong Feng, Xubing Kuang et Delong Wang. 2013. « Application of a new family of organosilicon quadripolymer as a fluid loss additive for drilling fluid at high temperature ». *Journal of Applied Polymer Science,* vol. 128, nº 1, p. 28-40.

Cocchi, Giovanni, Maria Grazia De Angelis et Ferruccio Doghieri. 2015. « Solubility and diffusivity of liquids for food and pharmaceutical applications in crosslinked polydimethylsiloxane (PDMS) films: I. Experimental data on pure organic components and vegetable oil ». *Journal of Membrane Science,* vol. 492, p. 600-611.

Crank, John. 1979. *The mathematics of diffusion*. Oxford university press.

Cui, Lili. 2009. *Polymer-organoclay nanocomposites by melt processing*. (Thèse de doctorat, The University of Texas, Austin)

Cui, Lili, Dimitri M Khramov, Christopher W Bielawski, DL Hunter, PJ Yoon et DR Paul. 2008. « Effect of organoclay purity and degradation on nanocomposite performance, Part 1: Surfactant degradation ». *Polymer,* vol. 49, nº 17, p. 3751-3761.

Cui, Yanbin, S Kumar, Balakantha Rao Kona et Daniel van Houcke. 2015. « Gas barrier properties of polymer/clay nanocomposites ». *Rsc Advances,* vol. 5, nº 78, p. 63669-63690.

Daab, Matthias, Natalie Jasmin Eichstaedt, Christoph Habel, Sabine Rosenfeldt, Hussein Kalo, Hubert Schießling, Stephan Förster et Josef Breu. 2018. « The Onset of Osmotic Swelling in Highly Charged Clay Minerals ». *Langmuir*.

Das, Amit, René Jurk, Klaus Werner Stöckelhuber et Gert Heinrich. 2008. « Effect of Vulcanization Ingredients on the Intercalation-Exfoliation Process of Layered Silicate in an Acrylonitrile Butadiene Rubber Matrix ». *Macromolecular Materials and Engineering,* vol. 293, nº 6, p. 479-490.

Dini, Maryam. 2013. *Improvement of Barrier Properties of Poly (Ethylene Terephthalate)/Organoclay Nanocomposites*. (Thèse de doctorat, École Polytechnique de Montréal, Montréal).

Dlamini, Derrick S, Jianxin Li et Bhekie B Mamba. 2019. « Critical review of montmorillonite/polymer mixed-matrix filtration membranes: Possibilities and challenges ». *Applied Clay Science,* vol. 168, p. 21-30.

Domenech, Trystan. 2012. « Structure et propriétés de nanocomposites polypropylène/argile lamellaire préparés par mélange à l'état fondu ». Paris, ENMP.

Domenech, Trystan, Edith Peuvrel-Disdier et Bruno Vergnes. 2013. « The importance of specific mechanical energy during twin screw extrusion of organoclay based polypropylene nanocomposites ». *Composites Science and Technology,* vol. 75, (2013/02/11/), p. 7-14.

Drioli, Enrico, Giuseppe Barbieri et Adele Brunetti. 2017. *Membrane Engineering for the Treatment of Gases Volume 2: Gas-separation Issues Combined with Membrane Reactors: Edition 2*. Royal Society of Chemistry.

Drioli, Enrico, Lidietta Giorno et Enrica Fontananova. 2017. *Comprehensive membrane science and engineering*. Elsevier.

Duncan, Bruce, Jeannie Urquhart et Simon Roberts. 2005. *Review of measurement and modelling of permeation and diffusion in polymers*. National Physical Laboratory Middlesex (UK).

Espinosa, Sánchez, et Cristian Stalin. 2017. « Estudio y caracterización reológica de fluidos de perforación basados en agua y bentonita sódica natural ». Universidad de las Fuerzas Armadas ESPE. Carrera de Ingeniería Mecánica.

Fajrin, A, LA Sari, N Rahmawati, OA Saputra et V Suryanti. 2017. « Preparation and Mechanical Properties of Chitosan-graft Maleic Anhydride Reinforced with Montmorillonite ». In *IOP Conference Series: Materials Science and Engineering*. Vol. 176, p. 012001. IOP Publishing.

Follain, Nadège, Jean-Marc Valleton, Laurent Lebrun, Benjamin Alexandre, Pierre Schaetzel, Michel Metayer et Stéphane Marais. 2010. « Simulation of kinetic curves in mass transfer phenomena for a concentration-dependent diffusion coefficient in polymer membranes ». *Journal of Membrane Science,* vol. 349, nº 1-2, p. 195-207.

Fornes, TD, DL Hunter et DR Paul. 2004a. « Effect of sodium montmorillonite source on nylon 6/clay nanocomposites ». *Polymer,* vol. 45, nº 7, p. 2321-2331.

Fornes, TD, DL Hunter et DR Paul. 2004b. « Nylon-6 nanocomposites from alkylammonium-modified clay: the role of alkyl tails on exfoliation ». *Macromolecules,* vol. 37, nº 5, p. 1793-1798.

Fornes, TD, PJ Yoon, DL Hunter, H Keskkula et DR Paul. 2002. « Effect of organoclay structure on nylon 6 nanocomposite morphology and properties ». *Polymer,* vol. 43, nº 22, p. 5915-5933.

Forrest, Martin John. 2001. *Rubber analysis: polymers, compounds and products*, 139. iSmithers Rapra Publishing.

Fu, Meng, Zepeng Zhang, Limei Wu, Guanzheng Zhuang, Shuo Zhang, Jiangyan Yuan et Libing Liao. 2016. « Investigation on the co-modification process of montmorillonite by anionic and cationic surfactants ». *Applied Clay Science,* vol. 132, p. 694-701.

Galimberti, Maurizio. 2011. *Rubber-clay nanocomposites: science, technology, and applications*. John Wiley & Sons.

Ganji, Fariba, Samira Vasheghani-Farahani et Ebrahim Vasheghani-Farahani. 2010. « Theoretical description of hydrogel swelling: a review ». *Iran Polym J,* vol. 19, nº 5, p. 375-398.

García-López, David, José Francisco Fernández, Juan Carlos Merino, Julio Santarén et José María Pastor. 2010. « Effect of organic modification of sepiolite for PA 6 polymer/organoclay nanocomposites ». *Composites Science and Technology,* vol. 70, nº 10, p. 1429-1436.

Gates, Will P, Uzma Shaheen, Terence W Turney et Antonio F Patti. 2016. « Cyclic carbonate–sodium smectite intercalates ». *Applied Clay Science,* vol. 124, p. 94-101.

Gatos, Konstantinos G, Nikolaos S Sawanis, Anton A Apostolov, Ralf Thomann et József Karger-Kocsis. 2004. « Nanocomposite formation in hydrogenated nitrile rubber (HNBR)/organo-montmorillonite as a function of the intercalant type ». *Macromolecular materials and engineering,* vol. 289, nº 12, p. 1079-1086.

Gatos, Konstantinos G, László Százdi, Béla Pukánszky et József Karger-Kocsis. 2005. « Controlling the deintercalation in hydrogenated nitrile rubber (HNBR)/organo-montmorillonite nanocomposites by curing with peroxide ». *Macromolecular rapid communications,* vol. 26, nº 11, p. 915-919.

George, S, KT Varughese et SABU Thomas. 2000. « Molecular transport of aromatic solvents in isotactic polypropylene/acrylonitrile-co-butadiene rubber blends ». *Polymer,* vol. 41, nº 2, p. 579-594.

George, Soney C, Sabu Thomas et KN Ninan. 1996. « Molecular transport of aromatic hydrocarbons through crosslinked styrene-butadiene rubber membranes ». *Polymer,* vol. 37, nº 26, p. 5839-5848.

George, Soney C., Manfred knörgen et Sabu Thomas. 1999. « Effect of nature and extent of crosslinking on swelling and mechanical behavior of styrene–butadiene rubber membranes ». *Journal of Membrane Science,* vol. 163, nº 1 (10/1/), p. 1-17.

George, Soney C., et Sabu Thomas. 2001. « Transport phenomena through polymeric systems ». *Progress in Polymer Science,* vol. 26, nº 6 (8//), p. 985-1017.

Ghari, Hedayatollah Sadeghi, et Azam Jalali-Arani. 2016. « Nanocomposites based on natural rubber, organoclay and nano-calcium carbonate: Study on the structure, cure behavior, static and dynamic-mechanical properties ». *Applied Clay Science,* vol. 119, p. 348-357.

Gierszewska-Drużyńska, Magdalena, et Jadwiga Ostrowska-Czubenko. 2012. « Mechanism of water diffusion into noncrosslinked and ionically crosslinked chitosan membranes ». *Prog. Chem. Appl. Chitin Deriv.,* vol. 17, p. 59-66.

Gilman, Jeffrey W. 1999. « Flammability and thermal stability studies of polymer layered-silicate (clay) nanocomposites1 ». *Applied clay science,* vol. 15, nº 1-2, p. 31-49.

Gilman, Jeffrey W, Takashi Kashiwagi, Alexander B Morgan, Richard H Harris, Lori Brassell, Walid H Awad, Rick D Davis, Leonard Chyall, Thomas Sutto et Paul C Trulove. 2001. « Recent advances in flame retardant polymer nanocomposites ». In *INTERNATIONAL SAMPE SYMPOSIUM AND EXHIBITION*. p. 2147-2158. SAMPE; 1999.

Greenkorn, Robert. 2018. *Momentum, heat, and mass transfer fundamentals*. CRC Press.

Griffith, May, KlasI Udekwu, Spyridon Gkotzis, Thien-Fah Mah et EmilioI Alarcon. 2015. « Anti-microbiological and Anti-infective Activities of Silver ». In *Silver Nanoparticle Applications* (2015/01/01), sous la dir. de Alarcon, Emilio I., May Griffith et Klas I. Udekwu. p. 127-146. Coll. « Engineering Materials ». Springer International Publishing.

Grinsted, Ronald A, Lori Clark et Jack L Koenig. 1992. « Study of cyclic sorption-desorption into poly (methyl methacrylate) rods using NMR imaging ». *Macromolecules,* vol. 25, nº 4, p. 1235-1241.

Haaf, F, A Sanner et F Straub. 1985. « Polymers of N-vinylpyrrolidone: synthesis, characterization and uses ». *Polymer Journal,* vol. 17, nº 1, p. 143-152.

Haider, Adnan, et Inn-Kyu Kang. 2015. « Preparation of Silver Nanoparticles and Their Industrial and Biomedical Applications: A Comprehensive Review ». *Advances in Materials Science and Engineering,* vol. 2015, p. 16.

Hainfeld, James F., Henry M. Smilowitz, Michael J. O'Connor, Farrokh Avraham Dilmanian et Daniel N. Slatkin. 2012. « Gold nanoparticle imaging and radiotherapy of brain tumors in mice ». *Nanomedicine,* vol. 8, nº 10 (2013/10/01), p. 1601-1609.

Haseeb, A. S. M. A., T. S. Jun, M. A. Fazal et H. H. Masjuki. 2011. « Degradation of physical properties of different elastomers upon exposure to palm biodiesel ». *Energy,* vol. 36, nº 3 (3//), p. 1814-1819.

Hasegawa, Naoki, Masaya Kawasumi, Makoto Kato, Arimitsu Usuki et Akane Okada. 1998. « Preparation and mechanical properties of polypropylene-clay hybrids using a maleic anhydride-modified polypropylene oligomer ». *Journal of Applied Polymer Science,* vol. 67, nº 1, p. 87-92.

Hasegawa, Naoki, et Arimitsu Usuki. 2004. « Silicate layer exfoliation in polyolefin/clay nanocomposites based on maleic anhydride modified polyolefins and organophilic clay ». *Journal of applied polymer science,* vol. 93, nº 1, p. 464-470.

Hatch, Courtney D, Jadon S Wiese, Cameron C Crane, Kenneth J Harris, Hannah G Kloss et Jonas Baltrusaitis. 2012. « Water adsorption on clay minerals as a function of relative humidity: application of BET and Freundlich adsorption models ». *Langmuir,* vol. 28, nº 3, p. 1790-1803.

Heinrich, Gert. 2011. *Advanced rubber composites*, 239. Springer Science & Business Media.

Hensen, Emiel JM, et Berend Smit. 2002. « Why clays swell ». *The Journal of Physical Chemistry B,* vol. 106, nº 49, p. 12664-12667.

Hsieh, Wen Yen, Kuo Bing Cheng et Chang Mou Wu. 2017. « Compatibilizer effect on Organosilicate reinforced NBR nanocomposites ». *Journal of Polymer Research,* vol. 24, nº 11, p. 205.

Huang, Nai-Jen, et Donald C Sundberg. 1995. « Fundamental studies of grafting reactions in free radical copolymerization. III. Grafting of styrene, acrylate, and methacrylate monomers onto cis-polybutadiene using benzoyl peroxide initiator in solution polymerization ». *Journal of Polymer Science Part A: Polymer Chemistry,* vol. 33, nº 15, p. 2571-2586.

Hui, C-Y, K-C Wu, Ronald C Lasky et Edward J Kramer. 1987. « Case-II diffusion in polymers. I. Transient swelling ». *Journal of Applied Physics,* vol. 61, nº 11, p. 5129-5136.

Hutter, Eliza, et Dusica Maysinger. 2013. « Gold-nanoparticle-based biosensors for detection of enzyme activity ». *Trends in Pharmacological Sciences,* vol. 34, nº 9 (9//), p. 497-507.

Hwang, Wei-Gwo, Kung-Hwa Wei et Chang-Mou Wu. 2004. « Preparation and mechanical properties of nitrile butadiene rubber/silicate nanocomposites ». *Polymer,* vol. 45, nº 16, p. 5729-5734.

Hári, J, F Horváth, J Móczó, K Renner et B Pukánszky. 2017. « Competitive interactions, structure and properties in polymer/layered silicate nanocomposites ». *Express Polymer Letters,* vol. 11, nº 6, p. 479.

Ibrahim, Maha M, Andreas Koschella, Ghada Kadry et Thomas Heinze. 2013. « Evaluation of cellulose and carboxymethyl cellulose/poly (vinyl alcohol) membranes ». *Carbohydrate polymers,* vol. 95, nº 1, p. 414-420.

Issaadi, Kahina, Abderrahmane Habi, Yves Grohens et Isabelle Pillin. 2015. « Effect of the montmorillonite intercalant and anhydride maleic grafting on polylactic acid structure and properties ». *Applied Clay Science,* vol. 107, p. 62-69.

Jauhari, Jenny, Chien-Yi Liao, Jau-Yu Chiou, Shinn-Jen Chang, Yu-Ting Tsai et Jiang-Jen Lin. 2017. « Functionalizing and molecular bonding nanoscale silicate-polymer composites of epoxies and Polyacrylates ». *Journal of Polymer Research,* vol. 24, nº 1, p. 6.

Joseph, Aji, Asha Elizabeth Mathai et Sabu Thomas. 2003. « Sorption and diffusion of methyl substituted benzenes through cross-linked nitrile rubber/poly (ethylene co-vinyl acetate) blend membranes ». *Journal of membrane science,* vol. 220, nº 1, p. 13-30.

Kader, MA, K Kim, Y-S Lee et C Nah. 2006. « Preparation and properties of nitrile rubber/montmorillonite nanocomposites via latex blending ». *Journal of materials science,* vol. 41, nº 22, p. 7341-7352.

Kamal, Tahseen, Soo-Young Park, Myong-Chan Choi, Young-Wook Chang, Wei-Tsung Chuang et U-Ser Jeng. 2012. « An in-situ simultaneous SAXS and WAXS survey of PEBAX® nanocomposites reinforced with organoclay and POSS during uniaxial deformation ». *Polymer,* vol. 53, nº 15, p. 3360-3367.

Karimi, Mohammad. 2011. *Diffusion in polymer solids and solutions*. INTECH Open Access Publisher.

Kato, Makoto, Arimitsu Usuki, Naoki Hasegawa, Hirotaka Okamoto et Masaya Kawasumi. 2011. « Development and applications of polyolefin–and rubber–clay nanocomposites ». *Polymer journal,* vol. 43, nº 7, p. 583.

Khoeini, M, S Bazgir, M Tamizifar, A Nemati et K Arzani. 2010. « Preparation and morphological study of epoxy/silane modified nanoclay nanocomposites ». *Asian Journal of Chemistry,* vol. 22, nº 1, p. 797.

Kiersnowski, Adam, Jochen S Gutmann et Jacek Pigłowski. 2007. « Influence of organic modifiers on morphology and crystallization of poly (ϵ-caprolactone)/synthetic clay intercalated nanocomposites ». *Journal of Polymer Science Part B: Polymer Physics,* vol. 45, nº 17, p. 2350-2367.

Kim, G-M, D-H Lee, B Hoffmann, J Kressler et G Stöppelmann. 2001. « Influence of nanofillers on the deformation process in layered silicate/polyamide-12 nanocomposites ». *Polymer,* vol. 42, nº 3, p. 1095-1100.

Kim, Jin-tae, Taeg-su Oh et Dong-ho Lee. 2004. « Curing and barrier properties of NBR/organo-clay nanocomposite ». *Polymer international,* vol. 53, nº 4, p. 406-411.

Kim, Younghoon, et James L White. 2005. « Formation of polymer nanocomposites with various organoclays ». *Journal of applied polymer science,* vol. 96, nº 5, p. 1888-1896.

Ko, Moon Bae. 2000. « Effects of acrylonitrile content on the properties of clay-dispersed poly (styrene-co-acrylonitrile) copolymer nanocomposite ». *Polymer Bulletin,* vol. 45, nº 2, p. 183-190.

Koo, Chong Min, Jong Hyun Kim, Ki Hyun Wang et In Jae Chung. 2005. « Melt-extensional properties and orientation behaviors of polypropylene-layered silicate nanocomposites ». *Journal of Polymer Science Part B: Polymer Physics,* vol. 43, nº 2, p. 158-167.

Kotal, Moumita, et Anil K Bhowmick. 2015. « Polymer nanocomposites from modified clays: Recent advances and challenges ». *Progress in Polymer Science,* vol. 51, p. 127-187.

Kraynov, Alexander, et Thomas E Müller. 2011. *Concepts for the stabilization of metal nanoparticles in ionic liquids*. INTECH Open Access Publisher.

Kumar, Anil, Xu Zhang et Xing-Jie Liang. 2013. « Gold nanoparticles: Emerging paradigm for targeted drug delivery system ». *Biotechnology Advances,* vol. 31, nº 5 (9//), p. 593-606.

Kumar, H. 2005. « A study of sorption/desorption and diffusion of substituted aromatic probe molecules into semi interpenetrating polymer network of polyurethane/polymethyl methacrylate ». *Polymer,* vol. 46, nº 18, p. 7140-7155.

Kwan Jr, Kermit S. 1998. « The role of penetrant structure on the transport and mechanical properties of a thermoset adhesive ».

Laske, Stephan. 2015. *Polymer nanoclay composites*. William Andrew.

Lawson, David F, William L Hergenrother et Mark G Matlock. 1990. « Preparation and characterization of heterophase blends of polycaprolactam and hydrogenated polydienes ». *Journal of Applied Polymer Science,* vol. 39, nº 11-12, p. 2331-2352.

LeBaron, Peter C, et Thomas J Pinnavaia. 2001. « Clay nanolayer reinforcement of a silicone elastomer ». *Chemistry of Materials,* vol. 13, nº 10, p. 3760-3765.

Lennerová, Dana, František Kovanda et Jiří Brožek. 2015. « Preparation of Mg–Al layered double hydroxide/polyamide 6 nanocomposites using Mg–Al–taurate LDH as nanofiller ». *Applied Clay Science,* vol. 114, p. 265-272.

Lertwimolnun, Wiboon, et Bruno Vergnes. 2005. « Influence of compatibilizer and processing conditions on the dispersion of nanoclay in a polypropylene matrix ». *Polymer,* vol. 46, nº 10, p. 3462-3471.

Lertwimolnun, Wiboon, et Bruno Vergnes. 2006. « Effect of processing conditions on the formation of polypropylene/organoclay nanocomposites in a twin screw extruder ». *Polymer Engineering & Science,* vol. 46, nº 3, p. 314-323.

Leszczyńska, A, James Njuguna, Krzysztof Pielichowski et JR Banerjee. 2007. « Polymer/montmorillonite nanocomposites with improved thermal properties: Part I. Factors influencing thermal stability and mechanisms of thermal stability improvement ». *Thermochimica Acta,* vol. 453, nº 2, p. 75-96.

Li, Hui, Min Wang, Chongzhi Wang, Wei Li, Weibing Qiang et Danke Xu. 2013. « Silver Nanoparticle-Enhanced Fluorescence Resonance Energy Transfer Sensor for Human Platelet-Derived Growth Factor-BB Detection ». *Analytical Chemistry,* vol. 85, nº 9 (2013/05/07), p. 4492-4499.

Liang, Yurong, Yuanhao Guo, Enmin Wang et Miko Cakmak. 2015. « Details of molecular organization during strain-induced crystallization in natural rubber/clay systems as revealed by real-time mechano-optical behavior ». *Macromolecules,* vol. 48, nº 7, p. 2299-2304.

Lim, Yong Taik, et O Ok Park. 2001. « Phase morphology and rheological behavior of polymer/layered silicate nanocomposites ». *Rheologica Acta,* vol. 40, nº 3, p. 220-229.

Lin, Meihua, Hao Pei, Fan Yang, Chunhai Fan et Xiaolei Zuo. 2013. « Applications of Gold Nanoparticles in the Detection and Identification of Infectious Diseases and Biothreats ». *Advanced Materials,* vol. 25, nº 25, p. 3490-3496.

Manias, E. 2007. « Polymer nanocomposite technology, fundamentals of barrier ». *J Nature Mater,* vol. 6, p. 9-11.

Masaro, L., et X. X. Zhu. 1999. « Physical models of diffusion for polymer solutions, gels and solids ». *Progress in Polymer Science,* vol. 24, nº 5 (8//), p. 731-775.

Massey, Liesl K. 2003. *Permeability properties of plastics and elastomers: a guide to packaging and barrier materials*. William Andrew.

Mathai, Asha Elizabeth, RP Singh et Sabu Thomas. 2002. « Transport of substituted benzenes through nitrile rubber/natural rubber blend membranes ». *Journal of membrane science,* vol. 202, nº 1, p. 35-54.

Mathew, Aji P, S Packirisamy, MG Kumaran et Sabu Thomas. 1995. « Transport of styrene monomer through natural rubber ». *Polymer,* vol. 36, nº 26, p. 4935-4942.

Mathew, Aji P, S Packirisamy, Ranimol Stephen et Sabu Thomas. 2002. « Transport of aromatic solvents through natural rubber/polystyrene (NR/PS) interpenetrating polymer network membranes ». *Journal of membrane science,* vol. 201, nº 1-2, p. 213-227.

McKeen, Laurence W. 2016. *Permeability properties of plastics and elastomers*. William Andrew.

Miller-Chou, Beth A, et Jack L Koenig. 2003. « A review of polymer dissolution ». *Progress in Polymer Science,* vol. 28, nº 8, p. 1223-1270.

Mittal, Vikas. 2009. « Polymer layered silicate nanocomposites: a review ». *Materials,* vol. 2, nº 3, p. 992-1057.

Mittal, Vikas. 2010. *Barrier properties of polymer clay nanocomposites*. Nova Science Publishers.

Modesti, M., A. Lorenzetti, D. Bon et S. Besco. 2005. « Effect of processing conditions on morphology and mechanical properties of compatibilized polypropylene nanocomposites ». *Polymer,* vol. 46, nº 23 (2005/11/14/), p. 10237-10245.

Morgan, Alexander B. 2006. « Flame retarded polymer layered silicate nanocomposites: a review of commercial and open literature systems ». *Polymers for Advanced Technologies,* vol. 17, nº 4, p. 206-217.

Möller, Kenneth, et Thomas Gevert. 1994. « An FTIR solid-state analysis of the diffusion of hindered phenols in low-density polyethylene (LDPE): The effect of molecular size on the diffusion coefficient ». *Journal of applied polymer science,* vol. 51, nº 5, p. 895-903.

Müller, Kerstin, Elodie Bugnicourt, Marcos Latorre, Maria Jorda, Yolanda Echegoyen Sanz, José M Lagaron, Oliver Miesbauer, Alvise Bianchin, Steve Hankin et Uwe Bölz. 2017. « Review on the processing and properties of polymer nanocomposites and nanocoatings and their applications in the packaging, automotive and solar energy fields ». *Nanomaterials,* vol. 7, nº 4, p. 74.

Nakason, C, A Kaesaman et P Supasanthitikul. 2004. « The grafting of maleic anhydride onto natural rubber ». *Polymer Testing,* vol. 23, nº 1, p. 35-41.

Naveau, Elodie, Zita Dominkovics, Christophe Detrembleur, Christine Jérôme, József Hári, Károly Renner, Michaël Alexandre et Béla Pukánszky. 2011. « Effect of clay modification on the structure and mechanical properties of polyamide-6 nanocomposites ». *European Polymer Journal,* vol. 47, nº 1, p. 5-15.

Okada, Akane, Masaya Kawasumi, Arimitsu Usuki, Yoshitsugu Kojima, Toshio Kurauchi et Osami Kamigaito. 1989. « Nylon 6–clay hybrid ». *MRS Online Proceedings Library Archive,* vol. 171.

Osman, Azlin Fazlina, Hussein Kalo, Mohd Saifullah Hassan, Tew Wei Hong et Farehah Azmi. 2016. « Pre-dispersing of montmorillonite nanofiller: Impact on morphology and performance of melt compounded ethyl vinyl acetate nanocomposites ». *Journal of Applied Polymer Science,* vol. 133, nº 11.

Osman, Maged A, Vikas Mittal et Hans Rudolf Lusti. 2004. « The aspect ratio and gas permeation in polymer-layered silicate nanocomposites ». *Macromolecular Rapid Communications,* vol. 25, nº 12, p. 1145-1149.

Ostiguy, Claude, Gilles Lapointe, Luc Ménard, Yves Cloutier, Mylène Trottier, Michel Boutin, Monty Antoun et Christian Normand. 2006. « Nanoparticles Actual Knowledge about Occupational Health and Safety Risks and Prevention Measures ».

Pal, Kaushik, R Rajasekar, Dong Jin Kang, Zhen Xiu Zhang, Samir K Pal, Chapal K Das et Jin Kuk Kim. 2010. « Effect of fillers on natural rubber/high styrene rubber blends with nano silica: morphology and wear ». *Materials & Design,* vol. 31, nº 2, p. 677-686.

Pandey, Shruti, Karun K Jana, Vinod K Aswal, Dipak Rana et Pralay Maiti. 2017. « Effect of nanoparticle on the mechanical and gas barrier properties of thermoplastic polyurethane ». *Applied Clay Science,* vol. 146, p. 468-474.

Park, Geoffrey Sheard, et John Crank. 1968. « Diffusion in polymers ».

Paul, DR, et Lioyd M Robeson. 2008. « Polymer nanotechnology: nanocomposites ». *Polymer,* vol. 49, nº 15, p. 3187-3204.

Pavlidou, S, et CD Papaspyrides. 2008. « A review on polymer–layered silicate nanocomposites ». *Progress in polymer science,* vol. 33, nº 12, p. 1119-1198.

Perron, G, TN Banh, L Pelletier, JE Desnoyers et J Lara. 2000. « Volumetric and swelling techniques for studying the permeation of protective gloves to solvents ». In *Performance of Protective Clothing: Issues and Priorities for the 21 st Century: Seventh Volume*. ASTM International.

Perron, Gérald, Jacques E Desnoyers et Jaime Lara. 2002a. « Permeation of mixtures of organic liquids through polymeric membranes: role of liquid–liquid interactions ». *Journal of applied polymer science,* vol. 86, nº 1, p. 195-215.

Perron, Gérald, Jacques Desnoyers et Jaime Lara. 2002b. *Résistance des vêtements de protection aux mélanges de solvants industriels: développement d'un outil de sélection*. Institut de recherche Robert-Sauvé en santé et en sécurité du travail.

Philipse, Albert P. 2018. « A First Round of Brownian Motion ». In *Brownian Motion*. p. 1-8. Springer.

Poon, K, V Castellino et YL Cheng. 2007. « Polymeric hydrophilic polymers in targeted drug delivery ». In *Artificial Cells, Cell Engineering and Therapy*. p. 42-71. Woodhead Publishing.

Powell, Clem E, et Greg G Qiao. 2006. « Polymeric CO2/N2 gas separation membranes for the capture of carbon dioxide from power plant flue gases ». *Journal of Membrane Science,* vol. 279, nº 1-2, p. 1-49.

Pramoda, KP, Tianxi Liu, Zhehui Liu, Chaobin He et Hung-Jue Sue. 2003. « Thermal degradation behavior of polyamide 6/clay nanocomposites ». *Polymer degradation and Stability,* vol. 81, nº 1, p. 47-56.

Prasad, A, R Shroff, S Rane et G Beaucage. 2001. « Morphological study of HDPE blown films by SAXS, SEM and TEM: a relationship between the melt elasticity parameter and lamellae orientation ». *Polymer,* vol. 42, nº 7, p. 3103-3113.

Puglia, D, E Fortunati, David Alberto D'Amico, Valérie Miri, Grégory Stoclet, Liliana Beatriz Manfredi, Viviana Paola Cyras et JM Kenny. 2016. « Influence of processing conditions on morphological, thermal and degradative behavior of nanocomposites based on plasticized poly (3-hydroxybutyrate) and organo-modified clay ». *Journal of Polymers and the Environment,* vol. 24, nº 1, p. 12-22.

Pulat, Mehlika, et Doğan Babayiğit. 2001. « Graft copolymerization of PU membranes with acrylic acid and crotonic acid using benzoyl peroxide initiator ». *Journal of applied polymer science,* vol. 80, nº 14, p. 2690-2695.

Purkait, Mihir K, et Randeep Singh. 2018. *Membrane Technology in Separation Science*. CRC Press.

Raheem, Dele. 2013. « Application of plastics and paper as food packaging materials-An overview ». *Emirates Journal of Food and Agriculture*, p. 177-188.

Rajasekar, R, Kaushik Pal, Gert Heinrich, Amit Das et CK Das. 2009. « Development of nitrile butadiene rubber–nanoclay composites with epoxidized natural rubber as compatibilizer ». *Materials & Design,* vol. 30, nº 9, p. 3839-3845.

Rao, B Madhusudhan, P Raghunath Rao et B Sreenivasulu. 1999. « Grafting of maleic anhydride onto acrylonitrile-butadiene-styrene terpolymer: Synthesis and characterization ». *Polymer-Plastics Technology and Engineering,* vol. 38, nº 5, p. 967-977.

Rao, KSV Krishna, MCS Subha, M Sairam, NN Mallikarjuna et TM Aminabhavi. 2007. « Blend membranes of chitosan and poly (vinyl alcohol) in pervaporation dehydration of isopropanol and tetrahydrofuran ». *Journal of applied polymer science,* vol. 103, nº 3, p. 1918-1926.

Ray, Suprakas Sinha. 2013. *Clay-containing polymer nanocomposites: from fundamentals to real applications*. Newnes.

Ray, Suprakas Sinha, et Masami Okamoto. 2003. « Polymer/layered silicate nanocomposites: a review from preparation to processing ». *Progress in polymer science,* vol. 28, nº 11, p. 1539-1641.

Reichert, P, J Kressler, R Thomann, R Müllhaupt et G Stöppelmann. 1998. « Nanocomposites based on a synthetic layer silicate and polyamide-12 ». *Acta Polymerica,* vol. 49, nº 2-3, p. 116-123.

Ren, Jie, Yanxia Huang, Yan Liu et Xiaozhen Tang. 2005. « Preparation, characterization and properties of poly (vinyl chloride)/compatibilizer/organophilic-montmorillonite nanocomposites by melt intercalation ». *Polymer testing,* vol. 24, nº 3, p. 316-323.

Rhim, Jong-Whan, Hwan-Man Park et Chang-Sik Ha. 2013. « Bio-nanocomposites for food packaging applications ». *Progress in polymer science,* vol. 38, nº 10-11, p. 1629-1652.

Roe, Ryong-Joon. 2000. « Methods of X-Ray and neutron scattering in polymer science (Topics in polymer science) ». *Oxford University Press,* vol. 9, p. 10-12.

Roque-Malherbe, Rolando MA. 2018. *Adsorption and diffusion in nanoporous materials*. CRC press.

Rudin, Alfred, et Phillip Choi. 2012. *The elements of polymer science and engineering*. Academic press.

Rusina, Tatsiana P, Foppe Smedes et Jana Klanova. 2010. « Diffusion coefficients of polychlorinated biphenyls and polycyclic aromatic hydrocarbons in polydimethylsiloxane and low-density polyethylene polymers ». *Journal of applied polymer science,* vol. 116, nº 3, p. 1803-1810.

Saad, Gamal R, Enas E Abd Elhamid et Said A Elmenyawy. 2011. « Dynamic cure kinetics and thermal degradation of brominated epoxy resin–organoclay based nanocomposites ». *Thermochimica acta,* vol. 524, nº 1-2, p. 186-193.

Sadhu, Susmita, et Anil K Bhowmick. 2004. « Preparation and properties of styrene–butadiene rubber based nanocomposites: the influence of the structural and processing parameters ». *Journal of Applied Polymer Science,* vol. 92, nº 2, p. 698-709.

Schnablegger, H, et S Yashveer. « The SAXS Guide, Getting Acquainted with the Principles (Anton Paar GmbH, Austria, 2013) ». *Google Scholar*.

Sclavons, Michel, Véronique Carlier, B De Roover, P Franquinet, Jacques Devaux et Roger Legras. 1996. « The anhydride content of some commercial PP-g-MA: FTIR and titration ». *Journal of applied polymer science,* vol. 62, nº 8, p. 1205-1210.

Sclavons, Michel, P Franquinet, V Carlier, G Verfaillie, I Fallais, R Legras, M Laurent et FC Thyrion. 2000. « Quantification of the maleic anhydride grafted onto polypropylene by chemical and viscosimetric titrations, and FTIR spectroscopy ». *Polymer,* vol. 41, nº 6, p. 1989-1999.

Sclavons, Michel, Michèle Laurent, Jacques Devaux et Véronique Carlier. 2005. « Maleic anhydride-grafted polypropylene: FTIR study of a model polymer grafted by ene-reaction ». *Polymer,* vol. 46, nº 19, p. 8062-8067.

Sedničková, Michaela, Daniela Jochec Mošková, Ivica Janigová, Juraj Kronek, Luboš Jankovič, Miroslav Šlouf et Ivan Chodák. 2017. « Properties of natural rubber composites with structurally different clay intercalable surfactants ». *Journal of Polymer Research,* vol. 24, nº 7, p. 105.

Shah, Rhutesh K, et DR Paul. 2006. « Organoclay degradation in melt processed polyethylene nanocomposites ». *Polymer,* vol. 47, nº 11, p. 4075-4084.

Shanthamurthy, UA, et TM Aminabhavi. 1990. « Measurement of diffusivity of organic liquids through polymer membranes ». *J. Chem. Educ,* vol. 67, nº 1, p. 82-85.

Shi, Jingyu. 2002. « MSE ».

Siepmann, Juergen, et Nicholas A Peppas. 2011. « Higuchi equation: derivation, applications, use and misuse ». *International journal of pharmaceutics,* vol. 418, nº 1, p. 6-12.

Silvestre, Clara, Donatella Duraccio et Sossio Cimmino. 2011. « Food packaging based on polymer nanomaterials ». *Progress in polymer science,* vol. 36, nº 12, p. 1766-1782.

Singala, KJ, AA Mungray et AK Mungray. 2012. « Degradation behavior of polypropylene–organically modified clay nanocomposites ». *Industrial & Engineering Chemistry Research,* vol. 51, nº 32, p. 10557-10564.

Singh, Preeti, Ali Abas Wani et Horst-Christian Langowski. 2017. *Food Packaging Materials: Testing & Quality Assurance*. CRC Press.

Sinha Ray, Suprakas, Pralay Maiti, Masami Okamoto, Kazunobu Yamada et Kazue Ueda. 2002. « New polylactide/layered silicate nanocomposites. 1. Preparation, characterization, and properties ». *Macromolecules,* vol. 35, nº 8, p. 3104-3110.

Siracusa, Valentina, Laura Genovese, Carlo Ingrao, Andrea Munari et Nadia Lotti. 2018. « Barrier Properties of Poly (Propylene Cyclohexanedicarboxylate) Random Eco-Friendly Copolyesters ». *Polymers,* vol. 10, nº 5, p. 502.

Sirinakorn, Thipwipa, Kamonnart Imwiset, Sareeya Bureekaew et Makoto Ogawa. 2018. « Inorganic modification of layered silicates toward functional inorganic-inorganic hybrids ». *Applied Clay Science,* vol. 153, p. 187-197.

Sridhar, S, B Smitha, Satyajai Mayor, B Prathab et TM Aminabhavi. 2007. « Gas permeation properties of polyamide membrane prepared by interfacial polymerization ». *Journal of materials science,* vol. 42, nº 22, p. 9392-9401.

Srikhirin, Toemsak, Abdelsamie Moet et Jerome B Lando. 1998. « Polydiacetylene–inorganic clay nanocomposites ». *Polymers for Advanced Technologies,* vol. 9, nº 8, p. 491-503.

Standard Test Method for Resistance of Chemical Protective Clothing Materials to Liquid Permeation-Permeation Cup Method. 2017. Pennsylvania, United States: American Society for Testing and Materials.

Standard Test Methods for Rubber-Evaluation of NBR (Acrylonitrile-Butadiene Rubber) - D3187-06. 2016.

Starmer, Philip H. 1993. « Swelling of Nitrile Rubber Vulcanizates-Part 3: Factors Affecting Maximum Swelling ». *Journal of Elastomers and Plastics,* vol. 25, nº 3 (July 1, 1993), p. 188-215.

Stephen, Ranimol, Siby Varghese, Kuruvilla Joseph, Zachariah Oommen et Sabu Thomas. 2006. « Diffusion and transport through nanocomposites of natural rubber (NR), carboxylated styrene butadiene rubber (XSBR) and their blends ». *Journal of membrane science,* vol. 282, nº 1, p. 162-170.

Suter, James L, Derek Groen et Peter V Coveney. 2015. « Mechanism of Exfoliation and Prediction of Materials Properties of Clay–Polymer Nanocomposites from Multiscale Modeling ». *Nano letters,* vol. 15, nº 12, p. 8108-8113.

Swamy, BK Kendaganna. 2003. « Sorption and diffusion of chlorinated aliphatic hydrocarbon penetrants into diol chain extended polyurethane membranes ». *Journal of hazardous materials,* vol. 99, nº 2, p. 177-190.

Tagad, Chandrakant K., Sreekantha Reddy Dugasani, Rohini Aiyer, Sungha Park, Atul Kulkarni et Sushma Sabharwal. 2013. « Green synthesis of silver nanoparticles and their application for the development of optical fiber based hydrogen peroxide sensor ». *Sensors and Actuators B: Chemical,* vol. 183, nº 0 (7/5/), p. 144-149.

Tan, Bowen, et Noreen L Thomas. 2016. « A review of the water barrier properties of polymer/clay and polymer/graphene nanocomposites ». *Journal of Membrane Science,* vol. 514, p. 595-612.

Tan, Bowen, et Noreen Louise Thomas. 2017. « Tortuosity model to predict the combined effects of crystallinity and nano-sized clay mineral on the water vapour barrier properties of polylactic acid ». *Applied Clay Science,* vol. 141, p. 46-54.

Teh, PL, ZA Mohd Ishak, AS Hashim, J Karger-Kocsis et US Ishiaku. 2004. « Effects of epoxidized natural rubber as a compatibilizer in melt compounded natural rubber–organoclay nanocomposites ». *European Polymer Journal,* vol. 40, nº 11, p. 2513-2521.

« The Global Nitrile Butadiene Rubber Market ». 2018. <https://www.apnews.com/279415807a544aceb4ff9206ab5e43f1> (Consulté le 10 mars 2019).

Thomas, Sabu, et Ranimol Stephen. 2010. *Rubber nanocomposites: preparation, properties, and applications*. John Wiley & Sons.

Thomas, Saliney, Soney C George et Sabu Thomas. 2017. « Rigid amorphous phase: mechanical and transport properties of nitrile rubber/clay nanocomposites ». *Progress in Rubber Plastics and Recycling Technology,* vol. 33, nº 2, p. 103-126.

Tiemblo, P, J Guzmán, E Riande, C Mijangos, M Herrero, J Espeso et H Reinecke. 2002. « Diffusion of small molecules through modified poly (vinyl chloride) membranes ». *Journal of Polymer Science Part B: Polymer Physics,* vol. 40, nº 10, p. 964-971.

Treece, Mark A., et James P. Oberhauser. 2007. « Processing of polypropylene–clay nanocomposites: Single-screw extrusion with in-line supercritical carbon dioxide feed versus twin-screw extrusion ». *Journal of Applied Polymer Science,* vol. 103, nº 2, p. 884-892.

Trivedi, Be. 2013. *Maleic anhydride*. Springer Science & Business Media.

Turner, DT, et AK Abell. 1987. « Water sorption of poly (methyl methacrylate): 2. Effects of crosslinks ». *Polymer,* vol. 28, nº 2, p. 297-302.

Unnikrishnan, G, et Sabu Thomas. 1997. « Sorption and diffusion of aliphatic hydrocarbons into crosslinked natural rubber ». *Journal of Polymer Science Part B: Polymer Physics,* vol. 35, nº 5, p. 725-734.

Vaia, Richard A, Klaus D Jandt, Edward J Kramer et Emmanuel P Giannelis. 1996. « Microstructural evolution of melt intercalated polymer− organically modified layered silicates nanocomposites ». *Chemistry of Materials,* vol. 8, nº 11, p. 2628-2635.

Vainio, Ulla. 2016. « A size-independent law to describe the alignment of shape-anisotropic objects ». *arXiv preprint arXiv:1604.05156*.

Valapa, Ravi Babu, Sravanthi Loganathan, G Pugazhenthi, Sabu Thomas et TO Varghese. 2017. « An Overview of Polymer–Clay Nanocomposites ». In *Clay-Polymer Nanocomposites*. p. 29-81. Elsevier.

Varghese, S, J Karger-Kocsis et KG Gatos. 2003. « Melt compounded epoxidized natural rubber/layered silicate nanocomposites: structure-properties relationships ». *Polymer,* vol. 44, nº 14, p. 3977-3983.

Vinches, L, C Peyrot, L Lemarchand, N Boutrigue, M Zemzem, KJ Wilkinson, S Hallé et N Tufenkji. 2015. « Towards understanding the mechanisms and the kinetics of nanoparticle penetration through protective gloves ». In *Journal of Physics: Conference Series*. Vol. 617, p. 012030. IOP Publishing.

Vinches, Ludwig, Gérald Perron, Patricia Dolez, Kevin J Wilkinson et Stéphane Hallé. 2012. « Swelling of Elastomers in Solutions of Nanoparticles ». *ISRN Polymer Science,* vol. 2012.

Vinches, Ludwig, Nicolas Testori, Patricia Dolez, Gérald Perron, Kevin J. Wilkinson et Stéphane Hallé. 2013. « Experimental evaluation of the penetration of TiO2 nanoparticles through protective clothing and gloves under conditions simulating occupational use ». *Nanoscience Methods,* vol. 2, nº 1 (2013/12/01), p. 1-15.

Vrtis, JK, et RJ Farris. 1996. « Mass diffusion coefficients of polymer films using real-time holographic interferometry ». *Journal of applied polymer science,* vol. 59, nº 12, p. 1849-1855.

Wang, Jianquan, Wenhui Wu et Zhihui Lin. 2008. « Kinetics and thermodynamics of the water sorption of 2-hydroxyethyl methacrylate/styrene copolymer hydrogels ». *Journal of applied polymer science,* vol. 109, nº 5, p. 3018-3023.

Wang, Ke, Cong Wang, Jiang Li, Juanxia Su, Qin Zhang, Rongni Du et Qiang Fu. 2007. « Effects of clay on phase morphology and mechanical properties in polyamide 6/EPDM-g-MA/organoclay ternary nanocomposites ». *Polymer,* vol. 48, nº 7, p. 2144-2154.

Wang, Yeh, Feng-B Chen, Yann-C Li et Kai-C Wu. 2004. « Melt processing of polypropylene/clay nanocomposites modified with maleated polypropylene compatibilizers ». *Composites Part B: Engineering,* vol. 35, nº 2, p. 111-124.

Wang, Yizhong, Liqun Zhang, Chunhong Tang et Dingsheng Yu. 2000. « Preparation and characterization of rubber–clay nanocomposites ». *Journal of Applied Polymer Science,* vol. 78, nº 11, p. 1879-1883.

Williams-Daryn, S, et RK Thomas. 2002. « The intercalation of a vermiculite by cationic surfactants and its subsequent swelling with organic solvents ». *Journal of colloid and interface science,* vol. 255, nº 2, p. 303-311.

Wilson, Runcy, Sajeev Martin George, Hanna J Maria, Tomás S Plivelic, Anil Kumar S et Sabu Thomas. 2012. « Clay intercalation and its influence on the morphology and transport properties of EVA/clay nanocomposites ». *The Journal of Physical Chemistry C,* vol. 116, nº 37, p. 20002-20014.

Wu, Chang, Wen Hsieh, Kuo Cheng, Chiu-Chun Lai et Kuei Lee. 2018. « Barrier properties of layered-silicate reinforced ethylenepropylenediene monomer/chloroprene rubber nanorubbers ». *Nanomaterials,* vol. 8, nº 5, p. 314.

Wu, You-Ping, Qing-Xiu Jia, Ding-Sheng Yu et Li-Qun Zhang. 2003. « Structure and properties of nitrile rubber (NBR)–clay nanocomposites by co-coagulating NBR latex and clay aqueous suspension ». *Journal of Applied Polymer Science,* vol. 89, nº 14, p. 3855-3858.

Xi, Yunfei, Zhe Ding, Hongping He et Ray L Frost. 2004. « Structure of organoclays—an X-ray diffraction and thermogravimetric analysis study ». *Journal of colloid and interface science,* vol. 277, nº 1, p. 116-120.

Xie, Wei, Zongming Gao, Kunlei Liu, Wei-Ping Pan, Richard Vaia, Doug Hunter et Anant Singh. 2001. « Thermal characterization of organically modified montmorillonite ». *Thermochimica Acta,* vol. 367, p. 339-350.

Yang, K., et R. Ozisik. 2006. « Effects of processing parameters on the preparation of nylon 6 nanocomposites ». *Polymer,* vol. 47, nº 8 (2006/04/05/), p. 2849-2855.

Yang, Liqun, Farao Zhang, Takashi Endo et Takahiro Hirotsu. 2003. « Microstructure of maleic anhydride grafted polyethylene by high-resolution solution-state NMR and FTIR spectroscopy ». *Macromolecules,* vol. 36, nº 13, p. 4709-4718.

Zabihi, Omid, Mojtaba Ahmadi, Saeid Nikafshar, Karthik Chandrakumar Preyeswary et Minoo Naebe. 2018. « A technical review on epoxy-clay nanocomposites: Structure, properties, and their applications in fiber reinforced composites ». *Composites Part B: Engineering,* vol. 135, p. 1-24.

Zanetti, Marco, Pierangiola Bracco et Luigi Costa. 2004. « Thermal degradation behaviour of PE/clay nanocomposites ». *Polymer degradation and stability,* vol. 85, nº 1, p. 657-665.

Zemzem, Mohamed, Ludwig Vinches et Stéphane Hallé. 2017a. « Diffusion of nanoparticles in solution through elastomeric membrane ». In *Journal of Physics: Conference Series*. Vol. 829, p. 012003. IOP Publishing.

Zemzem, Mohamed, Ludwig Vinches et Stéphane Hallé. 2017b. « Sorption and diffusion of gold and silver nanoparticles in solution through nitrile rubber membrane ». *Journal of Applied Polymer Science,* vol. 134, nº 39.

Zemzem, Mohamed, Ludwig Vinches et Stéphane Hallé. 2019a. « Influence of processing parameters on barrier properties of nitrile rubber/nanoclay nanocomposite membrane against organic solvent ». *Journal of Polymer Research,* vol. 26, nº 3, p. 64.

Zemzem, Mohamed, Ludwig Vinches et Stéphane Hallé. 2019b. « Morphological investigation of maleic anhydride-grafted nitrile rubber/nanoclay nanocomposites ». *Submitted to European Polymer Journal*.

Zhang, Chi, Xiandong Liu, Xiancai Lu, Mengjia He, Evert Jan Meijer et Rucheng Wang. 2017. « Surface complexation of heavy metal cations on clay edges: insights from first principles molecular dynamics simulation of Ni (II) ». *Geochimica et Cosmochimica Acta,* vol. 203, p. 54-68.

Zhang, Ru Liang, Li Fen Zhao, Yu Dong Huang et Li Liu. 2016. « Effect of silane coupling agent on the mechanical properties of nitrile butadiene rubber (NBR)/organophilic montmorillonite (OMMT) nanocomposites ». *Science and Engineering of Composite Materials,* vol. 23, nº 3, p. 277-282.

Zhou, Qin, Ray L Frost, Hongping He, Yunfei Xi et Marek Zbik. 2007. « TEM, XRD, and thermal stability of adsorbed paranitrophenol on DDOAB organoclay ». *Journal of colloid and interface science,* vol. 311, nº 1, p. 24-37.

Zhu, Ming, et D. Vesely. 2007. « The effect of polymer swelling and resistance to flow on solvent diffusion and permeability ». *European Polymer Journal,* vol. 43, nº 10 (10//), p. 4503-4515.